DIFFERENTIAL MECHANISMS OF MONOAMINE-INDUCED OSCILLATIONS IN THE LOBSTER PYLORIC PACEMAKER NEURON

A Dissertation

Presented to the Faculty of the Graduate School

of Cornell University

In Partial Fulfillment of the Requirements for the Degree of

Doctor of Philosophy

by

Lolahon Rustam Qizi Kadiri

May 2010

DIFFERENTIAL MECHANISMS OF MONOAMINE-INDUCED OSCILLATIONS IN THE LOBSTER PYLORIC PACEMAKER NEURON

Lolahon Rustam Qizi Kadiri, Ph. D.

Cornell University 2010

Central pattern generator (CPG) is a specialized neuronal circuit that can produce rhythmic motor pattern in the absence of sensory or descending inputs that carry specific timing information. CPGs control basic rhythmic motor functions, such locomotion, respiration, mastication, peristalsis and others. The lobster pyloric circuit is a classical CPG, driven by a pacemaker neuron called the anterior burster (AB). In a synaptically isolated AB neuron, dopamine (DA) and serotonin (5HT) can each evoke rhythmic bursting, but appear to use different sets of currents to drive the burst (Harris-Warrick and Flamm, 1987). DA-induced bursting in the AB neuron is critically dependent on external calcium, minimally affected by external sodium concentration and insensitive to tetrodotoxin (TTX). In contrast, 5HT-induced bursting is critically dependent on the concentration of external sodium: low (50%) external sodium prevents bursting, and TTX abolishes bursting, while low external calcium only slows down the 5HT bursting without completely blocking it.

I have tested the hypothesis that DA evokes oscillations by enhancing the calcium-activated non-selective current (I_{CAN}), while 5HT induces oscillations by enhancing the persistent sodium current ($I_{Na(P)}$). First, I have studied the properties of these slow inward currents in three different pyloric neurons: the

anterior burster (AB) and two motor neurons: the pyloric dilator (PD) and the lateral pyloric (LP). Both currents exhibit cell-type specificity in their properties and modulation. The results of this project are presented in Chapter 2.

In Chapters 3 and 4, I look at the functional significance of I_{CAN} and $I_{Na(P)}$ in the pacemaker neuron AB in more detail. I have established that DA triggers the release of calcium ions from intracellular stores, which results in an activation of the calcium-activated non-selective current and rhythmic oscillations. It is particularly interesting that DA evokes AB bursting in part by modulating a conductance that has no intrinsic voltage dependence. Serotonin, on the other hand, inhibits two potassium outward currents, thereby uncovering the depolarizing effect of the persistent sodium current and generating bursting. Most likely, these two mechanisms are complementary *in vivo* and constitute a fail-proof system in regulating a vitally important physiological function. This system redundancy may represent a common design principle in biology.

BIOGRAPHICAL SKETCH

Lola was born in Tashkent, Uzbekistan in the family of engineers. She excelled in her studies, especially in math and chemistry and graduated cum laude from high school. Her interest in biology and medicine led her to the medical school which she has completed in 1987. After completing residency training Lola practiced medicine for 7 years. During this time she became drawn to the basic biomedical research which she pursued in the Tashkent State Pediatric Medical Institution, while teaching the first and second year medical students anatomy and endocrinology courses. Her desire to study genetics and neurobiology of psychiatric disorders took her to the USA: first, to Rutgers University, where she obtained her master's degree in biology and eventually to the Department of Neurobiology and Behavior at Cornell.

During her years in Ithaca, Lola has come to appreciate the extent of the neuroscience field and different levels of analysis used by the faculty at the NB&B Department. She had chosen early in her graduate career Ron Harris-Warrick as her adviser and conducted her dissertation project in his laboratory. The past 6 years were exciting years, full of opportunities for both personal and professional growth. Although electrophysiology experiments require meticulous and painstaking work, and sometimes can be even frustrating, Lola was rewarded greatly by the vigorous intellectual atmosphere in the RHW lab and the Department of NB&B, known for its enthusiastic and cerebral students, as well as stimulating and inspirational faculty members. She feels that her years at Cornell had prepared her well to pursue her dream of working with animal models of psychiatric disorders and hopes to make original contributions to this fast developing and exciting field. After completing her thesis, Lola is going to join Dr. Osten group in the Cold Spring Harbor Laboratory to study the anatomy and physiology of the cortical circuitry in the mouse models of autism and schizophrenia.

To my parents

ACKNOWLEDGMENTS

I would like to thank my thesis adviser Dr. Ron Harris-Warrick and my PhD committee members Drs. David McCobb, Mariana Wolfner and Ron Hoy for providing me with guidance and setting up the highest standards of scientific scholarship. Ron's vision and uppermost expertise in the neurophysiology and motor systems gave me the necessary knowledge and skills to excel in the program. Dr. McCobb was instrumental in thinking through the experimental design and data interpretation. Dr. Hoy always brought his view of the bigger picture into our discussions and taught me how to look at the problem from different perspectives. Dr. Wolfner was an invaluable mentor and a model of scholarly excellence and provided me with remarkably thorough comments on my thesis. Although not officially on my committee, Dr. Bruce Johnson shared with me his expertise and vast knowledge of STG research on a daily basis. Also, I would like to thank Dr. Mary Lou Zeeman for being an admirable friend and an exceptionally supportive mentor throughout my years at Cornell.

I feel very privileged to have been a part of the Neurobiology and Behavior program at Cornell and considerably benefited from its stimulating and rigorous intellectual environment. I thank the Department for awarding me with the pre-doctoral traineeship. All the NB&B students and postdoctoral fellows inspired me and made the life in Ithaca so much fun. I am especially grateful to Laurieanne Dent for being an extraordinary officemate, and to my labmates Marie-Luise Goeritz, Qing Ouang, Matt Gruhn, Matt Abbinnatti, Giusheng Zhong, and Nate Cramer. Alex Kwan from Cornell physics department was a great collaborator and taught me the two-photon imaging techinque. Highly professional administrative staff of the NB&B, especially Terri Natoli, Suzanne Kohl, Lori Miller, Stacey Cole and Dawn Potter made my life easier

My dearest childhood friend Inga Gasman (Pevchin) was the most enthusiastic supporter of my endeavors. Inga was relentlessly cheering me up and making me laugh even when I thought I was unable to do so. I love you as my sister that I have never had, but always wanted.

Most importantly, I would like to thank my family: my parents for always believing in me, my brothers Bakh and Anvar for supporting my dreams however unattainable they might have seemed at the time, my dear friend and a life partner Corey Washington who made it all possible, and my wonderful children: son Mukhammad Ali and daughter Zika for their infinite love; you make my life happy and worthwhile.

TABLE OF CONTENTS

BIOGRAPHICAL SKETCH…….....iii

DEDICATION……...iv

ACKNOWLEDGMENTS……..v

TABLE OF CONTENTS…….....vii

LIST OF FIGURES……...ix

LIST OF ABBREVIATIONS……xi

CHAPTER 1……...1

CHAPTER 2 …….....24

Introduction …….24

Materials and Methods…….27

Results……..29

Discussion……48

References……57

CHAPTER 3 ……68

Introduction …….68

Materials and Methods…….69

Results……..73

Discussion…….99

References……120

CHAPTER 4 ……130

Introduction …….....130

Materials and Methods…….....132

Results……...133

Discussion…….144

References…….158

CHAPTER 5 ……..168

LIST OF FIGURES

Figure 2.1 Properties of I_{CAN} in the AB neuron…….30

Figure 2.2 Properties of I_{CAN} in the PD neuron…….35

Figure 2.3 Properties of I_{CAN} in the LP neuron……..38

Figure 2.4 Properties of $I_{Na(P)}$ in the AB neuron……41

Figure 2.5 Absence of $I_{Na(P)}$ in the PD neuron……..44

Figure 2.6 Properties of $I_{Na(P)}$ in the LP neuron……46

Figure 2.7 Cell-type differences in the properties of the slow inward currents….50

Figure 3.1 FFA blocks dopamine-induced oscillations in the AB neuron…….74

Figure 3.2 DA enhances the amplitude of I_{CAN} while inhibiting $I_{Ca(v)}$…….....78

Figure 3.3 DA un-couples the I_{CAN} deactivation from the $I_{Ca(v)}$……82

Figure 3.4 DA reduces the leak current in the AB neuron…….....85

Figure 3.5 Release of calcium from intracellular stores is essential for DA-induced AB bursting……..87

Figure 3.6 Anterior Burster neuron filled with calcium indicator Indo-1……..90

Figure 3.7 DA induces intracellular Ca^{2+} accumulation in fine neurites……92

Figure 3.8 The onset of the DA-induced calcium rise precedes the onset of membrane potential oscillations……95

Figure 3.9 Degree of calcium rise increases with bursting intensity……..98

Figure 3.10 Pre-treatment with intracellular calcium channel blockers dampens or prevents the rise in $[Ca^{2+}]_{in}$ and voltage oscillations during DA application……...100

Figure 3.11 The AB neuron calcium signal oscillates in phase but with a delay compared with voltage oscillations…….107

Figure 3.12 Overlay of voltage and calcium traces……111

Figure 3.13 Intracellular Calcium dynamics……..113

Figure 3.14 Model of DA-induced bursting in the AB neuron…….115

Figure 4.1 Serotonin-induced oscillations in a synaptically isolated AB are highly sensitive to blockers of sodium currents…….135

Figure 4.2 Riluzole blocked the AB rhythm by reducing the rate of depolarization preceding the oscillation…….138

Figure 4.3 Serotonin does not modulate the persistent sodium current in the AB neuron.....140

Figure 4.4 Serotonin effects on the outward currents in the AB…….142

Figure 4.5 Serotonin inhibits $I_{K(Ca)}$, but not $I_{K(V)}$ in the AB……146

Figure 4.6 Ionic mechanisms of serotonin and dopamine bursting in the AB neuron……151

LIST OF ABBREVIATIONS

5HT, serotonin

AB, anterior burster

$[Ca^{2+}]_{in}$, intracellular calcium concentration

CG-1, Calcium Green 1

CICR, calcium-induced calcium release

CPG, central pattern generator

DA, dopamine

ER, endoplasmic reticulum

FFA, Flufenamic acid

G, conductance

GPCR, G-protein coupled receptor

I_A, transient potassium current

$I_{CAN,}$ calcium-activated nonselective current

$I_{h,}$ hyperpolarization-activated current

$I_{K(Ca),}$ calcium-activated potassium current

I_{Kv}, delayed rectifier potassium current

I_{leak}, leak current

$I_{Na(P),}$ persistent sodium current

IP_3, inositol triphosphate

IP_3R, IP_3-sensitive receptor

MNJ, neuromuscular junction

Nif, Nifedipine

PKC, protein kinase C

PreBC, pre-Botzinger complex

PTX, picrotoxin

Ril, Riluzole

ROI, region of interest

Ry, Ryanodine

RyR, Ryanodine-sensitive receptor

SERCA, sarco-endoplasmic reticulum calcium ATPase

STG, stomatogastric ganglion

STNS, stomatogastric nervous system

TEA, tetraethylammonium chloride

Tg, Thapsigargin

TTX, tetrodotoxin

VC, voltage clamp

V_m, membrane potential

Xe, Xestospongin C

CHAPTER 1

PRINCIPLES OF RHYTHM GENERATION: AN OVERVIEW

Animals survive and adapt their physiology and behavior to various external and internal factors with the help of their nervous system. The neural processes span time scales from less than a millisecond to the lifetime of the organism. Examples encompass the fastest processes such as channel gating and action potentials to the slowest processes such as seasonal and developmental transformations and long-term memory. Control of rhythmic behaviors occurs at all levels of the nervous system, from the neocortex to peripheral ganglia. In the vertebrate brain, practically all known microcircuits demonstrate oscillatory behavior, each at different preferred frequencies (Yuste *et al.,* 2005; Grillner *et al.*, 2005). For example, rhythmic oscillations in neocortical and cerebellar cortical microcircuits are involved in vastly different tasks related to perception, cognition, memory and control of movement (Clemens *et al* ; 2005; Rizzuto, 2003; Steriade, 2001; Maex *et al*., 2005). At another level, in the hippocampus, γ-frequency oscillations are implicated in encoding and retrieval of memory, while the θ- frequency has been associated with place representation and memory functions (Bragin et al., 1995; Buszaki et al., 2002). Finally, brainstem and spinal cord microcircuits that generate rhythmic respiratory and locomotor activity have been analyzed in considerable detail in different animal models, from the lamprey to mammals (reviewed in Grillner, 2003; Smith et al., 1991; Feldman, 2003; Kiehn, 2006). The respiratory, locomotor and other similar neural circuits governing basic rhythmic motor functions are collectively termed “central pattern generators”, or CPGs.

CPGs are specialized neuronal circuits that can produce rhythmic motor patterns in the absence of sensory or descending inputs that carry specific timing

information (Marder and Bucker, 2001). Each CPG are constructed from three fundamental building blocks: specific cellular properties (endogenous bursting, plateau potentials, postinhibitory rebound, and spike-frequency adaptation), the pattern of synaptic connectivity and neuromodulation (Marder and Bucher, 2001). Traditionally, CPGs are divided into the network-driven and the pacemaker-driven, depending on the predominant mechanism for generation of rhythmic output. Most likely, both mechanisms of rhythmogenesis normally work together *in vivo*.

Pacemaker-based rhythmogenesis

This mechanism relies on the intrinsic properties of a single cell, called the "pacemaker" that, under the appropriate modulatory conditions, endogenously generates rhythmic output and drives the whole network. The best-known known example of a pacemaker-driven CPG is the pyloric network in the crustacean stomatogastric ganglion (STG). Much insight has been gained from studying this CPG for feeding motor behavior in crabs and lobsters (Harris-Warrick and Marder, 1991; Katz and Harris-Warrick, 1999; Harris-Warrick, 2002; Selverston, 1999; Marder and Calabrese, 1996; Katz, 1998; Marder and Bucker, 2001, 2007; Marder et al., 2005, Nusbaum and Beenhakker, 2002, Hooper and DiCaprio, 2004).

The Crustacean Stomatogastric Ganglion

The crustacean stomatogastric ganglion is one of the best experimental models to understand the mechanisms of pacemaker activity because it contains only 30 neurons and each neuron and synapse are reliably identifiable from animal to animal. Moreover, its structural organization, function and neuromodulation are well-described (Harris-Warrick and Marder, 1992, Marder and Bucher, 2007, 2001; Nusbaum and Beenhakker, 2002; Selverston et al., 1998). The STG

contains two distinct, but interconnected CPGs: a slower gastric mill circuit and a faster pyloric circuit. The pyloric rhythm is a triphasic motor pattern with a period of 1–2 s. The pyloric subcircuit consists of 14 neurons, including one interneuron (the anterior burster, or AB) and 13 motoneurons that fall into 5 types: pyloric dilator (PD), lateral pyloric (LP), pyloric constrictor (PY), ventricular dilator (VD) and inferior cardiac (IC). Each pyloric neuron type has a unique electrophysiological profile and the cells form identified electrical and inhibitory chemical synapses which define the network (Harris-Warrick et al., 1992; Selverston and Moulins, 1987). In addition to sensory input and history of activity, the final motor output is modulated by multiple compounds coming from the anterior (commissural and esophageal) ganglia and the brain or as neurohormones in the hemolymph: monoamines, peptides, hormones, growth factors (Flamm and Harris-Warrick, 1986; Hooper and Marder, 1987; Skiebe etal., 1994; Nusbaum and Marder 1988; Marder and Thirumalai, 2002; Turrigiano and Selverston, 1989; Swensen et al., 2002).

The power of this model system lies in the ability to isolate any neuron or a subset of neurons with selected synapses using a combination of three methods: blockade of the descending modulatory inputs by TTX, pharmacological block of chemical synapses within STG and photoinactivation of electrically coupled neurons (Miller, 1979; Bidaut, 1980). Much insight into rhythmogenesis has been gained from studies of the reduced preparations of the pyloric network. First, elimination of the pacemaker neuron AB does not stop oscillations of the remaining network provided that modulatory input is intact (Miller and Selverston, 1982a), although it slows down considerably. In fact, two neurons (LP and PD) connected with mutually inhibitory synapses are able to form so-called “half-center oscillator” and generate rhythmic output in the presence of

depolarizing current (Miller and Selverston 1982b). However, AB is the only pyloric neuron that is capable of endogenous bursting in the presence of monoamines. Second, descending modulatory input from the anterior ganglia is required for bursting of the pacemaker neuron AB as well as the entire network, as removal of these modulatory inputs terminates the rhythm (Miller and Selverston, 1982a; Russell and Hartline, 1978). Photoinactivation makes it possible to study the function of the pacemaker kernel and its components in isolation. The pyloric pacemaker kernel is made up of the AB and two PD neurons; all three neurons are strongly electrically coupled (Harris-Warrick et al., 1992; Selverston and Moulins, 1987). Modulatory effects on the oscillatory frequency of the isolated AB are different from their effects on the pacemaker kernel (ABx2PDs or ABxPD) (Ayali and Harris-Warrick, 1999).

Multiple modes of pyloric pacemaker bursting

In a synaptically isolated AB neuron, dopamine and serotonin can each evoke rhythmic bursting, but appear to use different sets of currents to drive the burst (Harris-Warrick and Flamm, 1987). Dopamine-induced bursting in the AB neuron is critically dependent on external calcium, minimally affected by external sodium concentration and insensitive to tetrodotoxin (TTX). In contrast, serotonin-induced bursting is critically dependent on the concentration of external sodium: low (50%) external sodium prevents bursting, and TTX abolishes bursting, while low external calcium only slows down the 5HT bursting without completely blocking it. Thus, dopamine may activate a bursting mode that is critically dependent on calcium or calcium-dependent currents, while 5HT activates a separate bursting mode that depends critically upon sodium currents. Elevated bath temperature was shown to alter this ionic dependence (Johnson et al., 1992). Building upon the previous work in the lab, I sought to determine the

exact currents targeted by DA and 5HT, and the mechanisms of monoamine-induced bursting in the AB neuron.

Mechanisms of the DA-induced AB bursting

Dopamine has numerous effects on the intrinsic and synaptic properties of the different stomatogastric neurons. First, on the pyloric network level, DA slightly decreases cycle frequency and changes the phase relationships, with PD and VD phase delayed while LP, PY, and IC are phase advanced relative to the AB pacemaker (Flamm and Harris-Warrick, 1986a, b). Second, the individual synapses, both chemical and electrical, may be either strengthened or weakened by DA (Johnson *et al.,* 1990, 1993, 1995; Johnson and Harris-Warrick, 1997; Cleland and Selverston, 1997, Ayali *et al.,* 1998). Third, each isolated pyloric neuron changes its intrinsic electrophysiological behavior upon DA application: AB becomes an endogenous oscillator (sometimes called "burster") (Harris-Warrick and Flamm, 1987), while LP, PY, and IC neurons depolarize and fire tonically and the PD and VD neurons are inhibited and may fall silent (Harris-Warrick *et al.,* 1993). Finally, the individual conductances are modified in a cell-type specific manner. For instance, DA increases the transient potassium current I_A in the PD, while reducing it in LP, PY, IC and AB neurons (Peck et al., 2001). DA also affects other conductances, such as the hyperpolarization-activated current I_h (Peck et al., 2006) and various types of potassium currents (Kloppenberg et al., 1999; Gruhn et al., 2005). DA enhances the voltage-dependent calcium current $I_{Ca(v)}$ in the LP, and importantly for the bursting mechanism under the current study, it strongly inhibits $I_{Ca(v)}$ in the AB neuron (Johnson et al., 2003).

Dopamine is not synthesized within the STG; instead, it is produced by the neurons that are located in the anterior ganglia and the brain and send their axons

down to the STG via the stomatogastric nerve (Kushner, 1977; Sullivan *et al.* 1977; Barker *et al.* 1979; Kushner and Barker 1983; Cournil, 1994). DA is also present as a neurohormone in the hemolymph surrounding the STG (Sullivan *et al.,* 1977), although in the lobster, DA concentrations in the blood are probably too low to affect the STG DA receptors.

Three types of DA receptors that belong to the superfamily of G-protein coupled receptors (GPCRs) have so far been identified in the lobster STG: $D_{1\alpha Pan}$, $D_{1\beta Pan}$ and $D_{2\alpha Pan}$ (Clark and Baro 2006, 2007). The $D_{1\alpha Pan}$ receptor couples with G_s and G_q, while the $D_{1\beta Pan}$ receptor couples with G_s, and the $D_{2\alpha Pan}$ receptor couples with G_i (Clark *et al.,* 2008). All three receptor types are localized exclusively to the synaptic neuropil, but the cell type specific distribution of the DA receptors is currently unknown. As described above, the effect of DA on the intrinsic properties of the individual pyloric cell types varies greatly (Flamm and Harris-Warrick, 1986a,b; Harris-Warrick and Flamm, 1987; Ayali and Harris-Warrick, 1999; Kloppenburg et al.,2000, 2007; Peck *et al.,* 2001, 2006; Johnson *et al.,* 2003; Gruhn *et al.,* 2005); it is expected that each cell type has its own unique complement of DA receptors, secondary messengers, and effector proteins (Clark *et al.,* 2008; Oginsky *et al.,* 2010) which remains to be identified for the AB neuron.

One of the most striking effects of DA in the STG, on which I am focusing in this thesis, is its ability to induce endogenous bursting in the pyloric pacemaker AB neuron, even when isolated from all synaptic inputs (Flamm and Harris-Warrick, 1986a; Harris-Warrick and Flamm, 1987). Dopamine-induced bursting in the AB neuron is critically dependent on external calcium, minimally affected by external sodium concentration and insensitive to tetrodotoxin (TTX) (Harris-Warrick and Flamm, 1987). This calcium-dependence of DA-induced bursting suggests an

involvement of voltage-gated calcium currents (VGCC) and/or the calcium-activated non-selective current (I_{CAN}); both currents have been described as critical players in many rhythmic neurons (Partridge and Swandulla, 1987; Büschges *et al.,* 2000; Perrier *et al.,* 2000; Pace *et al.,* 2007a). However, in the AB neuron, the voltage-gated calcium current is inhibited by up to 75% by DA (Johnson *et al.* 2003), significantly reducing the influx of calcium ions to the cytoplasm. Thus, the calcium current described by Johnson *et al* cannot be the major driving force behind the slow depolarization in AB when DA is added, nor can it be the prime driver for the DA-evoked oscillations. Interestingly, DA still enhances calcium-dependent properties in the AB, such as an increase in its synaptic output (Johnson *et al.,* 1995; Harris-Warrick *et al.,* 1998) and an augmentation of $I_{K(Ca)}$ (Johnson *et al.,* 2003). Therefore, I tested the hypothesis that DA may also enhance the calcium-activated non-specific current, I_{CAN}, in the AB neuron for rhythm generation in the pyloric network.

Properties, function and DA modulation of I_{CAN}

Calcium-activated non-selective (CAN) channels are cationic channels with slow activation kinetics. They permeable to calcium, sodium and potassium ions to various degrees; channel opening creates a net inward current leading to depolarization of the membrane potential. In the literature, different terms have been used to denote this current: it may be called a calcium-activated "nonspecific", "cationic" or "slow inward" current, as well as non-selective cationic (NSC) in different sources. CAN channels were first described (Colquhoun, 1981; Maruyama, 1981) and later extensively studied in non-neuronal cells, where they are involved in diverse processes including, for instance, cytokine production by T lymphocytes (Launay *et al.,* 2004) and arrhythmias in ventricular cardiomyocytes (Guinamard *et al.,* 2002, 2004).

CAN channels are directly activated by accumulation of intracellular calcium ions that bind to a specialized domain on the cytoplasmic side of the channels and increase their open probability. They typically do not show any voltage- or time-dependent inactivation (Partridge *et al.,* 1994, Hille, 2001). Finally, they provide an alternative route for calcium entry into the cell and generate net inward current. These unique properties of the CAN channels put them into an exceptional position to couple intracellular calcium dynamics with many processes in the plasma membrane such as channel gating and synaptic release. First, as a result of their voltage-independent activation, CAN channels may be active at subthreshold voltages and may contribute to the initiation of V_m depolarization, before voltage-gated channels turn on. Second, their lack of voltage- or time-dependent inactivation renders them functionally important in supporting sustained depolarizations such as plateau potentials or bursting. Third, these channels' permeability to calcium contributes to self-activation creating an additional basis for sustained depolarization (Partridge *et al.,* 1994), although some types of CAN channels strongly prefer Na^+ and K^+ over Ca^{2+} and hence may lack this property (Payne *et al.,* 1992; Razani-Boroujerdi *et al.,* 1993; Zucker *et al.,* 1998).

Monoamine modulation of CAN channel gating is most likely mediated by GPCRs and can involve changes in calcium handling (discussed below) or the gating properties of the channel itself. One possible result of modulator-evoked phosphorylation is an increase in the Hill coefficient of the calcium-binding site of the channel, which would lower its dependence on calcium concentration, as has been demonstrated for calcium-activated potassium or chloride channels (Reinhart *et al.,* 1991; Marunaka *et al.,* 1990; Golowasch *et al.,* 1986). It is also

possible that phosphorylation of the channel directly targets the gating particle and alters the activation and inactivation properties of the channel in a manner that is independent of calcium binding (Partridge *et al.,* 1984). CAN channels are thought to be encoded by members of *trp* family of genes in both vertebrates and invertebrates (Montell, 2001; Venkatachalam and Montell, 2007; Matsuura *et al.*, 2009). However genes encoding the arthropod CAN channels are unknown. Known physiological functions of I_{CAN} include modulation of firing properties (bursting and plateau potentials) of central neurons, shaping sensory receptor activity and endocrine/hormone responses, as well as contribution to pathological processes such as excitotoxicity. Here, I focus on the I_{CAN}'s role in the generation of plateau potentials and bursting. Plateau potentials, or the phenomenon of membrane potential bistability, rely at least in part on activation of the CAN current in the dorsal gastric (DG) neuron in the crab STG (Zhang et al., 1995a), mouse brain stem neurons (Rekling and Feldman, 1997), rat deep dorsal horn neurons (Morisset and Nagy 1999), and rat substantia nigra GABAergic neurons (Lee and Tepper, 2007). However, I_{CAN} does not participate in generation of plateau potentials in turtle spinal motoneurons **(**Perrier and Hounsgaard, 1990). The CAN current contributes to bursting in molluscan neurons (Partridge and Swandulla, 1987) and in the mammalian inspiratory CPG, Pre-Bötzinger Complex (PreBC). In the neonate mouse PreBC, the CAN current was proposed to generate bursting in one type of pacemaker neurons, thus contributing to fictive eupneic activity both in vitro and in vivo (Pena et al., 2004; Del Negro et al., 2005; Tryba et al., 2006). However, this view, and the relevance of the CAN current in respiratory rhythm generation, is still highly disputed (St-John, 2008.). In the crustacean stomatogastric ganglion, I_{CAN} has been demonstrated to play a critical role in the generation of plateau potentials in the dorsal gastric (DG)

motor neuron (Zhang *et al.,* 1995b). The current is blocked by blockers of calcium currents and intracellular injection of calcium chelators, and abolished when calcium ions are replaced by barium. However, CAN channels in the DG appear to be predominantly calcium-permeable, as a substitution of sodium ions does not affect the reversal potential of the current (-27 mV). The CAN current is not directly enhanced by 5HT, even though it underlies the 5HT-evoked plateau potentials; instead, 5HT enhances the voltage-gated calcium current which triggers I_{CAN} activation (Zhang et al., 1995a). The properties and physiological functions of the CAN current in the pyloric network is unknown, and it is possible that I_{CAN} is involved in LP's prolonged plateau potentials and AB's bursting in the presence of DA.

Calcium sources for the activation of I_{CAN}

The open probability of CAN channels increases with binding of the calcium ions to a cytoplasmic site on the channels. Overall, calcium dynamics in neurons is determined by membrane flux via ion channels and pumps, as well as by intracellular organelle release and uptake and cytoplasmic buffering. Thus the calcium that activates I_{CAN} can come from the extracellular space via ion channels, and/or from release from intracellular stores. Calcium influx from the extracellular space occurs via voltage-gated or receptor-gated calcium channels (Hall *et al.,* 2002, Mackay *et al.,* 2007; Pace *et al.,* 2007). Calcium from intracellular calcium stores can come from the smooth endoplasmic reticulum (ER) or mitochondria. I_{CAN} can be activated by IP_3-sensitive calcium release from the ER (Partridge and Swandulla, 1987; Sawada *et al.,* 1990; Partridge and Valenzuela 1999; Crowder *et al.,* 2007; Pace *et al.,* 2007a), as a result of Thapsigargin blockade of the sarco-endoplasmic reticular calcium pump

(SERCA) (Knox *et al*. 1996), or by caffeine activation of Ryanodine-sensitive calcium release (Currie & Scott, 1992; Vinogradova *et al.,* 2006).

In Chapter 2, I describe the properties of the CAN current in three classes of pyloric neurons. In Chapter 3, I present the results of electrophysiology experiments combined with two-photon calcium imaging to test the role of DA-induced increase in $[Ca^{2+}]_{in}$ and I_{CAN} in AB neuron bursting.

Mechanisms of 5HT-induced AB bursting

In the lobster *P. interruptus,* serotonin has multiple effects on the intrinsic and synaptic properties in the crustacean STNS. It alters the biophysical properties of ion channels located in different STG neurons (Harris-Warrick et al. 1998; Kiehn and Harris-Warrick 1992; Peck et al. 2001; Zhang and Harris-Warrick 1995). In the lobster pyloric network, serotonin induces sustained bursting in the anterior burster (AB) neuron (Ayali and Harris-Warrick 1999; Harris-Warrick and Flamm 1987), inhibits the lateral pyloric (LP) and ventricular dilator (VD) neurons, excites the inferior cardiac (IC) neuron, and has no effect on the pyloric dilator (PD) or pyloric constrictor (PY) neurons (Ayali and Harris-Warrick 1999; Flamm and Harris-Warrick 1986b). In addition, 5HT modulates the strength of electrotonic coupling and chemical synapses within the pyloric circuit (Johnson and Harris-Warrick 1990; Johnson et al. 1993, 1994, 1995).

There are no serotonergic input fibers to the STG. The STG is located inside a blood vessel, and is thus accessible to hemolymph containing 5HT (Sullivan et al., 1977; Beltz et al., 1984; Beltz, 1999). It is generally agreed that 5HT acts as a neurohormone in the *P. interruptus* stomatogastric nervous system (STNS). Arthropods express multiple 5HT receptor (5HTR) types (Tierney, 2001). Five arthropod 5HTR subtypes have been cloned and characterized to date. In the spiny lobster, two different 5HT receptors subtypes have been cloned to date:

$5HT_{1\alpha Pan}$ and $5HT_{2\beta Pan}$ (Clark et al., 2004; Sosa et al., 2004; Spitzer et al., 2008). Activation of the $5HT_{1\alpha Pan}$ receptor inhibits forskolin-stimulated cAMP accumulation, presumably *via* $G_{i/o}$ inhibition of adenylyl cyclase (Spitzer et al., 2008). The $5HT_{2\beta Pan}$ receptor couples to G_q to activate PLC and the IP_3 and PKC pathways, and is constitutively active when stably expressed in HEK cells; it is expressed in the fine neuropil and the NMJ, mostly presynaptically (Clark et al., 2004). It has been suggested that there are three more putative monoamine receptors in the STG yet to be cloned (Clark and Baro, 2007; Clark et al., 2004). All STG cells express identified types of the 5HT receptors, and, while the cellular distribution of these receptors is currently unknown, it is expected that different cell types will express different receptors or sets of receptors, which then could be correlated with the established electrophysiological actions of 5HT. In the lobster pyloric pacemaker neuron AB, serotonin-induced bursting is critically dependent on the concentration of the external sodium (Harris-Warrick and Flamm, 1987). Low (50%) external sodium prevents bursting; in agreement with this sensitivity to low external sodium, 5HT-induced bursting is blocked by 10^{-7}M TTX, a specific blocker of sodium channels (Harris-Warrick and Flamm, 1987). In contrast to its effects on DA-induced bursting described above, low external calcium only slows down the 5HT bursting without completely blocking it. Based on these results, I hypothesized that a persistent sodium current may underlie 5HT bursting in the AB neuron.

Properties, function and 5HT modulation of $I_{Na(P)}$ and its role in cellular excitability

The molecular mechanisms that cause the persistent opening of sodium channels are still debated. The classical "transient" sodium current, which drives action potentials, activates within a millisecond of depolarization and inactivates within

several milliseconds. It was first described by Hodgkin and Huxley in their seminal paper (1952). Their model of the sodium channel predicted an existence of a "window current", a small amplitude steady-state sodium current at intermediate voltages, where both activation and inactivation are incomplete (Attwell *et al.,* 1979). However, later research suggested that a persistent sodium current outside this window voltage range may arise from a subset of sodium channels with altered gating properties (Alzheimer *et al.,* 1993; Crill, 1996). These channels favor the non-inactivating or "persistent" mode of activity (Raman *et al.,* 1997; Smith *et al.,* 1998), perhaps because of a modulation via G-protein coupled receptors (GPCR) (Numann *et al.,* 1991; Ma *et al.,* 1997) or an association with auxiliary beta subunits modulating their inactivation kinetics (Paton *et al.,* 1994; Morgan *et al.,* 2000). In tuberomammillary neurons of the hypothalamus, Taddese and Bean (2002) proposed an alternative explanation for $I_{Na(P)}$, where it is once again a normal property of the fast sodium channels which do not inactivate completely upon depolarization; a small fraction remains active for much longer than usual. To explain this, they generated an allosteric model where depolarization promotes transitions through successive activation states, each with higher affinity for the inactivation particle.

In invertebrate neurons, $I_{Na(P)}$ is present in cockroach (Christensen *et al.,* 1988; Lapied *et al.,*1989), Drosophila (Saito and Wu, 1991) and honeybee (Schäfer *et al.,* 1994) neurons, in the heart interneurons of the medicinal leech (Opdyke and Calabrese, 1994), in squid giant axons (Rakowski *et al.,* 2002; Clay *et al.,* 2003), and in snail interneurons (Nikitin *et al*., 2006, 2008; Kiss *et al.,* 2009). $I_{Na(P)}$ is implicated in both synaptic and cellular plasticity and learning in molluscan neurons (Nikitin *et al*., 2008; Kiss *et al.,* 2009), while in leech heart interneurons, it underlies prolonged plateau potentials (Opdyke and Calabrese, 1994).

Biophysical properties, pharmacology, gene organization, and intron splice sites of invertebrate sodium channels are largely similar to the mammalian sodium channels (Goldin, 2002; Plummer and Meisler, 1999).

In vertebrate CPGs, the functional role of $I_{Na(P)}$ has been investigated more extensively. It was first suggested and tested in a mathematical model that in the inspiratory neurons of the pre-Bötzinger complex (preBC), $I_{Na(P)}$ can function as a primary voltage-dependent burst-generating mechanism (Butera et al. 1999a,b; Del Negro et al., 2001). Later it was demonstrated experimentally in the in *vitro* brainstem slice preparation, that bursting behavior depends on a balance between the persistent sodium and the leak conductances (Smith et al., 2000; Del Negro, 2001, 2002, 2005; Koizumi and Smith, 2008). In fact, $I_{Na(P)}$ is present in all respiratory neurons, both pacemakers and non-pacemakers; the only difference between the cell types is the ratio of the persistent sodium conductance relative to the leak conductance: the higher the ratio, the more likely a neuron to burst. However, the necessity of this current in network rhythmogenesis *in vivo* is still controversial (DelNegro, 2005; Pena et al., 2007).

In the locomotor CPG, $I_{Na(P)}$ is critical in network function, as application of the $I_{Na(P)}$ blocker Riluzole stops rhythmic firing in neurons of neonatal mouse spinal cord at concentrations that partially block $I_{Na(P)}$ (Zhong *et al.,* 2007; Tazerart *et al*., 2007; Ziskind-Conhaim *et al.*,2008). Furthermore, in rat mesencephalic trigeminal neurons, the mammalian CPG for mastication, $I_{Na(P)}$ along with the resurgent sodium current, is also essential for generation of rhythmic activity (Wu et al., 2005; Enomoto et al., 2006). Serotonin potently facilitates the persistent sodium current in numerous mammalian neurons, generating (Cramer et al., 2005) and modulating (Hsiao et al., 1998; Harvey et al., 2006a,b) rhythmic firing. In pre-BötC neurons of neonatal mice, activation of the 5HT2A receptors, and a

subsequent enhancement of $I_{Na(P)}$, have been proposed to be required for rhythmogenesis (Peña and Ramirez, 2002). However, in rat medullary preparations, Ptak and colleagues (2009) did not find such an enhancing effect on the persistent sodium current, although application of 5HT clearly transformed non-intrinsic bursters into intrinsic bursters, at least in part by affecting the leak conductances in respiratory neurons.

In the lobster pyloric pacemaker AB neuron, the exact conductances mediating 5HT bursting are unknown. Elsen and Selverston previously suggested, based on indirect evidence, that $I_{Na(P)}$ is present and helps drive the gastric mill rhythm in the STNS (Elsen and Selverston, 1997), but to date this current has not been directly measured in any STG neurons. I describe the physiological and pharmacological properties of this current in three classes of pyloric neurons in Chapter 2, and analyze the current's functional role during 5HT-evoked AB bursting in Chapter 4.

Multiple mechanisms of bursting

In this thesis, I describe two inward currents with slow kinetics and look at their functional significance in the pacemaker neuron AB. Both DA and 5HT elicit bursting behavior in the AB neuron, but each monoamine uses a distinct and independent mechanism of action to evoke depolarization. DA triggers the release of calcium ions from intracellular stores, which results in an activation of the calcium-activated non-selective current and rhythmic oscillations. It is particularly interesting that DA evokes AB bursting in part by modulating a conductance that has no intrinsic voltage dependence. Serotonin, on the other hand, inhibits two potassium outward currents, thereby uncovering the depolarizing effect of the persistent sodium current and generating bursting. Most likely, these two mechanisms are complimentary *in vivo* and provide a necessary

redundancy in regulating a vitally important physiological function, which can constitute a common biological design principle. For example, within the respiratory CPG, two different populations of pacemaker neurons with distinct pharmacology and physiological functions employ two different mechanisms of bursting, the cadmium-insensitive (sodium-dependent) and cadmium-sensitive (sodium- and calcium-dependent) (Pena et al., 2004; Viemari JC, Ramirez JM., 2006; Peña and Aguileta, 2007). However, direct evidence for multiple bursting mechanisms employed by a single neuron has not been presented in any system. Here, for the first time I show that two different ionic mechanisms of intrinsic bursting may be employed by a single neuron to generate a rhythmic output.

REFERENCES

Ayali A, Johnson BR, Harris-Warrick RM. (1998) Dopamine modulates graded and spike-evoked synaptic inhibition independently at single synapses in pyloric network of lobster. *J Neurophysiol.* 79(4):2063-9.

Beltz B, Eisen JS, Flamm R, Harris-Warrick RM, Hooper SL, Marder E (1984) Serotonergic innervation and modulation of the stomatogastric ganglion of three decapod crustaceans (Panulirus interruptus, Homarus americanus and Cancer irroratus). *J Exp Biol* 109: 35–54.

Bidaut, M. 1980. Pharmacological dissection of pylo ric network of the lobster stomatogastric ganglion using picrotoxin. *J. Neurophysiol*. 44: 1089–1101.

Clark M.C., T.E. Dever, J.J. Dever, P. Xu, V. Rehder, M.A. Sosa and D.J. Baro, Arthropod 5-HT2 receptors: a neurohormonal receptor in decapod crustaceans that displays agonist independent activity resulting from an evolutionary alteration to the DRY motif, *J. Neurosci.* **24** (2004), pp. 3421–3435.

Clark, M.C. and D.J. Baro, Molecular cloning and characterization of crustacean type-one dopamine receptors: D(1alphaPan) and D(1betaPan), *Comp. Biochem. Physiol. Part B Biochem. Mol. Biol.* **143** (2006), pp. 294–301.

Cleland TA, Selverston AI. (1997) Dopaminergic modulation of inhibitory glutamate receptors in the lobster stomatogastric ganglion. *J Neurophysiol*. 78(6):3450-2.

Colquhoun, D., Neher, E., Reuter, H., Stevens, CF., (1981) Inward current channels activated by intracellular Ca in cultured cardiac cells, *Nature*, 294 752-754.

Cournil, I. (1994) Dopamine in the lobster Homarus gammarus. I. Comparative analysis of dopamine and tyrosine hydroxylase immunoreactivities in the nervous system of the juvenile. *J. Comp. Neurol*. 344: 455–469.

Del Negro, C.A. ,C. Morgado-Valle, J.A. Hayes, D.D. Mackay, R.W. Pace, E.A. Crowder and J.L. Feldman, Sodium and calcium current-mediated pacemaker neurons and respiratory rhythm generation, *J. Neurosci.* **25** (2005), pp. 446–453.

Elson RC, Selverston AI. (1997) Evidence for a persistent Na+ conductance in neurons of the gastric mill rhythm generator of spiny lobsters. *J Exp Biol*. 200(Pt 12):1795-807.

Flamm RE, Fickbohm D, Harris-Warrick RM (1987) cAMP elevation modulates physiological activity of pyloric neurons in the lobster stomatogastric ganglion. *J Neurophysiol* 58: 1370–1386.

Flamm RE, Harris-Warrick RM (1986a) Aminergic modulation in lobster stomatogastric ganglion. I. Effects on motor pattern and activity of neurons within the pyloric circuit. *J Neurophysiol* 55: 847–865.

Flamm RE, Harris-Warrick RM (1986b) Aminergic modulation in lobster stomatogastric ganglion. II. Target neurons of dopamine, octopamine, and serotonin within the pyloric circuit. *J Neurophysiol* 55: 866–881.

Golowasch, J., Kirkwood, A. and Miller, C. (1986) Allosteric effects of Mg2+ on the gating of Ca2+ -activated K channels from mammalian skeletal muscle, *J. Exp. Biol.* 124: 5-13.

Gruhn, M., J. Guckenheimer, B. Land and R.M. Harris-Warrick, Dopamine modulation of two delayed rectifier potassium currents in a small neural network, *J Neurophysiol.* **94** (2005), pp. 2888–2900

Guinamard R, Chatelier A, Lenfant J, Bois P. (2004) Activation of the Ca(2+)-activated nonselective cation channel by diacylglycerol analogues in rat cardiomyocytes. *J. Cardiovasc Electrophysiol.* 2004 Mar;15(3):342-8.

Guinamard R, Rahmati M, Lenfant J, Bois P. (2002) Characterization of a Ca2+-activated nonselective cation channel during dedifferentiation of cultured rat ventricular cardiomyocytes. *J Membr Biol*. 188(2):127-35.

Harris-Warrick RM, Coniglio LM, Barazangi N, Guckenheimer J, Gueron S (1995b) Dopamine modulation of transient potassium current evokes phase shifts in a central pattern generator network. *J Neurosci* 15: 342–358.

Harris-Warrick RM, Coniglio LM, Levini RM, Gueron S, Guckenheimer J (1995a) Dopamine modulation of two subthreshold currents produces phase shifts in activity of anidentified motoneuron. *J Neurophysiol* 74: 1404–1420.

Harris-Warrick RM, Flamm RE (1987) Multiple mechanisms of bursting in a conditional bursting neuron. *J Neurosci* 7: 2113–2128.

Harris-Warrick RM, Johnson BR, Peck JH, Kloppenburg P, Ayali A, Skarbinski J (1998) Distributed effects of dopamine modulation in the crustacean pyloric network. *Ann NY Acad Sci* 860: 155–167.

Harris-Warrick RM, Marder E, Selverston AI, Moulins M. Editors. (1992) *Dynamic biological networks: the stomatogastric nervous system.* Cambridge, MA: MIT.

Johnson B.R., P. Kloppenburg and R.M. Harris-Warrick. (2003) Dopamine modulation of calcium currents in pyloric neurons of the lobster stomatogastric ganglion, *J. Neurophysiol.* 90 pp. 631–643.

Johnson BR, Harris-Warrick RM (1990) Aminergic modulation of graded synaptic transmission in the lobster stomatogastric ganglion. J Neurosci 10: 2066–2076.

Johnson BR, Harris-Warrick RM. (1997) Amine modulation of glutamate responses from pyloric motor neurons in lobster stomatogastric ganglion. *J Neurophysiol.* 78(6):3210-21.

Johnson BR, Peck JH, Harris-Warrick RM (1993) Amine modulation of electrical coupling in the pyloric network of the lobster stomatogastric ganglion. *J Comp Physiol [A]* 172: 715–732.

Johnson BR, Peck JH, Harris-Warrick RM (1995) Distributed amine modulation of graded chemical transmission in the pyloric network of the lobster stomatogastric ganglion. *J Neurophysiol* 74: 437–452.

Katz PS, Eigg MH, Harris-Warrick RM (1989) Serotonergic/cholinergic muscle receptor cells in the crab stomatogastric nervous system. I. Identification and characterization of the gastropyloric receptor cells. *J Neurophysiol* 62: 558–570.

Katz PS, Harris-Warrick RM (1990) Neuromodulation of the crab pyloric central pattern generator by serotonergic/cholinergic proprioceptive afferents. *J Neurosci* 10: 1495–1512.

Kiehn O, Harris-Warrick RM (1992a) Serotonergic stretch receptors induce plateau properties in a crustacean motor neuron by a dual-conductance mechanism. *J Neurophysiol* 68: 485–495.

Kiehn O, Harris-Warrick RM (1992b) 5-HT modulation of hyperpolarization-activated inward current and calcium-dependent outward current in a crustacean motor neuron. *J Neurophysiol* 68: 496–508.

Kloppenburg, P., R.M. Levini and R.M. Harris-Warrick.(1999) Dopamine modulates two potassium currents and inhibits the intrinsic firing properties of an identified motor neuron in a central pattern generator network, *J. Neurophysiol.* 81, pp. 29–38.

Kloppenburg. P,W.R. Zipfel, W.W. Webb and R.M. Harris-Warrick (2000) Highly localized Ca(2+) accumulation revealed by multiphoton microscopy in an identified motoneuron and its modulation by dopamine, *J. Neurosci.* 20, pp. 2523–2533.

Kushner, P. D. (1977). Localization of monoamine fluorescence in the stomatogastric nervous system of lobsters. *Brain Res*. 129: 13–28.

Launay P, Cheng H, Srivatsan S, Penner R, Fleig A, Kinet JP. (2004) TRPM4 regulates calcium oscillations after T cell activation. *Science*. 306(5700):1374-7.

M.P. Nusbaum and M.P. Beenhakker, (2002), A small-systems approach to motor pattern generation, *Nature* 417 pp. 343–350.

Marder E, Bucher D, Schulz DJ, Taylor AL. (2005) Invertebrate central pattern moves along.

Marder E, Bucher D. (2001) Central pattern generators and the control of rhythmic movements. *Curr Biol*. 11(23):R986-96.

Marder E, Bucher D. (2007) Understanding circuit dynamics using the stomatogastric nervous system of lobsters and crabs. *Annu Rev Physiol*. 69:291-316.

Marder E, Eisen JS (1984) Electrically coupled pacemaker neurons respond differently to same physiological inputs and neurotransmitters. *J Neurophysiol* 51: 1362–1374.

Marder, E. and D. Bucher, (2001) Central pattern generators and the control of rhythmic movements, *Curr. Biol.* 11: 986–R996.

Marunaka, Y. and Eaton, D.C., (1990) Effects of insulin and phosphatase on a Ca2+-dependent Cl channel in a distal nephron cell line, J. *Gen. Physiol*., 95: 773-789.

Maruyama, Y. and Petersen, O.H., (1981) Single-channel currents in isolated patches of plasma membrane from basal surface of pancreatic acini, *Nature, 299 159-161*.

Miller, J. P. (1979). Rapid killing of single neurons by irradiation of intracellularly injected dye. *Science* 206: 702–704.

Oginsky MF, Rodgers EW, Clark MC, Simmons R, Krenz WD, Baro DJ. (2010) D(2) receptors receive paracrine neurotransmission and are consistently targeted to a subset of synaptic structures in an identified neuron of the crustacean stomatogastric nervous system. *J Comp Neurol*. 518(3):255-76.

Payne, R., Corson, D.W. and Fein, A., (1992) Pressure injection of Ca2+ both excites and adapts *Limulus,* ventral photoreceptors, J. Gen. *Physiol.,* 88 107-126.

Peck, J.H., S.T. Nakanishi, R. Yaple and R.M. Harris-Warrick, (2001) Amine modulation of the transient potassium current in identified cells of the lobster stomatogastric ganglion, *J. Neurophysiol.* 86, pp. 2957–2965.

Peña, F. M.A. Parkis, A.K. Tryba and J.M. Ramirez, (2004) Differential contribution of pacemaker properties to the generation of respiratory rhythms during normoxia and hypoxia, *Neuron.* 43: 105–117

Ramirez, J.M., A.K. Tryba and F. Pena, (2004) Pacemaker neurons and neuronal networks: an integrative view, *Curr. Opin. Neurobiol.* 14**:** 665–674

Razani-Boroujerdi, S. and Partridge, L.D., (1993) Activation and modulation of calcium-activated non-selective cation channels from embryonic chick sensory neurons*, Brain Res***,** 623 195-200

Reinhart, P.H., Chung, S., Martin, B.L., Brautigan, D.L. and Levitan, I.B., (1991) Modulation of calcium-activated potassium channels from rat brain by protein kinase and phosphatase 2A, J. *Neurosci.***,** 11 1627-1635.

Sosa MA, Spitzer N, Edwards DH, Baro DJ. (2004) A crustacean serotonin receptor: cloning and distribution in the thoracic ganglia of crayfish and freshwater prawn. *J Comp Neurol*. 473(4):526-37.

Spitzer N, Cymbalyuk G, Zhang H, Edwards DH, Baro DJ. (2008) Serotonin transduction cascades mediate variable changes in pyloric network cycle

frequency in response to the same modulatory challenge. *J Neurophysiol*. 99(6):2844-63.

Spitzer N, Edwards DH, Baro DJ. (2008) Conservation of structure, signaling and pharmacology between two serotonin receptor subtypes from decapod crustaceans, Panulirus interruptus and Procambarus clarkii. *J Exp Biol* 211: 92–105.

St-John WM. (2008) Eupnea of in situ rats persists following blockers of in vitro pacemaker burster activities. *Respir Physiol Neurobiol*. 160(3):353-6.

Tierney AJ (2001) Structure and function of invertebrate 5-HT receptors: a review. *Comp Biochem Physiol A Mol Integr Physiol* 128: 791–804.

Tierney AJ, Godleski MS, Rattananont P (1999) Serotonin-like immunoreactivity in the stomatogastric nervous systems of crayfishes from four genera. *Cell Tissue Res* 295: 537–51.

Tryba, A.K. F. Peña and J.M. Ramirez, (2006)Gasping activity in vitro: a rhythmic behavior dependent on 5HT2A receptors, *J. Neurosci.* 26, pp. 2623–2634.

Turrigiano GG, Marder E (1993) Modulation of identified stomatogastric ganglion neurons in primary cell culture. *J Neurophysiol* 69: 1993–2002.

Zhang B, Harris-Warrick RM (1994) Multiple receptors mediate the modulatory effects of serotonergic neurons in a small neural network. *J Exp Biol* 190: 55–77.

Zhang B, Harris-Warrick RM (1995a) Calcium-dependent plateau potentials in a crab stomatogastric ganglion motor neuron. I. Calcium current and its modulation by serotonin. *J Neurophysiol* 74: 1929–1937.

Zhang B, Wootton JF, Harris-Warrick RM (1995b) Calcium-dependent plateau potentials in a crab stomatogastric ganglion motor neuron. II. Calcium-activated slow inward current. *J Neurophysiol* 74: 1938–1946.

CHAPTER 2

CHARACTERIZATION OF TWO INWARD CURRENTS WITH SLOW INACTIVATION KINETICS IN PYLORIC NEURONS

INTRODUCTION

Slowly inactivating or non-inactivating inward currents are thought to be critical in rhythmogenesis (Harris-Warrick, 2002; Ramirez et al., 2004; Tazerart et al., 2008; Rubin et al., 2009). In particular, the calcium-activated non-selective current (I_{CAN}) and the persistent sodium current ($I_{Na(P)}$) play important roles in shaping the firing properties of motoneurons (Cramer et el, 2006; Wu et al., 2005) and interneurons (Kramer and Zucker, 1985; Swandulla and Lux, 1985; DelNegro 2002, 2005; Pace et al., 2007a and b; Zhong et al., 2007; Tazerart et al., 2007). In this Chapter I describe biophysical and pharmacological properties of these two persistent inward currents in lobster pyloric neurons. In the following two chapters, I address their modulation by monoamines and their functional importance in the physiology of the pyloric pacemaker neuron.

The calcium-activated non-specific current, I_{CAN}, is carried through ionic channels thought to be encoded by members of *trp* superfamily of genes in both vertebrates and invertebrates (Montell, 2001; Venkatachalam and Montell, 2007; Matsuura *et al.*, 2009); however, their exact structure in lobster STNS is unknown. The total number of insect TRP family members is 13 or 14, approximately half that of mammalian TRP family members (Matsuura *et al.,* 2009). Although the majority of *trp*-related channels are expressed in sensory neurons and function to shape sensory physiology (Montell, 2001), here I am focusing on the role of these channels in regulating neuronal excitability.

CAN channels were first described in non-neuronal cells, including cardiomyocytes (Colquhoun et al., 1981) and pancreatic acinar cells (Maruyama

et al., 1981). In sensory systems, calcium-activated inward currents shape receptor and central neuron physiology (Cho *et al.,* 2003; Van den Abbeele *et al.,* 1994; Zufall *et at.,* 1991). In motor systems they have been shown to be critical in such neuronal properties as calcium-dependent prolonged plateau potentials (Zhang *et al.,* 1995; Lee and Tepper, 2007), afterdepolarizations (Haj-Dahmane *et al.,* 1997) and pacemaker bursting (Swandulla and Lux, 1987; Sawada et al., 1990; Pace *et al.,* 2007a). Indeed, CAN channels possess certain properties that allow them to generate neuronal bistability: they pass depolarizing current; they are voltage-independent and activated by accumulation of intracellular calcium; they do not show any voltage or calcium-dependent inactivation; and the kinetics of activation and deactivation of the current are very slow (Partridge *et al.,* 1994). Additionally, CAN channels can be calcium-permeable themselves and hence are capable of self-activation and amplification of depolarizing mechanism. The permeability of these channels to different cations, however, varies between different types: in cardiomyocytes (Guinamard *et al.,* 2006), photoreceptors, rat dorsal root ganglion cells and an *Aplysia* pacemaker neuron (Kramer and Zucker, 1985) they are virtually impermeable to calcium, while in a *Helix* bursting neuron (Swandulla and Lux, 1985), a crab stomatogastric neuron (Zhang *et al.,* 1995), a *Lymnaea* pacemaker neuron (Yazenian and Byerly, 1989), the respiratory pacemaker neurons (Pace *et al.,* 2007) and rat Substantia Nigra neurons (Lee and Tepper, 2007) they are permeable to both sodium and calcium.

I_{CAN} does not have any intrinsic voltage dependence; instead it is activated by calcium ions binding to the cytoplasmic side of the channels which increases the probability of the opening of the channel. I_{CAN}-activating calcium ions can come from the extracellular space via voltage-gated or receptor-gated calcium channels (Hall *et al.,* 2002, Mackay *et al.,* 2007; Pace *et al.,* 2007a) or can be released from

intracellular calcium stores such as smooth endoplasmic reticulum (ER) or mitochondria. Specifically, in rhythmic cells, I_{CAN} can be activated by IP_3 sensitive calcium release from the ER (Partridge and Swandulla, 1987; Sawada *et al.,* 1990; Partridge and Valenzuela 1999; Crowder *et al.,* 2007; Pace *et al.,* 2007a); or by caffeine activation of Ryanodine-sensitive calcium release (Currie & Scott, 1992; Vinogradova *et al.,* 2006).

In the lobster STG, Zhang and colleagues previously described I_{CAN} in the dorsal gastric neuron and showed that it can be evoked by a depolarizing pre-step or by caffeine puff, but the presence and properties of this current in pyloric neurons were still unknown. I have characterized the biophysical and pharmacological properties of this current in three pyloric cell types, the pacemaker interneuron (Anterior Burster, AB) and two motoneurons (Lateral Pyloric, LP and Pyloric Dilator, PD)..

The persistent sodium current is exclusively carried by sodium ions and is thought to represent the small fraction of sodium channels that fail to inactivate rapidly during a voltage step, thus appearing to be persistent during the step (Crill 1996; Magistretti et al. 1999, Alzheimer et al. 1993, Brown et al. 1994, Taddese and Bean 2002). The exact mechanism of this current is not known, although some contribution of a window current (Attwell et al., 1979), as well as regulation by sodium channel auxiliary beta subunits have been suggested (Aman et a al., 2009). $I_{Na(P)}$ is widely expressed in neurons and regulates cellular excitability and synaptic transmission. In peripheral and central sensory neurons, it is involved in mediating neuropathic pain sensation (Lampert et al., 2006)

Because of its biophysical properties, $I_{Na(P)}$ was shown to be important in regulating neuronal excitability and contribute to bursting in several motor systems (Bevan and Wilson, 1999; Thoby-Brisson and Ramirez, 2001; Taddese

and Bean, 2002; Darbon *et al.,* 2004; Del Negro *et al.,* 2005; Wu *et al.,* 2005; Enomoto *et al.,* 2006; Paton *et al.,* 2006; Van Drongelen *et al.,* 2006; Cramer et al, 2007; Zhong *et al.,* 2007; Tazerart, *et al.,* 2008). $I_{Na(P)}$ in these neurons activates around -60 mV and peaks at -40mV in most neurons, although some neurons can have an unusually hyperpolarized activation voltage (Huang and Trussell, 2009). In the STG, based on the current clamp experiments and a mathematical model, $I_{Na(P)}$ was suggested to play a putative role in the STG (Elson and Selverston, 1997), but it was never systematically studied in voltage clamp. Here I have characterized this current in three pyloric neuronal types, the AB, PD and LP neurons.

MATERIALS AND METHODS

Animals and preparation. Adult California spiny lobsters (*Panulirus interruptus*) were supplied by Don Tomlinson Commercial Fishing (San Diego, CA) and kept in tanks with artificial sea water. Lobsters were anesthetized in ice; the STNS was dissected out and pinned on a Sylgard-coated Petri dish and superfused with oxygenated lobster physiological saline. The temperature of the bath saline was kept at 16-17°C unless specified otherwise. The STG was desheathed and cells were identified as previously described (Selverston *et al*. 1976). The experiments in this chapter were done on the anterior burster (AB), pyloric dilator (PD) and lateral pyloric (LP) neurons.

Electrophysiology. Two-electrode voltage clamp (TEVC) was performed using Axoclamp-2B amplifier, Digidata 1440 board and pCLAMP10 software (all from Molecular Devices, Sunnyvale, CA).

I_{CAN} measurements. Lack of inherent voltage-dependence presents a challenge to measuring I_{CAN} in voltage clamp. Generally, there are two ways to measure this current: by using a depolarizing pre-step to 0 mV to activate voltage-gated

calcium influx or by application of caffeine or IP_3 to trigger a release from ER calcium-release channels. To measure I_{CAN} activated by influx of external calcium in voltage clamp, I used depolarizing pre-steps to 0 mV from V_h=-50mV to activate the voltage-dependent calcium currents. For the determination of the I_{CAN} reversal potential, an activating pre-step was followed by series of hyperpolarizing steps from -80 mV to -30 mV in increments of 5 mV to evoke a tail current (Fig 2.1). The peak tail current amplitude was measured and plotted against the value of the voltage step. The deactivating portion of the current trace was fitted with an exponential function using Clampex; the time constants were then plotted against voltage steps. All measured currents were leak subtracted before data analysis.

$I_{Na(P)}$ measurements. $I_{Na(P)}$ was measured in voltage clamp by either driving the neuron with a slow depolarizing ramp (with the rate of 25-100 mV/s) or by long depolarizing steps. Both methods measure the slowly inactivating or non-inactivating (persistent) portion of the current without contribution from the fast, rapidly inactivating sodium current. The peak current was measured, and $I_{Na(P)}$ was calculated as a difference between the currents measured in the absence and the presence of one of the sodium blockers (0.1 μM TTX for the AB neuron and 5-10 μM Riluzole for the LP neuron).

For all VC experiments, leak subtraction was done either on-line (P/N=6 protocol) or off-line (direct measure of the leak current and post-hoc digital leak subtraction); both methods gave similar results.

Solutions. *Panulirus* physiological saline had the following composition (in mM): 479 NaCl, 12.8 KCl, 13.7 $CaCl_2$, 3.9 Na2SO4, 10.0 MgSO4, 2 Glucose, and 11.1 Tris base, pH 7.4 (Mulloney and Selverston 1974). To pharmacologically isolate the currents of interest, I used the following blockers:

50 mM tetraethyl-ammonium chloride (TEA) and 4 mM 4-aminopyridine (4-AP) to block potassium currents, 5 mM CsCl to block the hyperpolarization-activated current, 0.1 μM TTX to block the sodium currents (excluded when measuring $I_{Na(P)}$), 0.6 mM $CdCl_2$ to block calcium currents (excluded when measuring I_{CAN}), and $5 \cdot 10^{-6}$ M picrotoxin (PTX) to block glutamatergic synapses within the STG; the amount of NaCl was adjusted to compensate for high TEA. In addition to the bath-applied blockers, I loaded the cell body with internal K^+ channel blockers by iontophoresis, injecting small negative current steps through electrodes loaded with 2M TEA and 2M CsCl for 1-1.5 hours; the cell was allowed to recover for 1-1.5 hours before starting the experiment. I used Nifedipine (Nif, 200 μM) to block the $I_{Ca(V)}$, Flufenamic acid (FFA 0.1-30 μM) to block I_{CAN}, Riluzole (Ril,10 μM) to block $I_{Na(P)}$. To determine the effective concentrations of blockers, serial dilution experiments were performed. The chemicals were purchased from Sigma, Tocris, or Cayman Chemical.

Data analysis. Current measurements and current fits were performed using Clampex. The statistical analysis was performed using JMP7 (SAS). The figures were prepared using Excell, Origin and Adobe Illustrator. All values are presented as mean+/-SE, the effect was considered statistically significant at $p<0.05$.

RESULTS

CHARACTERIZATION OF THE CALCIUM-ACTIVATED NON-SELECTIVE CURRENT

I have measured the following physiological and pharmacological properties of I_{CAN}: its reversal potential (E_{rev}), deactivation time constant, and sensitivity to a specific blocker of this current, flufenamic acid (FFA). Because this current lacks intrinsic voltage-sensitivity, and due to problems of space clamp in these highly

Figure 2.1. Properties of I_{CAN} in the AB neuron

A. The I_{CAN} is measured as a slowly deactivating tail current evoked by an activating pre-step to 0 mV and a series of hyperpolarizing steps (top, voltage protocol; bottom, current traces from an AB neuron; an arrowhead marks peak $I_{Ca(V)}$ activated by the depolarizing pre-step, an arrow marks the peak I_{CAN}, tail currents).
B. Current-voltage relationship of the tail current measured at the peak (the arrow in A). To find the reversal potential of the current, the data points were fitted with a linear function and the E_{rev} was extrapolated (-29 mV, n=8).
C. For each current trace the decay of the tail current was fitted with an exponential function and the mean time constants from all neurons were plotted against voltage steps. There was no voltage dependence of the time constant of I_{CAN} deactivation; the mean τ was 74±14 ms (n=6).
D. The current traces in control (black), in 100 µM FFA (red) and in 0.6mM $CdCl_2$ (gray). The FFA blocked I_{CAN} (arrow), but not $I_{Ca(V)}$ (arrowhead).
E. The dose response curve for FFA block of I_{CAN} at 21℃ (black, IC_{50}=13±7 µM, n=3) and 16℃ (red, IC_{50}=247±5 µM, n=4). The amplitude of the blocked current is expressed as the % of the control amplitude.
F. DA more than doubled the CAN conductance at -65 mV (n=5, $p<0.05$, student's t-test)

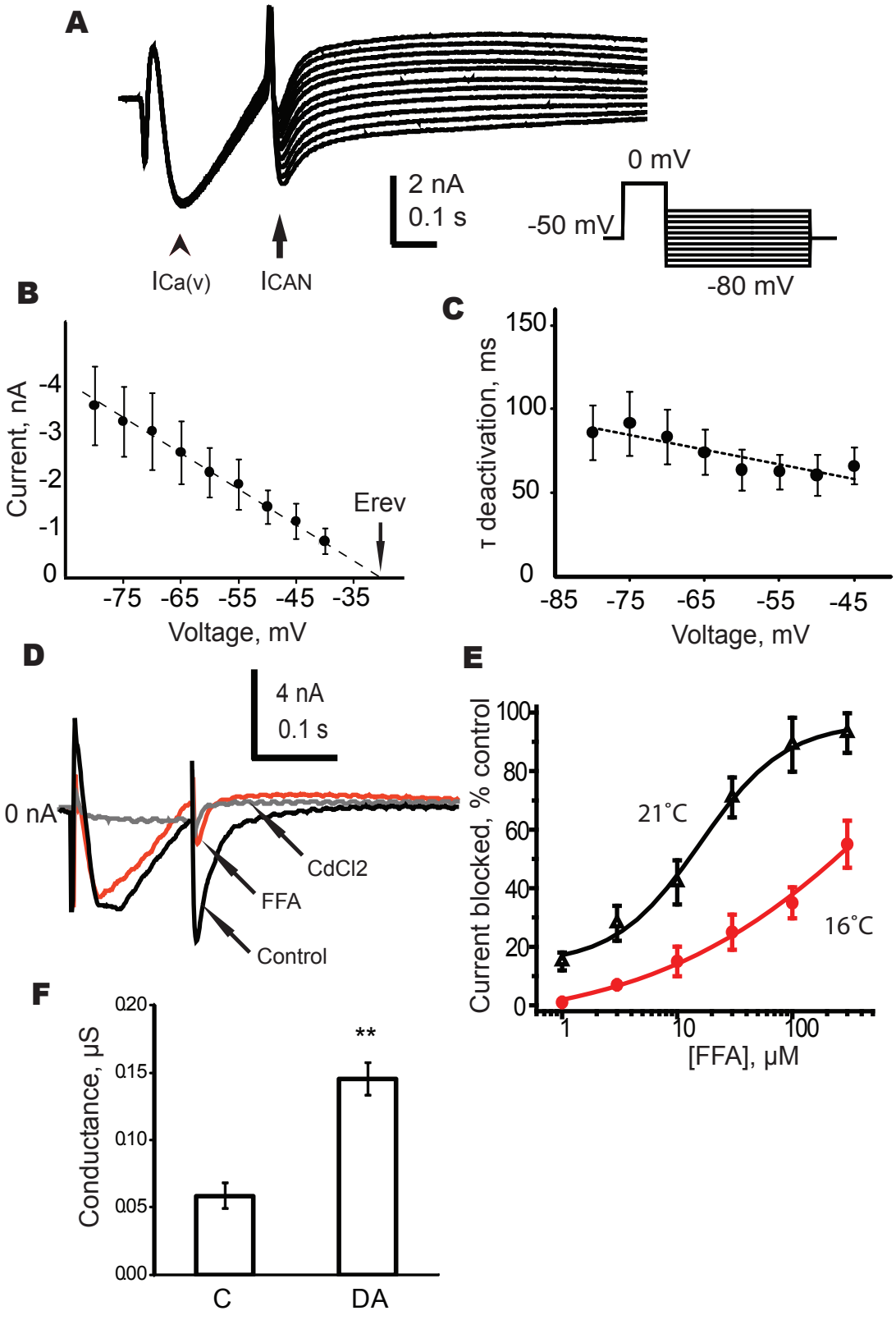
A
2 nA
0.1 s
0 mV
-50 mV
-80 mV
ICa(v)
ICAN
B
Current, nA
-4
-3
-2
-1
0
Erev
-75 -65 -55 -45 -35
Voltage, mV
C
τ deactivation, ms
150
100
50
0
-85 -75 -65 -55 -45
Voltage, mV
D
4 nA
0.1 s
0 nA
CdCl2
FFA
Control
E
Current blocked, % control
100
80
60
40
20
0
21˚C
16˚C
1
10
100
[FFA], μM
F
Conductance, μS
020
015
010
005
000
**
C
DA

branched neurons (Kloppenburg et al. 2000), I was unable to carry out a full biophysical analysis.

To measure I_{CAN}, all voltage-dependent ionic currents other than calcium currents were blocked by bath application of the following blockers: TTX to block the sodium currents, PTX to block glutamatergic transmission in the STG, 4-AP to block the transient potassium current (I_A), CsCl to block the hyperpolarization-activated current I_h, and TEA to block the calcium-activated and delayed rectifier potassium currents. To ensure that the potassium currents, which are quite large in these neurons, were blocked as completely as possible, TEA and CsCl were iontophoretically loaded into a cell 1 hour before VC measurements. I_{CAN} was measured as a slow tail current activated by the voltage-gated calcium current evoked by a depolarizing pre-step to 0 mV. The tail current was recorded at the range of voltages from -80mV to -30 mV in 5mV increments (Fig. 2.1). The peak amplitude of this tail current was measured at the beginning of the hyperpolarizing step, taking advantage of the difference in deactivation kinetics of the calcium current and that of I_{CAN}. The tail current was leak-subtracted and plotted for each voltage step. As expected for a voltage-independent current, the I-V plot had a linear shape (Figure 2.1B). The data points were fit with a linear function, and E_{rev} was extrapolated for each cell type. The decay of the I_{CAN} tail current was fitted with an exponential function, and resulting *time constant*s τ were plotted against tail current voltage. The current properties were analyzed for each cell type separately, and the results were compared between cell types.

Properties of I_{CAN} in the Anterior Burster Neuron

Figure 2.1 shows the voltage clamp protocol, sample current traces and the I-V plot showing averaged data from 8 AB neurons (Figure 2.1A). At -65 mV, the mean amplitude of the peak I_{CAN} in the AB was -2.7± 0.7 nA (n=8). The average

reversal potential was -29 mV (extrapolated from all inward currents in Fig. 2.1B). The current decayed during the hyperpolarizing step, reflecting the time constant of channel deactivation. I fitted the current traces from their peaks to the end of the hyperpolarizing steps with an exponential function to measure the time constant of deactivation (τ deactivation). I tested whether there was any voltage dependence of the deactivation rate. The current tended to decay somewhat more rapidly at the voltages more depolarized than -60 mV, but there was no statistically significant difference between τ values at different voltages (Figure 2.1C). The average τ was 74±14 ms (n=8).

I measured the pharmacological properties of the tail current by blocking it with FFA (an I_{CAN} blocker), BAPTA-AM (a membrane-permeable form of intracellular calcium chelator) and $CdCl_2$ (wide-spectrum calcium current blocker).

FFA is a fairly specific blocker of the I_{CAN} at concentrations 100-300 μM (Korbmacher et al., 1995; Lee and Tepper, 2007; Pace et al, 2007), but it blocked only 37 % of the tail current at 100 μM in my preliminary experiments, which were performed at 16℃. However, FFA visibly precipitated out of solution at 16℃, and I had to raise the temperature to 21℃ to maintain the drug in solution in the lobster saline (which has higher osmolarity than vertebrate solutions). The average amplitude of the I_{CAN} was higher at 21℃ compared to 16℃ (at -65mV -5.9±0.7 and -2.7±0.7 nA respectively), making it easier to measure. When I compared the FFA dose response experiments at 16℃ and 21℃, FFA had a significantly lower IC_{50} (15.9±6.8 μM, n=3, Figure 2.1E) and more complete block at 21℃ than at 16℃ (247.4 μM, n=4). Figure 2.1D shows sample traces of the currents measured in control (black), after block by 100 μM FFA (red) and 0.6mM $CdCl_2$ (gray); the baselines were aligned. Note that 100μM FFA blocked

the tail current (arrowheads) with little effect on the voltage-dependent calcium current (arrows); $CdCl_2$ eliminated $I_{Ca(V)}$ and thus also I_{CAN}.

Properties of I_{CAN} in the Pyloric Dilator Neuron

The mean amplitude of the leak-subtracted peak current in the PD was -2.6±0.8 nA at the -65mV step (n=5, Figure 2.2A). As was seen with the AB neuron, the current showed a linear relation to the hyperpolarizing step voltage, with an average reversal potential of -31.8±0.3 mV (n=5, Figure 2.2B). I measured the deactivation of I_{CAN} during the maintained hyperpolarizing voltage steps and fit it to an exponential function to determine the time constant (τ) of deactivation. This time constant was considerably slower than the deactivation time constant in the AB neuron; for instance at -65 mV I_{CAN} deactivated with mean τ of 66±14 ms in the AB and 226±32 ms in the PD. Additionally, in the PD there was an inverse linear dependence of the deactivation time constant on voltage step (Figure 2.2C, R^2=0.78, n=3), so the current decayed more slowly at hyperpolarized than at depolarized voltages (Figure 2.2C).

Next, I measured the pharmacological properties of the tail current in the PD neuron, using the same methods as for the AB neuron. I measured the FFA effect at 21℃ because FFA visibly precipitated out of saline at 16℃ (see above). Figure 2.3D shows sample traces of the currents measured under control conditions (black), in the presence of 30μM FFA (red), and 0.6mM $CdCl_2$ (gray). Note that 30μM FFA blocked much of the tail current but had minimal effect on the voltage-dependent calcium current; $CdCl_2$ blocked both currents; there was a small inward tail current in the presence of 0.6mM $CdCl_2$ equal to 10% of the control I_{CAN}. FFA blocked I_{CAN} with a mean IC_{50}=37±16 μM (Figure 2.3E, n=4). The effects of other blockers on the I_{CAN} amplitude were: 63±10% in 30μM

Figure 2.2. Properties of I_{CAN} in the PD neuron

A. Current traces showing activation of I_{CAN} in a PD neuron; an arrowhead marks $I_{Ca(V)}$ activated by the depolarizing pre-step, while an arrow marks the peak I_{CAN}, tail currents activated at the beginning of the hyperpolarizing steps. The voltage clamp protocol is shown on the right.
B. I-V relationship of the tail current measured at the peak (the arrow in A). To find the reversal potential of the current, the data points were fitted with a linear function. The E_{rev} was extrapolated to -32 mV (n=5).
C. Measurements of the time constant for deactivation of I_{CAN} in the PD neuron, measured as in Fig. 1.The time constant of deactivation linearly decreased at more depolarized voltages (R^2=0.78, n=3), ranging from 272±34 ms to 163±44 ms.
D. I_{CAN} current traces under control conditions (black), in 30 μM FFA (red) and in 0.6 mM $CdCl_2$ (gray). The FFA blocked I_{CAN}, but not $I_{Ca(V)}$, although it changed the activation kinetics of $I_{Ca(V)}$.
E. The dose response curve for FFA block of I_{CAN} at 21℃, IC_{50}=37±16 μM (n=4).
F. CAN conductance at -65 mV under control conditions and in DA was not different (n=5).

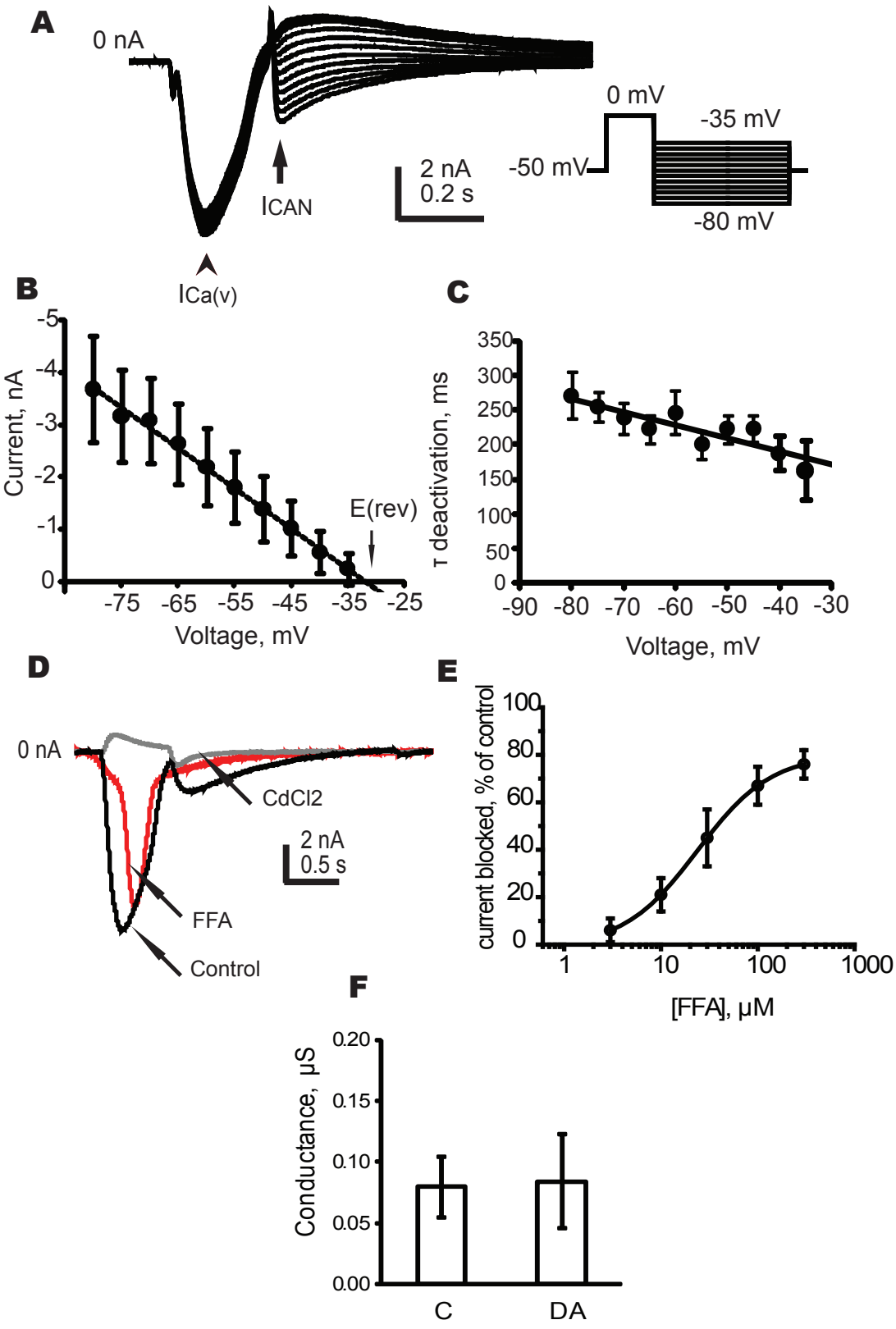
A
0 nA
ICAN
ICa(v)
2 nA
0.2 s
0 mV
-35 mV
-50 mV
-80 mV
B
Current, nA
-5
-4
-3
-2
-1
0
E(rev)
-75
-65
-55
-45
-35
-25
Voltage, mV
C
τ deactivation, ms
350
300
250
200
150
100
50
0
-90
-80
-70
-60
-50
-40
-30
Voltage, mV
D
0 nA
CdCl2
2 nA
0.5 s
FFA
Control
E
current blocked, % of control
100
80
60
40
20
0
1
10
100
1000
[FFA], μM
F
Conductance, μS
0.20
0.15
0.10
0.05
0.00
C
DA

BAPTA-AM (n=3), 11 ±2% in 0.6mM $CdCl_2$ (amplitude of the remaining current, expressed as a percentage of the control current, n=5).

Properties of I_{CAN} in the Lateral Pyloric Neuron

The mean amplitude of the peak current in the LP was -6.7±1.2 nA at -65 mV (n=4, Figure 2.3A, two LP cells), which is significantly larger than in the PD or AB neurons (n=4, $p<0.05$). The average reversal potential of I_{CAN} in the LP neuron was -31.8±0.4 mV (n=4) (Figure 2.4B). When held at the hyperpolarizing voltages, the current decayed with extremely variable rates for different LP neurons (the range of τ deactivation for different cells was over two orders of magnitude (Fig. 2.3A), which in part may reflect a large unclamped $I_{Ca(V)}$ in the neuropil, typical for LP neurons (Johnson *et al*, 2003). Hence I excluded from analysis the LP cells with τ values more than 3 SD above or below the mean. As with the PD, the LP deactivation time constants were voltage-dependent ($R^2=0.9$, n=5) and significantly slower than in the AB (n=5, $p<0.05$).

Finally, I tested the pharmacological properties of the tail current in the LP neuron. Figure 2.3D shows the does-response curve for FFA; the peak current decreased with an IC_{50}=32±0.7 μM (n=3, Figure 2.3D). FFA did not affect $I_{Ca(V)}$ at concentrations below 300 μM. The intracellular calcium chelator BAPTA-AM also blocked half of the tail current amplitude at 30μM, while 0.6mM $CdCl_2$ completely blocked both $I_{Ca(V)}$ and I_{CAN}.

Dopamine Modulation of I_{CAN} in the Pyloric Neurons

Dopamine is endogenous to the STNS and has multiple effects on both synaptic and intrinsic properties of the pyloric cells. I measured its effect on CAN currents in AB, PD and LP. To compare between different cells, I calculated the mean conductance at -65 mV for all cells tested. Dopamine had a statistically significant effect on this conductance only in the AB neuron (Figure 2.1F). The

Figure 2.3. Properties of I_{CAN} in the LP neuron

A. Current traces from two LP neurons; $I_{Ca(V)}$ was activated by the depolarizing pre-step to 20 mV and -10 mV and I_{CAN} was measured at tail currents activated at the beginning of the hyperpolarizing steps. The voltage clamp protocol is shown above the current traces.
B. I-V relationship of the tail current measured at the peak of I_{CAN} (the arrowheads in A and B). A linear function extrapolated E_{rev} to -32 mV (n=4). Note the larger $I_{Ca(V)}$ and I_{CAN} amplitude compared to AB and PD.
C. Voltage-dependence of deactivation time constant (R^2=0.9, n=5).
D. The dose response curve for the FFA at 21°C; IC_{50}=32±1 μM (n=4).
E. CAN conductance at -65 mV under control conditions and in DA was not statistically different (n=3, p>0.05).

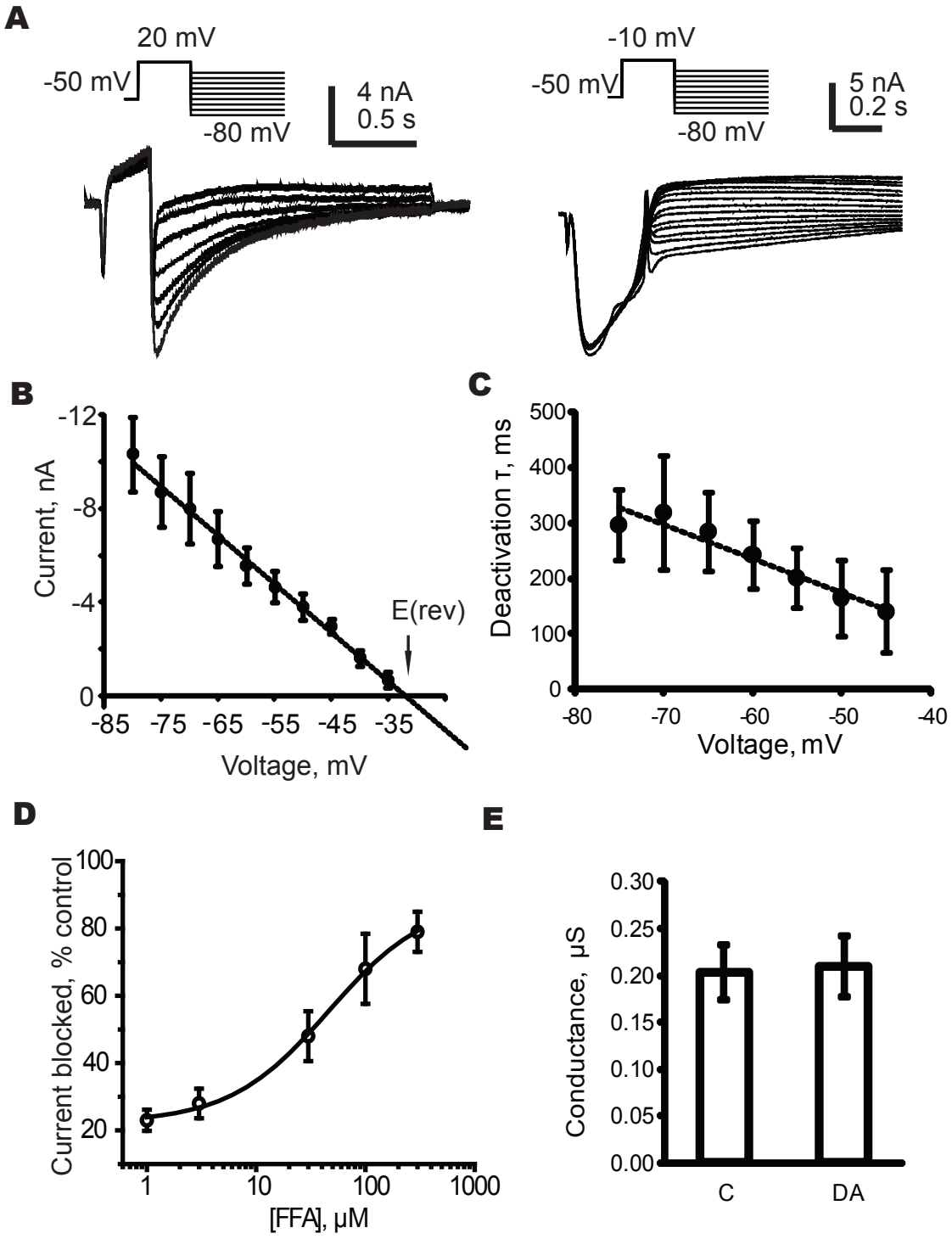
A
20 mV
-50 mV
-80 mV
4 nA
0.5 s
-10 mV
-50 mV
-80 mV
5 nA
0.2 s
B
Current, nA
-12
-8
-4
0
E(rev)
-85 -75 -65 -55 -45 -35
Voltage, mV
C
Deactivation τ, ms
500
400
300
200
100
0
-80 -70 -60 -50 -40
Voltage, mV
D
Current blocked, % control
100
80
60
40
20
1 10 100 1000
[FFA], μM
E
Conductance, μS
0.30
0.25
0.20
0.15
0.10
0.05
0.00
C
DA

CAN conductance in AB increased from 58±9 nS under control conditions to 145±12 nS in the presence of DA (n=5, $p<0.05$), while it did not change in the PD (Figure 2.2F, n=2) or the LP (Figure 2.3E, n=3) neurons. This effect of DA in the AB neuron is further explored in Chapter 3.

CHARACTERIZATION OF THE PERSISTENT SODIUM CURRENT

The persistent sodium current $I_{Na(P)}$ represents the portion of the sodium current flowing via non- or slowly-inactivating sodium channels. Because this current is very small, I used a cocktail of blockers to suppress all other voltage-gated currents and synaptic transmission by bath application and iontophoresis (Materials and Methods, this chapter). To separate the fast sodium current $I_{Na(T)}$ and the persistent sodium current $I_{Na(P)}$ in voltage clamp I used differences in their inactivation kinetics: from a holding potential of -90 mV, I injected depolarizing ramps (25 mV/s to 100 mV/s) which depolarize slowly enough to inactivate the rapid $I_{Na(T)}$; this allowed me to measure $I_{Na(P)}$ without contribution from $I_{Na(T)}$. Pharmacologically, the persistent sodium current is blocked by TTX and Riluzole, though some persistent currents were reported to be TTX -resistant (Elliot and Elliot, 1993; Dib-Hajj et al., 2002; Kiss, 2003). $I_{Na(P)}$ was defined as the difference between the currents measured in the presence and absence of TTX or Riluzole. I have also tested the serotonin modulation of $I_{Na(P)}$ in the pyloric neurons: the AB, the PD and the LP.

Properties of $I_{Na(P)}$ in the Anterior Burster Neuron

In the AB, the current recorded during a slow depolarizing ramp initially rose linearly as a leak, but then showed an inward dip of a negative slope conductance region at a threshold of -62±8mV (n=5) and reaching its negative peak at -46±5mV (n=5). The mean peak current amplitude was -2.6±0.8 nA (n=5). Sample ramp current traces are shown on Figure 2.4A, where the gray trace is the

Figure 2.4. Properties of $I_{Na(P)}$ in the AB neuron

A. $I_{Na(P)}$ was measured during slow depolarizing voltage ramps from -80 mV to 10 mV (top, voltage clamp protocol) as a region of negative slope conductance (bottom, current trace: gray is total ramp current, black is leak-subtracted ramp current). The fast sodium current inactivated during the slow ramps and did not contribute to the $I_{Na(P)}$ amplitude.
B. The rate of the depolarizing ramp had minimal effect on the maximal $I_{Na(P)}$ current amplitude (top, voltage ramps of different rates, gray is 133 mV/s, black is 33m V/s; bottom, the current traces for the corresponding voltage ramps).
C. Current-voltage relationship of $I_{Na(P)}$, a small inward current activating at about -60 mV and reaching its peak at about -45 mV on average (n=4). The apparent reversal potential at 0 mV was more hyperpolarized than expected +50 mV, probably because of partially unblocked outward currents.
D. Block of $I_{Na(P)}$ by Riluzole. The traces are examples of the currents under control conditions (black), in 10 μM Riluzole (red) and in 100 μM Riluzole (gray).
E. Riluzole dose-response curve. The amplitude of the blocked portion of the current is shown as % of the control amplitude. IC_{50}=3.2±2 μM.
F. Serotonin did not affect maximum $G_{Na(P)}$ in the AB neuron (n=5, $p>0.05$, student's t-test)

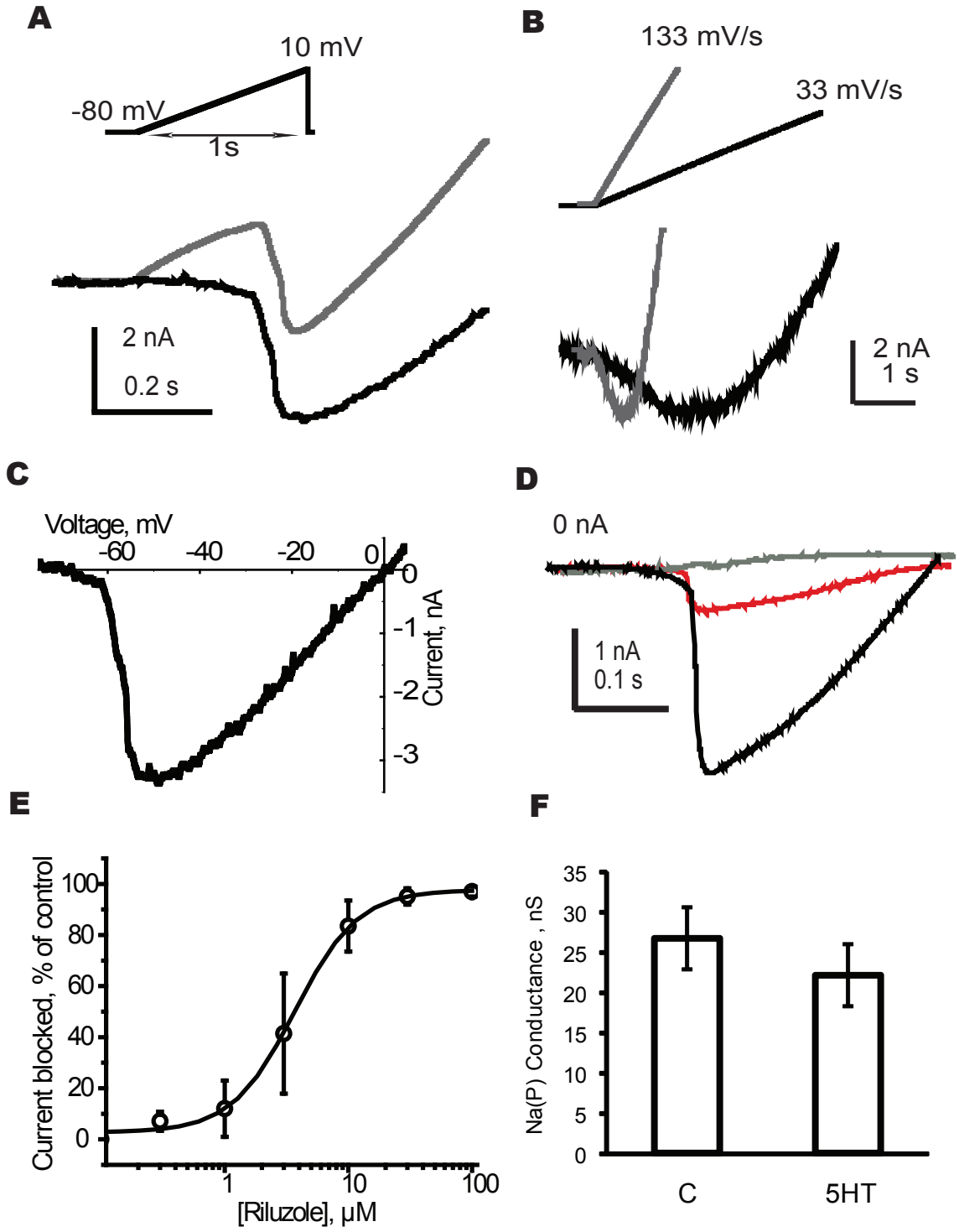
A
10 mV
-80 mV
1s
2 nA
0.2 s
B
133 mV/s
33 mV/s
2 nA
1 s
C
Voltage, mV
-60
-40
-20
0
0
-1
-2
-3
Current, nA
D
0 nA
1 nA
0.1 s
E
Current blocked, % of control
100
80
60
40
20
0
1
10
100
[Riluzole], µM
F
Na(P) Conductance , nS
35
30
25
20
15
10
5
0
C
5HT

total ramp current and the black trace is the leak subtracted ramp current. Varying the rate of the command voltage ramp had only minor effect on the peak amplitude of the current (Figure 2.4B, overlapped current trace at 133mV/s (gray),or 33mV/s (black)); I mostly used 100 mV/s ramps. The current-voltage relationship of the leak subtracted $I_{Na(P)}$ under control conditions is shown on Figure 2.4C. Note that the persistent sodium current reversed at 0 mV rather than +50 mV, probably because of the residual unblocked potassium currents. In pyloric neurons, amplitude of these outward currents are normally two orders of magnitude larger than the $I_{Na(P)}$ amplitude I measured in these experiments. Therefore, despite my efforts to block them as much as possible, residual potassium currents contaminated my recordings, shifting the reversal potential of the ramp current to more negative voltages.

I next tested the sensitivity of the AB's $I_{Na(P)}$ to sodium current blockers Riluzole and TTX. Fig. 2.4D shows sample traces of $I_{Na(P)}$ in the presence of Riluzole which completely blocked the current with an IC_{50} of 3.2±0.2 μM (n=3, dose response curve, Figure 2.4E). The current in the AB neuron was also completely blocked by 0.1μM TTX (not shown).

Serotonin had no effect on the amplitude of the persistent sodium current in the AB neuron (Fig. 2.1F, Na(P) maximum conductance under control conditions and in 5HT, n=5, $p>0.05$).

Absence of $I_{Na(P)}$ in the Pyloric Dilator Neuron

In all of 5 PD neurons tested, I was unable to detect a significant $I_{Na(P)}$. Examples of the current traces and I-V curve in the PD neuron are given in Figure 2.5A and B: total ramp current traces are gray and the leak subtracted currents traces are black. The slowest ramp rate I tested was 10 mV/s, at which all fast sodium current is presumably inactivated (Figure 2.5A), but I did not detect any region of

Figure 2.5. Absence of $I_{Na(P)}$ in the PD neuron

A. Failure to detect $I_{Na(P)}$ in a PD neuron. Voltage ramps of varying speed (3-10 sec) were used to evoke $I_{Na(P)}$ (inset). The absence of any inward rectification in the current trace, and the failure to block action potential generation during the slow ramp was typical for all PD neurons tested (n=5); total ramp current (gray) and leak-subtracted current (black).
B. Current-voltage relationship for a PD neuron (gray is the total ramp current, black is the leak subtracted current).
C. Application of 10 μM Riluzole did not alter the ramp current in a PD neuron: leak subtracted ramps under control conditions (black) and in the presence of Riluzole (red). The small region of the current trace is enlarged below to show the typical break out of VC, with action potentials generated in unclamped regions of the neuron.

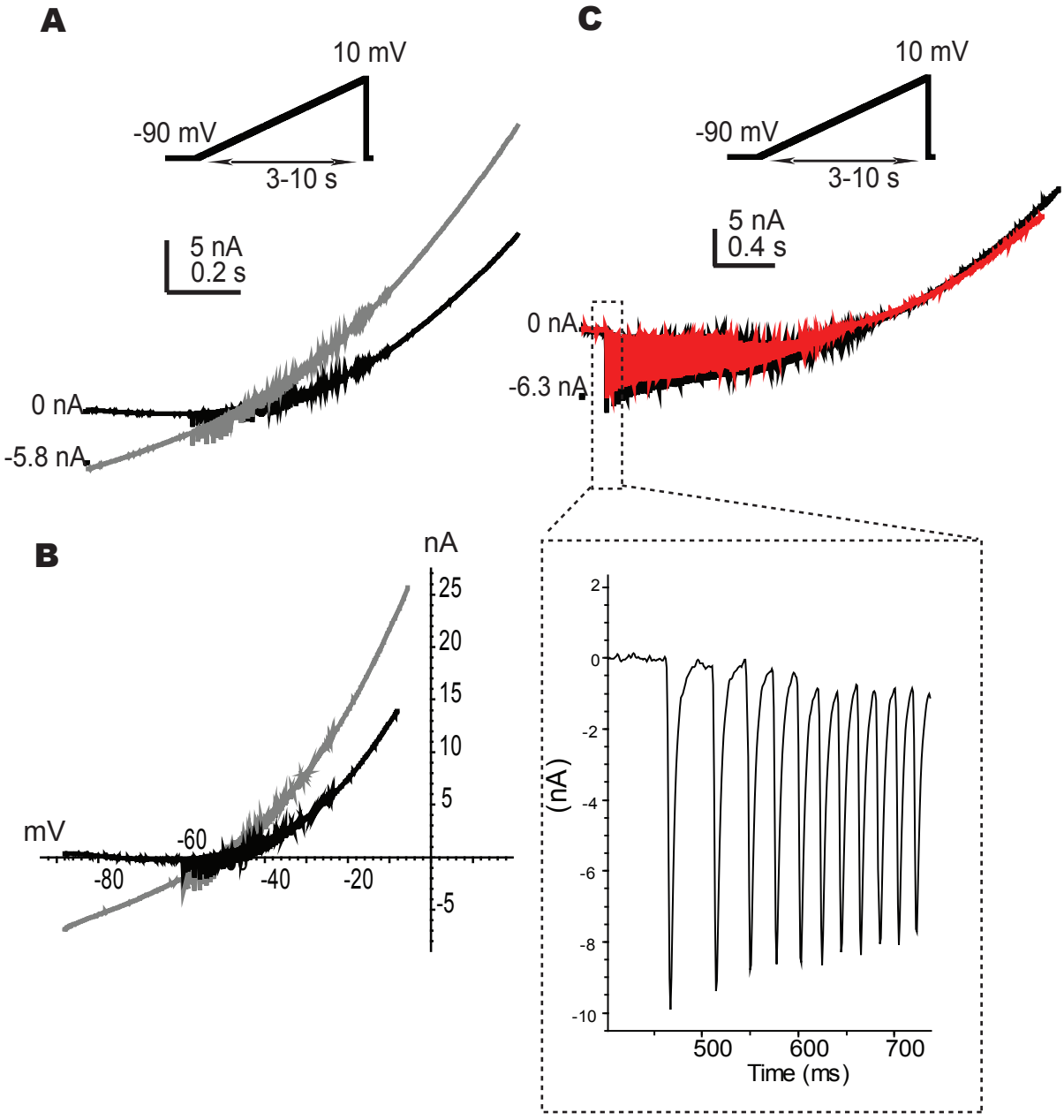
A
10 mV
-90 mV
3-10 s
5 nA
0.2 s
0 nA
-5.8 nA
B
nA
25
20
15
10
5
-5
mV
-80
-60
-40
-20
C
10 mV
-90 mV
3-10 s
5 nA
0.4 s
0 nA
-6.3 nA
2
0
-2
-4
-6
-8
-10
(nA)
500
600
700
Time (ms)

Figure 2.6. Properties of $I_{Na(P)}$ in the LP neuron

A. Block of $I_{Na(P)}$ by Riluzole in the LP neuron: control (black), in 10μM Riluzole (gray) and $I_{Na(P)}$ calculated as a difference between control and Riluzole currents (red trace). Compared to AB, LP neurons typically had much larger amplitude.
B. Block of $I_{Na(P)}$ by TTX in another LP neuron: control (black), in 0.1 mM TTX (gray) and the difference between the two (red trace). Lower concentrations of TTX only partially blocked $I_{Na(P)}$ in LP neurons.
C. Riluzole block of $I_{Na(P)}$ in the LP neuron. The current amplitude is expressed as % of control amplitude (n=1, IC_{50}=6 μM).
D. TTX block of $I_{Na(P)}$ in the LP neuron. Note that 0.1μM TTX, that is used to abolish action potentials in pyloric neurons, blocked only 38% of the $I_{Na(P)}$ (n=1, IC_{50}=330 nM).
E. Serotonin did not change maximum $G_{Na(P)}$ in the LP neuron (n=5, $p>0.05$, student's t-test).

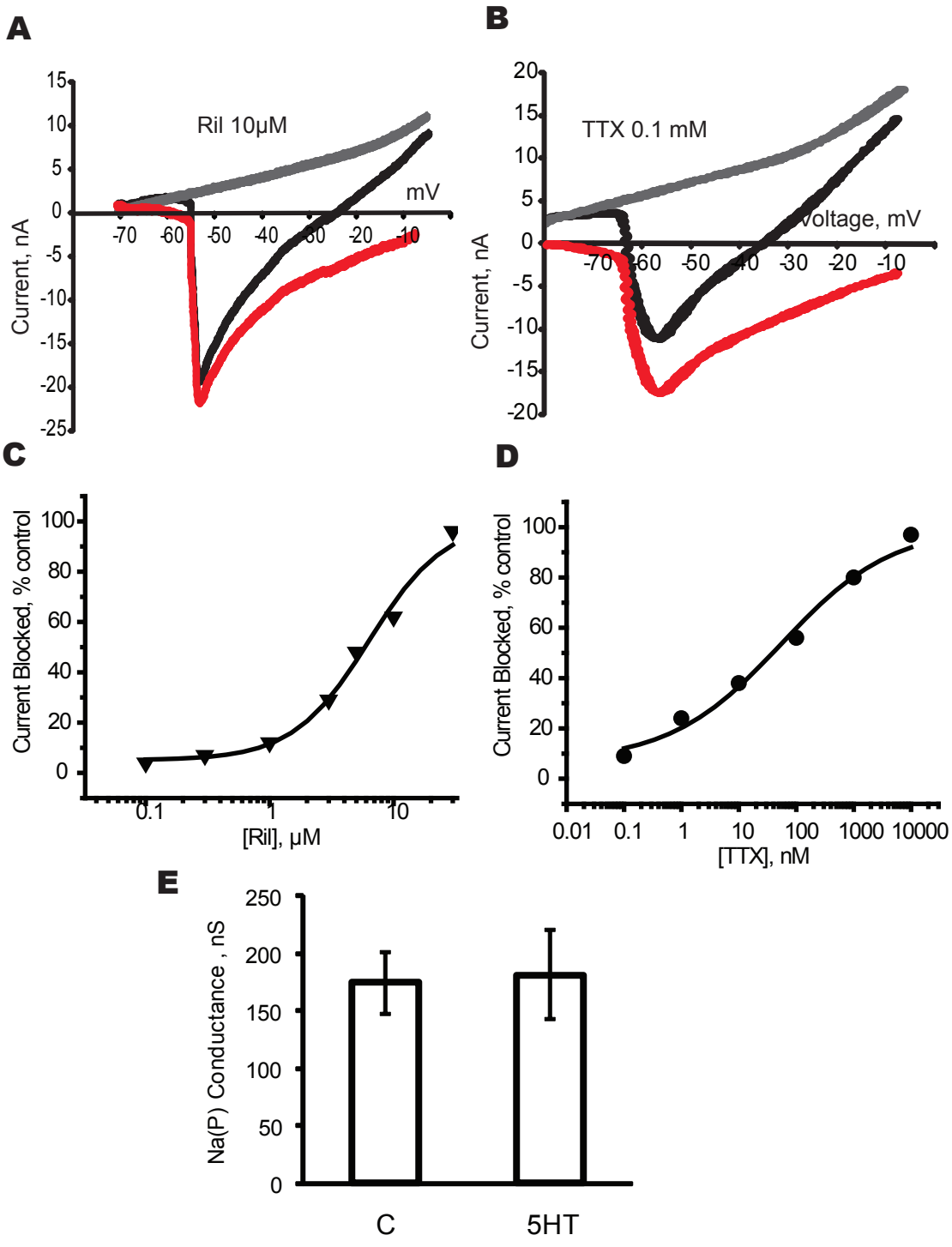
A
Ril 10μM
mV
Current, nA
B
TTX 0.1 mM
Voltage, mV
Current, nA
C
Current Blocked, % control
[Ril], μM
D
Current Blocked, % control
[TTX], nM
E
Na(P) Conductance , nS
C
5HT

negative slope conductance in the PD. PD cells usually escaped from the voltage clamp and began to fire, no matter how slow the slope of the voltage ramp, reflecting the electrotonic distance from the recording site to the spike initiation zone (Example in Fig. 2.5C). Application of 10μM Riluzole did not have any effect on the current-voltage relationship (Figure 2.5C, black trace is under control conditions, red trace is in the presence of 10μM Riluzole).

Properties of $I_{Na(P)}$ in the Lateral Pyloric Neuron

LP had the largest $I_{Na(P)}$ among three cell types tested, with a mean peak inward amplitude of 22±6 nA (n=5). The current started to activate at -60±2mV and reached its peak at -49±3 mV (n=5). Figure 2.6A shows sample current-voltage relation of the ramp current in control (black trace), and in the presence of 10 μM Riluzole (gray); $I_{Na(P)}$ was calculated as the difference between the control and Riluzole currents (red). The apparent IC_{50} for Riluzole block was 6 μM (Fig. 2.6C). TTX was not as effective in blocking $I_{Na(P)}$ as it was in the AB neuron: (Fig. 2.6B, control ramp current, black trace; in 10^{-4} M TTX, gray trace; and the difference current, $I_{Na(P)}$, red trace). The concentration of TTX (10^{-7}M) sufficient to block action potentials and hence fast sodium currents in lobster pyloric cells, was not adequate to block all of the persistent current in the LP neurons (Fig. 2.6D, IC_{50} for TTX=270 nM), which was different from the AB neuron.

As in the AB, serotonin did not alter the Na(P) maximum conductance in the LP neuron (Fig. 2.6E, n=5, $p>0.05$), although the absolute values of the conductance were significantly larger in the LP compared to the AB (Fig. 2.7E).

DISCUSSION

I have characterized two slow inward currents, I_{CAN} and $I_{Na(P)}$, in three different classes of the lobster pyloric neurons. As is the case with other ionic currents in the pyloric neurons that were characterized previously in our lab (Peck et al.,

2001, 2006; Johnson et al., 2003; Gruhn et al, 2006; Ouyang et al, 2006), the slow inward currents had cell-type specific properties. These distinct intrinsic properties are expected, given the different firing patterns and functional roles of these neurons: AB as an interneuron with endogenous bursting capabilities (Miller and Selverston, 1982a; Russell and Hartline, 1978, Flamm and Harris-Warrick, 1986), PD as a motoneuron with a tendency to fire tonically in isolation (Flamm and Harris-Warrick, 1986), and LP as a motoneuron with strong bistable properties in the presence of neuromodulators.

Cell-type specificity of I_{CAN}

I_{CAN} was measured in synaptically isolated cells under conditions of block of all voltage-gated currents except calcium current. Although some unblocked potassium currents could be a contributing factor, I tried to eliminate this possibility by using intracellular blockers of potassium channels (CsCl and TEA). I could not use pharmacological block of $I_{Ca(V)}$ to separate it from ICAN; hence I used their electrophysiological properties to do that. In the pyloric neurons, $I_{Ca(V)}$ activates above -40 mV and reaches its peak around -10 mV to 0 mV (Johnson et al., 2003). Therefore, to measure the CAN current on isolation I did it at the voltages below -40 mV. Additionally, $I_{Ca(V)}$ shows calcium-dependent inactivation in some neurons including pyloric neurons, while I_{CAN} does not show intrinsic inactivation (Partridge et al., 1994). Finally, $I_{Ca(V)}$ de-activates on a faster time scale than I_{CAN}; hence I measured the tail current at least 100 ms after the command voltage was stepped down to ensure the complete de-activation of the calcium current.

I have found that CAN current amplitude is much larger in the LP compared to the AB and PD. To compare between cell types, I have calculated the conductance at -65 mV step in all neurons tested. Under control conditions, the

Figure 2.7. Cell-type differences in the properties of the slow inward currents

A. Mean calcium-activated nonselective conductances (G_{CAN}) calculated from currents measured at -65 mV in AB (n=6), PD (n=5) and LP (n=4). G_{CAN} was significantly larger in the LP compared to the AB and the PD (n=4, $p<0.001$, student's t-test). There was no difference between AB and PD mean conductances.
B. Reversal potential for I_{CAN} in AB, PD and LP was not statistically different (n=5, $p>0.05$, student's t-test).
C. CAN current deactivation time constant at -65 mV was significantly shorter in the AB neuron compared to the PD and the LP (n=5, $p<0.05$, student's t-test).
D. DA significantly increased CAN conductance at -65 mV in the AB neuron (n=5, $p<0.05$, student's t-test), but not in the LP (n=3, $p>0.05$, student's t-test) or the PD (n=3).
E. There was no significant difference in $I_{Na(P)}$ activation and peak voltages between AB and LP neurons. Vact is the voltage at which $I_{Na(P)}$ starts activating; Vpeak is the voltage at which $I_{Na(P)}$ reaches its peak values as measured with slow depolarizing ramp (n=5, $p>0.05$, student's t-test).
F. Maximum persistent sodium conductance was significantly smaller in the AB neuron, compared to that in the LP neuron (n=5, $p<0.05$, student's t-test).

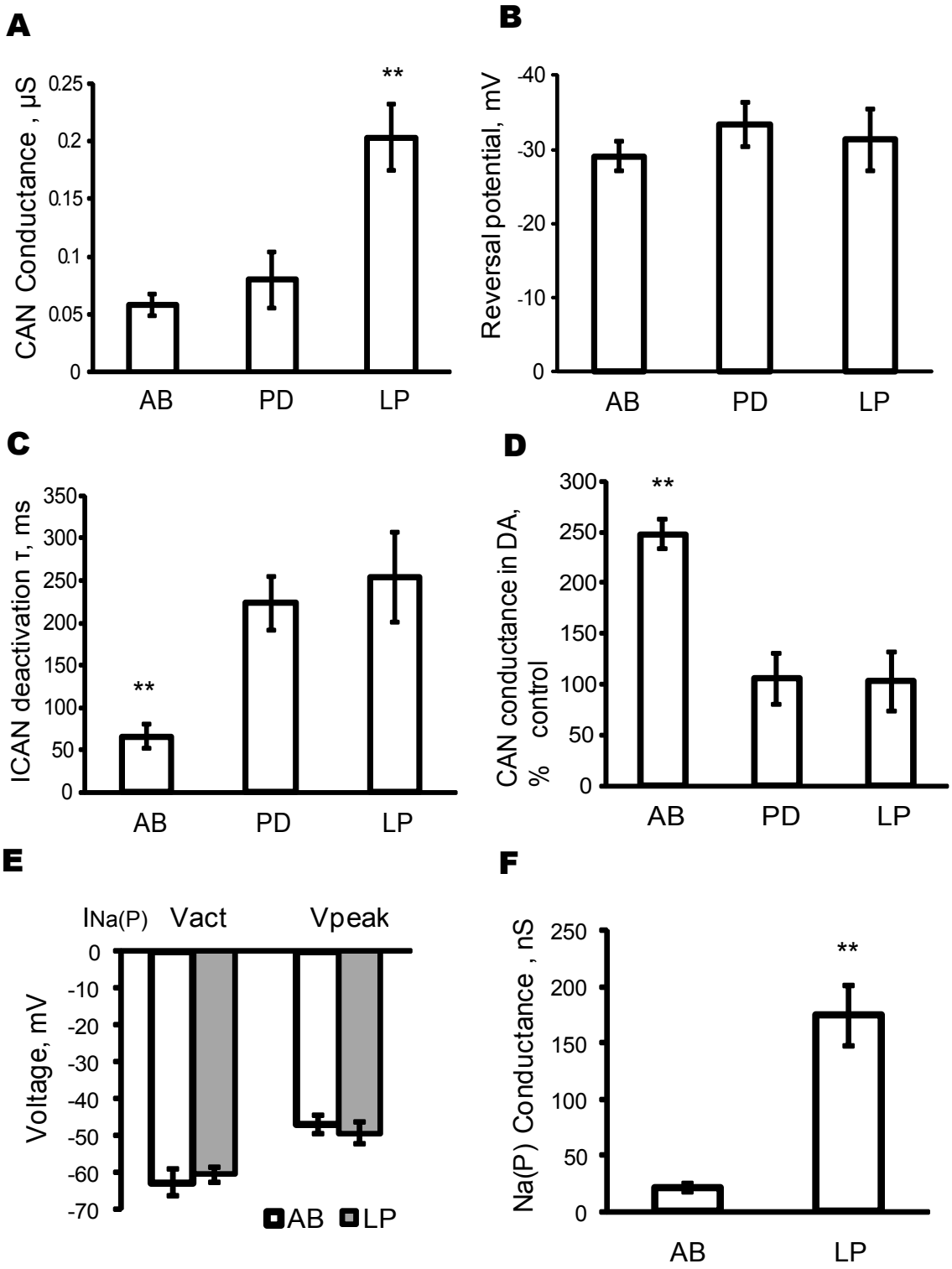
A
CAN Conductance , µS
0.25
0.2
0.15
0.1
0.05
0
**
AB
PD
LP
B
Reversal potential, mV
-40
-30
-20
-10
0
AB
PD
LP
C
ICAN deactivation τ, ms
350
300
250
200
150
100
50
0
**
AB
PD
LP
D
CAN conductance in DA, % control
300
250
200
150
100
50
0
**
AB
PD
LP
E
INa(P)
Vact
Vpeak
Voltage, mV
0
-10
-20
-30
-40
-50
-60
-70
AB
LP
F
Na(P) Conductance , nS
250
200
150
100
50
0
**
AB
LP

mean LP conductance (200±29 nS) was significantly larger compared to those of AB (58±9 nS) and PD (80±25 nS) (n=6, $p<0.05$). Larger I_{CAN} in the LP can be explained by several factors. First, CAN channels may be more densely expressed in this cell type which, together with larger surface area of LP, may lead to the larger whole-cell current. Based on our earlier measurements of the input capacitance (Baro et al., 1997), the I_{CAN} current density in the LP, AB and PD neurons is 136, 97 and 67 nS/nF, suggesting that the larger current in the LP neuron is not simply a reflection of its larger surface area. Second, I_{CAN} may be larger simply because of the larger $I_{Ca(V)}$: peak amplitude of the calcium current is well above 20 nA in the LP, about 15 nA in the PD, and less than 10 nA in the AB (Johnson et al., 2003). Without ability to measure single channel conductance it is impossible to make a reliable conclusion about this difference in CAN current between AB and LP.

A second property of I_{CAN} that showed cell-type specificity was its deactivation kinetics. In the AB, deactivation was independent of voltage, while both PD and LP showed significant voltage-dependence (Figs 2.1C, 2.2C, 2.3C), deactivating more rapidly at more depolarized voltages. When compared at -65 mV, the deactivation time constant after the 200 ms activating pre-step was significantly shorter in the AB (70 ms) compared to PD and LP (220 ms and 250 ms, respectively), while there was no difference between PD and LP deactivation kinetics (n=5, $p<0.05$ for AB, Fig. 2.7C).

In all three neurons, I_{CAN} was sensitive to FFA and BAPTA-AM; both had approximate half-block concentrations about 15-30 μM at 21°C. This was in agreement with earlier reported values in respiratory CPG, cardiomyocytes and brain slices (Pace et al., 2007; Demion et al., 2006; Lee and Tepper, 2007). In all cell types 0.6 mM Cd^{2+} completely blocked the calcium and the calcium-

dependent currents. Thus, there were no obvious cell-specific differences in the pharmacological blockade of I_{CAN}.

In many vertebrate and invertebrate neurons, the CAN current is subject to modulation by G-protein coupled receptor (GPCR)-activated pathways involving second messengers such as cAMP (Partridge et al., 1990; Van den Abbeele et al., 1994; Cho et al., 2003), DAG (Guinamard et al., 2004) and IP_3 (Congar *et al.* 1997; Partridge & Valenzuela, 1999; Pace *et al.,* 2007). In the STG, Clark and colleagues have cloned three different DA receptors that are coupled to the G_s, G_q and G_i pathways. It is possible that DA may act via Gq-PLC pathway to directly enhance I_{CAN} by DAG or to indirectly activate I_{CAN} by IP_3-sensitive calcium release from endoplasmic reticulum. Dopamine reversibly increased CAN conductance at -65 mV in the AB interneuron (248±15 % of control), but not in the PD or LP motor neurons (106±25 % and 103±29 % of control, respectively) (Fig.2.7D, n=5, $p<0.05$ for AB). DA enhancement of I_{CAN} may at least partially underlie AB's unique ability to burst endogenously upon dopamine application. In the next chapter, I will look in more detail at the dopamine modulation of I_{CAN} in the AB neuron and the functional implications of this modulation.

Cell-type specificity of $I_{Na(P)}$

As with I_{CAN}, I found that all three types of pyloric neurons have physiologically and pharmacologically distinct persistent sodium currents. The first cell type specific feature was a difference in the amount of $I_{Na(P)}$. The PD, a motoneuron electrically coupled to the AB to form the pacemaking kernel, completely lacked any detectable $I_{Na(P)}$ (Fig 2.5). Since there was no significant difference in the activation and peak voltages between the AB and LP neurons (Fig. 2.7E, n=5, $p>0.05$), I have calculated the maximum conductance for each cell type to compare $I_{Na(P)}$ in AB and LP. The AB, an interneuron capable of endogenous

bursting in the presence of monoamines (Miller and Selverston, 1982a; Russell and Hartline, 1978; Flamm and Harris-Warrick, 1986), typically had a small current (G_{max}=27±4 nS, n=5), while the LP, a motoneuron with bistable properties, had the largest (G_{max}=174±27 nS). The difference was statistically significant (Fig 2.7F, n=5, $p<0.05$). This disparity in the whole cell conductance between AB and LP may in part reflect the differences in the cell size: AB and LP have 50 µm and 150 µm diameters, respectively (Thuma et al., 2009). Based on our earlier measurements of input capacitance in pyloric neurons (Baro et al., 1997), the $I_{N(P)}$ current density in the AB and LP neurons is 41 and 118 nS/nF, suggesting that the difference between the two neurons is not entirely due to differences in surface area. Both experimental and theoretical work has shown that the relative balance of the opposing ionic currents in a neuron may have a profound effect on the neuron's functional state (Guckenheimer et al., 1993, Butera et al., 1999: Smith *et al.*, 2000). For instance, the ratio of $I_{Na(P)}$ to leak current was shown to be the main difference between pacemaker and non-pacemaker neurons in the respiratory CPG (Smith et al., 1985; Butera et al., 1999; Del Negro et al., 1998, 2002). Hence the final physiological outcome of a smaller or larger Na(P) conductance may depend on the differences in outward currents in AB and LP. For instance, the AB neuron has smaller I_A and leak currents, resulting in higher input resistance compared to the LP neuron (Peck et al., 2001). This balance between $I_{Na(P)}$ and outward currents may change upon monoamine application because of modulation of these currents. In the AB neuron, serotonin has no effect on the I_A (Peck et al., 2001); and while it did not enhance $I_{Na(P)}$ (Fig. 2.5F), serotonin-induced inhibition of other outward currents in this neuron may unmask $I_{Na(P)}$, leading to AB bursting as I will discuss in Chapter 4. As for my inability to detect $I_{Na(P)}$ in the PD neuron, it may stem from space clamp

difficulties due to the properties of gap-junction between PD and AB neurons. An experimental study of the effect of electrical coupling on measurements of voltage-gated currents in the spiny lobster determined the errors to be in the range of 5-10% of the measured conductance (Rabbah et al., 2005). However, their model predicted these errors rise up to 20% depending on the location of the electrical synapse (gap-junction) and even higher (up to 90%) for smaller conductances; they have also suggested that measurements of regenerative inward conductances may be complicated by the loss of voltage control.

A second difference between the AB and LP neurons was the differential TTX sensitivity of $I_{Na(P)}$. High specificity of TTX block comes from a unique TTX-binding site of the sodium channel, although some sodium channels have been reported to be TTX -resistant (Elliot and Elliot, 1993; Dib-Hajj et al., 2002; Kiss, 2003). In mammals, the binding site of the TTX-resistant channels differs in one residue from that of their TTX-sensitive counterparts; they belong to the subgroups encoded by $Na_V1.6$, 1.8 and 1.9. (Ogata and Ohishi, 2002) and are mostly involved in neuropathic pain (Silos-Santiago I., 2008). Recently, it was shown that TTX still binds to this altered binding site, but lacks the potency to block the current (Farmer et al., 2008). It appears that pyloric neurons may be expressing different subtypes of sodium channels: TTX-sensitive in the AB but less TTX-sensitive in the LP. TTX at the concentration that is routinely used in STNS experiments to block action potentials (0.1μM), was sufficient to block $I_{Na(P)}$ in the AB (Fig. 2.4. However, LP had a significantly lower sensitivity to TTX: the same concentration of TTX (0.1μM) blocked less than 40 % of the current amplitude, and it took 100 μM TTX for a complete block. However, $I_{Na(P)}$ in both cell types was still sensitive to low doses of Riluzole (IC_{50} in the range of low micromolar concentrations, Fig 2.4 and 2.6).

Functional significance of cell-type specificity of $I_{Na(P)}$. Neuronal excitability is linked to the patterns of expression of specific sodium channel isoforms with distinct biophysical and pharmacological characteristics. For instance, different neuronal subpopulations of DRG neurons were shown to differ in their sodium channel composition which affected their firing properties (Rush *et al.,* 2007). The AB neuron, as a pacemaker driving the whole pyloric network, has to have high level of excitability and be sensitive to descending neuromodulatory inputs. $I_{Na(P)}$ can provide this higher excitability at subthreshold voltages and ensure the pacemaking function in the AB. The PD neurons are not endogenously rhythmic in the presence of monoamines; instead they are driven by the AB and may act as a frequency regulating mechanism in the pacemaker kernel. PD neurons appear to have little or no $I_{Na(P)}$. Having biophysically and pharmacologically distinct subtypes of pacemaker neurons is not unique to the pyloric system. In the mammalian respiratory CPG, there are two different subtypes of the pacemaker neurons: the fast bursters are blocked by TTX and the slow bursters are blocked by a combination of TTX and $CdCl_2$ (Thoby-Brisson and Ramirez, 2000, 2001); each subgroup is thought to have distinct physiological functions. Finally, the LP is a motoneuron with very strong bistable properties. Since it provides the only synaptic feedback to the pacemaker kernel, the LP may need an additional boost to its depolarizing forces provided by $I_{Na(P)}$.

REFERENCES

Ahn HS, Choi JS, Choi BH, Kim MJ, Rhie DJ, Yoon SH, Jo YH, Kim MS, Sung KW, Hahn SJ (2005) Inhibition of the cloned delayed rectifier K^+ channels, Kv1.5 and Kv3.1, by riluzole. Neuroscience 133:1007–1019.

Butera, R., Rinzel, J., and Smith, J.C. Models of respiratory rhythm in the pre-Bötzinger complex. I. Bursting pacemaker neurons. *J Neurophysiol* 81 (1999), pp. 382–397.

Cao YJ, Dreixler JC, Couey JJ, Houamed KM (2002) Modulation of recombinant and native neuronal SK channels by the neuroprotective drug riluzole. *Eur J Pharmacol* 449:47–54

Chen Y, Yu FH, Sharp EM, Beacham D, Scheuer T, Catterall WA. 2008 Functional properties and differential neuromodulation of Na(v)1.6 channels. *Mol Cell Neurosci* 38(4):607-15

Cho H, Kim MS, Shim WS, Yang YD, Koo J, Oh U. (2003) Calcium-activated cationic channel in rat sensory neurons. *Eur J Neurosci*. 17(12):2630-8.

Colquhoun, D., Neher, E., Reuter, H., Stevens, CF. (1981) Inward current channels activated by intracellular Ca in cultured cardiac cells. *Nature* 294: 752-754.

Congar P, Leinekugel X, Ben-Ari Y & Crepel V (1997). A long-lasting calcium-activated nonselective cationic current is generated by synaptic stimulation or exogenous activation of group I metabotropic glutamate receptors in CA1 pyramidal neurons. *J Neurosci* 17, 5366–5379.

Congar P, Leinekugel X, Ben-Ari Y, Crépel V. (1997) A long-lasting calcium-activated nonselective cationic current is generated by synaptic stimulation or exogenous activation of group I metabotropic glutamate receptors in CA1 pyramidal neurons. *J Neurosci*. 17(14):5366-79.

Cramer NP, Li Y, Keller A. 2007 The whisking rhythm generator: a novel mammalian network for the generation of movement. *J Neurophysiol.* 97(3):2148-58.

Crill WE. (1996) Persistent sodium current in mammalian central neurons. *Annu Rev Physiol*. 58:349-62.

Dai Y, Jordan LM, Fedirchuk B. 2009 Modulation of transient and persistent inward currents by activation of protein kinase C in spinal ventral neurons of the neonatal rat. *J Neurophysiol*. 101(1):112-28.

Demion M, Bois P, Launay P, Guinamard R. (2007) TRPM4, a Ca2+-activated nonselective cation channel in mouse sino-atrial node cells. *Cardiovasc Res.* 73(3):531-8.

Dib-Hajj S, Black JA, Cummins TR, Waxman SG. (2002) NaN/Nav1.9: a sodium channel with unique properties. *Trends Neurosci*. 25(5):253-9.

Duprat F, Lesage F, Patel AJ, Fink M, Romey G, Lazdunski M (2000) The neuroprotective agent riluzole activates the two P domain K(+) channels TREK-1 and TRAAK. *Mol Pharmacol* 57:906–912.

Elliott, AA and Elliott, JR. (1993) Characterization of TTX-sensitive and TTX-resistant sodium currents in small cells from adult rat dorsal root ganglia. *J Physiol*. 463:39-56.

Elson RC, Selverston AI. (1997) Evidence for a persistent Na+ conductance in neurons of the gastric mill rhythm generator of spiny lobsters. *J Exp Biol.* 200(Pt 12):1795-807.

Farmer C, Smith K, Docherty R. (2008) Low concentrations of tetrodotoxin interact with tetrodotoxin-resistant voltage-gated sodium channels. *Br J Pharmacol*. 155(1):34-43.

Faustino EV, Donnelly DF. (2006) An important functional role of persistent Na+ current in carotid body hypoxia transduction. *J Appl Physiol.* 101(4):1076-84.

Fedida D, Noble D, Shimoni Y, Spindler AJ. (1987) Inward current related to contraction in guinea-pig ventricular myocytes. *J Physiol*. 385:565-89.

Flamm RE, Harris-Warrick RM. (1986) Aminergic modulation in lobster stomatogastric ganglion. II. Target neurons of dopamine, octopamine, and serotonin within the pyloric circuit. *J Neurophysiol*. 55(5):866-81

Golomb D, Yue C, Yaari Y. (2006) Contribution of persistent Na+ current and M-type K+ current to somatic bursting in CA1 pyramidal cells: combined experimental and modeling study. *J Neurophysiol*. 96(4):1912-26.

Guckenheimer J, Gueron S, Harris-Warrick RM. (1993) Mapping the dynamics of a bursting neuron. *Philos Trans R Soc Lond B Biol Sci.* 341(1298):345-59.

Guckenheimer J, Harris-Warrick R, Peck J, Willms A. Bifurcation, bursting, and spike frequency adaptation. *J Comput Neurosci*. (1997) 4(3):257-77.

Guinamard R, Chatelier A, Lenfant J, Bois P. (2004) Activation of the Ca(2+)-activated nonselective cation channel by diacylglycerol analogues in rat cardiomyocytes. *J Cardiovasc Electrophysiol*. 15(3):342-8.

Guinamard R, Demion M, Chatelier A, Bois P. (2006) Calcium-activated nonselective cation channels in mammalian cardiomyocytes. *Trends Cardiovasc Med*. 16(7):245-50.

Haj-Dahmane S, Andrade R. (1997) Calcium-activated cation nonselective current contributes to the fast afterdepolarization in rat prefrontal cortex neurons. *J. Neurophysiol*. 78(4):1983-9.

Hardie, R.C. and Minke, B. (1993) Novel Ca2+ channels underlying transduction in Drosophila photoreceptors: implications for phosphoinositide-mediated Ca" mobilization. *Trend Neurosci,* 16: 371-376.

Harris-Warrick, RM and Johnson, BR. (1987) Potassium channel blockade induces rhythmic activity in a conditional burster neuron. *Brain Res.* 416(2):381-6

Harris-Warrick RM. (2002). Voltage-sensitive ion channels in rhythmic motor systems. *Curr Opin Neurobiol*. 12(6):646-51.

Harvey PJ, Li X, Li Y, Bennett DJ. (2006) Endogenous monoamine receptor activation is essential for enabling persistent sodium currents and repetitive firing in rat spinal motoneurons. *J Neurophysiol*. 96(3):1171-86.

Huang CS, Song JH, Nagata K, Yeh JZ, Narahashi T (1997) Effects of the neuroprotective agent riluzole on the high voltage-activated calcium channels of rat dorsal root ganglion neurons. *J Pharmacol Exp Ther* 282:1280–1290.

Huang H, Trussell LO. (2008) Control of presynaptic function by a persistent Na(+) current. *Neuron.* 60(6):975-9.

Jones LS, Lewis DV. (1988) A calcium-activated, nonselective cationic conductance in Aplysia silent neurons. *Brain Res Bull*. 20(5):607-9.

Kang Y, Saito M, Sato H, Toyoda H, Maeda Y, Hirai T, Bae YC. (2007) Involvement of persistent Na+ current in spike initiation in primary sensory neurons of the rat mesencephalic trigeminal nucleus. *J Neurophysiol.* 97(3):2385-93.

Kiss, T. (2003) Evidence for a persistent Na-conductance in identified command neurones of the snail, Helix pomatia. *Brain Res*. 989(1):16-25.

Kloppenburg P, Zipfel WR, Webb WW, and Harris-Warrick RM. (2000) Highly localized Ca2+ accumulation revealed by multiphoton microscopy in an

identified motoneuron and its modulation by dopamine. *J Neurosci* 20: 2523–2533.

Korbmacher C, Volk T, Segal AS, Boulpaep EL, Frömter E. (1995) A calcium-activated and nucleotide-sensitive nonselective cation channel in M-1 mouse cortical collecting duct cells. *J Membr Biol*. 146(1):29-45.

Kramer, R. H. and R. S. Zucker. (1985) Calcium-dependent inward currents in Aplysia bursting pace-maker neurons. *J Physiol*. 362:107-130.

Kuo JJ, Lee RH, Zhang L, Heckman CJ (2006) Essential role of the persistent sodium current in spike initiation during slowly rising inputs in mouse spinal neurones. *J Physiol (Lond)* 574:819–834.

Lamanauskas N, Nistri A. (2008) Riluzole blocks persistent Na+ and Ca2+ currents and modulates release of glutamate via presynaptic NMDA receptors on neonatal rat hypoglossal motoneurons in vitro. *Eur J Neurosci.* 27(10):2501-14.

Lamas JA, Romero M, Reboreda A, Sánchez E, Ribeiro SJ. (2009) A riluzole- and valproate-sensitive persistent sodium current contributes to the resting membrane potential and increases the excitability of sympathetic neurones. *Pflugers Arc*h. 458(3):589-99.

Lampert A, Hains BC, Waxman SG. (2006) Upregulation of persistent and ramp sodium current in dorsal horn neurons after spinal cord injury. *Exp Brain Res.* 174(4):660-6.

Lapointe JY, Bell PD, Sabirov RZ, Okada Y (2003) Calcium-activated nonselective cationic channel in macula densa cells. *Am J Physiol Renal Physiol*. 285(2):F275-80.

Lee CR, Tepper JM. (2007) A calcium-activated nonselective cation conductance underlies the plateau potential in rat substantia nigra GABAergic neurons. *J Neurosci.* 27(24):6531-41.

Liu S, Shipley MT. (2008) Multiple conductances cooperatively regulate spontaneous bursting in mouse olfactory bulb external tufted cells. *J Neurosci.* 28(7):1625-39.

Maruyama, Y. and Petersen, O.H. (1981) Single-channel currents in isolated patches of plasma membrane from basal surface of pancreatic acini. *Nature* 299: 159-161.

Matsuura H, Sokabe T, Kohno K, Tominaga M, Kadowaki T. (2009) Evolutionary conservation and changes in insect TRP channels. *BMC Evol Biol* 9:228.

Miles GB, Dai Y, Brownstone RM (2005) Mechanisms underlying the early phase of spike frequency adaptation in mouse spinal motoneurones. *J Physiol (Lond)* 566:519–532.

Montell C. (2001) Physiology, phylogeny, and functions of the TRP superfamily of cation channels. *Sci STKE.* (90):re1.

Ogata N, Ohishi Y. (2002) Molecular diversity of structure and function of the voltage-gated Na+ channels. *Jpn J Pharmacol*. 88(4):365-77.

Pace RW, Mackay DD, Feldman JL, Del Negro CA. (2007a) Inspiratory bursts in the preBötzinger complex depend on a calcium-activated non-specific cation current linked to glutamate receptors in neonatal mice. *J Physiol*. 582:113-25.

Pace RW, Mackay DD, Feldman JL, Del Negro CA. (2007b) Role of persistent sodium current in mouse preBötzinger Complex neurons and respiratory rhythm generation. *J Physiol*. 580(Pt. 2):485-96.

Partridge LD & Valenzuela CF (1999). Ca2+ store-dependent potentiation of Ca2+-activated non-selective cation channels in rat hippocampal neurones in vitro. *J Physiol* 521, 617–627.

Partridge LD, Swandulla D, Müller TH. (1990) Modulation of calcium-activated non-specific cation currents by cyclic AMP-dependent phosphorylation in neurones of Helix. *J Physiol*. 429:131-45.

Pedersen SF, Owsianik G, Nilius B. (2005) TRP channels: an overview. *Cell Calcium*. 38(3-4):233-52.

Peña F, Aguileta MA. (2007) Effects of riluzole and flufenamic acid on eupnea and gasping of neonatal mice in vivo. *Neurosci Lett.* 415(3):288-93.

Peña F. 2008 Contribution of pacemaker neurons to respiratory rhythms generation in vitro. *Adv Exp Med Biol*. 605:114-8.

Penington NJ, Kelly JS. (1993) Ionic dependence of a slow inward tail current in rat dorsal raphe neurones. *J Physiol*. 464:33-48.

Perrier JF, Hounsgaard J. (1999) Ca(2+)-activated nonselective cationic current (I(CAN)) in turtle motoneurons. *J Neurophysiol*. 82(2):730-5.

Poronnik, P., Ward, M.C. and Cook, D.I. (1992) Intracellular Ca2+ release by flufenamic acid and other blockers of the non-selective cation channel, *FEBS Lett.* 296: 245.

Pressler RT, Inoue T, Strowbridge BW. (2007) Muscarinic receptor activation modulates granule cell excitability and potentiates inhibition onto mitral cells in the rat olfactory bulb. *J Neurosci*. 27(41):10969-81.

Qiao GF, Li BY, Zhou YH, Lu YJ, Schild JH. (2009) Characterization of persistent TTX-R Na+ currents in physiological concentration of sodium in rat visceral afferents. *Int J Biol Sci.* 5(3):293-7.

Ramirez JM, Tryba AK, Peña F (2004) Pacemaker neurons and neuronal networks: an integrative view. *Curr Opin Neurobiol* 14:665–674.

Rubin JE, Hayes JA, Mendenhall JL, Del Negro CA. (2009) Calcium-activated nonspecific cation current and synaptic depression promote network-dependent burst oscillations. *Proc Natl Acad Sci U S A.* 106(8):2939-44.

Rush AM, Cummins TR, Waxman SG. (2007) Multiple sodium channels and their roles in electrogenesis within dorsal root ganglion neurons. *J Physiol*. 579(Pt 1):1-14. .

Russo MJ, Mugnaini E, Martina M. (2007) Intrinsic properties and mechanisms of spontaneous firing in mouse cerebellar unipolar brush cells. *J Physiol*. 581(Pt 2):709-24.

Sawada, M., Ichinose, M. and Maeno, T. (1990) Activation of a non-specific cation conductance by intracellular injection of inositol 1,3,4,5 tetrakisphosphate into identified neurons of Aplysia. *Brain Res.*512: 333-338.

Silos-Santiago, I. (2008) The role of tetrodotoxin-resistant sodium channels in pain states: are they the next target for analgesic drugs? *Curr Opin Investig Drugs*. 9(1):83-9.

St-John, WM. (2008) Eupnea of in situ rats persists following blockers of in vitro pacemaker burster activities. *Respir Physiol Neurobiol*. 160(3):353-6.

Swandulla, D. and Lux, H.D. (1985) Activation of a non-specific cation conductance by intracellular Ca2+ elevation in bursting pacemaker neurons of Helix pomatia. *J. Neurophysiol.* 54: 1430-1443.

Taddese, A. and Bean, B.P. (2002) Subthreshold sodium current from rapidly inactivating sodium channels drives spontaneous firing of tuberomammillary neurons. *Neuron* 33:587–600

Tahvildari B, Alonso AA, Bourque CW. (2008) Ionic basis of ON and OFF persistent activity in layer III lateral entorhinal cortical principal neurons. *J Neurophysiol.* 99(4):2006-11.

Tazerart S, Viemari JC, Darbon P, Vinay L, Brocard F. (2007) Contribution of persistent sodium current to locomotor pattern generation in neonatal rats. *J Neurophysiol.* 98(2):613-28.

Tazerart S, Vinay L, Brocard F. (2008) The persistent sodium current generates pacemaker activities in the central pattern generator for locomotion and regulates the locomotor rhythm. *J Neurosci*. 28(34):8577-89.

Theiss RD, Kuo JJ, Heckman CJ. (2007) Persistent inward currents in rat ventral horn neurones. *J Physiol*. 580(Pt. 2):507-22

Thoby-Brisson, M and Ramirez JM. (2001) Identification of two types of inspiratory pacemaker neurons in the isolated respiratory neural network of mice. *J Neurophysiol* 86: 104-112

Thoby-Brisson, M and Ramirez, JM. (2000) Role of inspiratory pacemaker neurons in mediating the hypoxic response of the respiratory network in vitro. *J Neurosci*. 20(15):5858-66.

Thuma JB, White WE, Hobbs KH, Hooper SL. (2009) Pyloric neuron morphology in the stomatogastric ganglion of the lobster, Panulirus interruptus. *Brain Behav Evol*. 73(1):26-42.

Tien JH, Guckenheimer J. (2008) Parameter estimation for bursting neural models. *J Comput Neurosci*. 24(3):358-73.

Urbani, A. and Belluzzi, O. (2000) Riluzole inhibits the persistent sodium current in mammalian CNS neurons. *Eur J Neurosci* 12:3567–3574.

Van den Abbeele T, Tran Ba Huy P, Teulon J. (1994) A calcium-activated nonselective cationic channel in the basolateral membrane of outer hair cells of the guinea-pig cochlea. *Pflugers Arch*. 427(1-2):56-63.

van Drongelen W, Koch H, Elsen FP, Lee HC, Mrejeru A, Doren E, Marcuccilli CJ, Hereld M, Stevens RL, Ramirez JM. (2006) Role of persistent sodium

current in bursting activity of mouse neocortical networks in vitro. *J Neurophysiol.* 96(5):2564-77.

Willms AR, Baro DJ, Harris-Warrick RM, Guckenheimer J. (1999) An improved parameter estimation method for Hodgkin-Huxley models. *J Comput Neurosci.* 6(2):145-68.

Wu N, Enomoto A, Tanaka S, Hsiao CF, Nykamp DQ, Izhikevich E, Chandler SH (2005) Persistent sodium currents in mesencephalic v neurons participate in burst generation and control of membrane excitability. *J Neurophysiol* 93:2710–2722.

Yan HD, Villalobos C, Andrade R. (2009) TRPC Channels Mediate a Muscarinic Receptor-Induced Afterdepolarization in Cerebral Cortex. *J Neurosci.* 29(32):10038-46.

Yazenian, B. and Byerly, L. (1989) Voltage-independent Ba-permeable channel activated in Lymnaea neurons by internal perfusion or patch excision. *J. Mem. Biol*. 107: 63-75.

Yvon C, Czarnecki A, Streit J. (2007) Riluzole-induced oscillations in spinal networks. *J Neurophysiol*. 97(5):3607-20.

Zhang B, Wootton JF, Harris-Warrick RM. (1995) Calcium-dependent plateau potentials in a crab stomatogastric ganglion motor neuron. II. Calcium-activated slow inward current. *J Neurophysiol*. 74(5):1938-46.

Zhong G, Masino MA, Harris-Warrick RM. (2007) Persistent sodium currents participate in fictive locomotion generation in neonatal mouse spinal cord. *J Neurosci*. 27(17):4507-18.

Zhong G. (2007) Persistent sodium current in preBotzinger neurons is not necessary for respiratory rhythm generation in the neonatal mouse? *J Physiol.* 581(Pt 2):429.

Zhu ZT, Munhall A, Shen KZ, Johnson SW. (2004) Calcium-dependent subthreshold oscillations determine bursting activity induced by N-methyl-D-aspartate in rat subthalamic neurons in vitro. *Eur J Neurosci*. 19(5):1296-304.

Ziskind-Conhaim L, Wu L, Wiesner EP. (2008) Persistent sodium current contributes to induced voltage oscillations in locomotor-related hb9 interneurons in the mouse spinal cord. *J Neurophysiol*. 100(4):2254-64.

Zona C, Cavalcanti S, De Sarro G, Siniscalchi A, Marchetti C, Gaetti C, Costa N, Mercuri N, Bernardi G (2002) Kainate-induced currents in rat cortical neurons in culture are modulated by riluzole. *Synapse* 43:244–251.

Zona C, Siniscalchi A, Mercuri NB, Bernardi G (1998) Riluzole interacts with voltage-activated sodium and potassium currents in cultured rat cortical neurons. *Neuroscience* 85:931–938.

CHAPTER 3

DOPAMINE-INDUCED BURSTING IN THE PYLORIC PACEMAKER NEURON

INTRODUCTION

Dopamine (DA)-induced bursting in the pyloric pacemaker neuron (Anterior Burster, or AB) is critically dependent on external calcium, minimally affected by external sodium concentration and insensitive to tetrodotoxin (TTX) (Harris-Warrick and Flamm 1987). This calcium-dependence of DA-induced bursting suggests an involvement of the voltage-gated calcium current (VGCC) and/or the calcium-activated non-selective current (I_{CAN}); both currents have been described as critical players in many vertebrate and invertebrate rhythmic neurons (Partridge and Swandulla, 1987; Büschges *et al.,* 2000; Perrier *et al.,* 2000; Pace *et al.,* 2007a).

In the AB neuron, the voltage-gated calcium current is inhibited by up to 75% by 0.1mM DA (Johnson *et al.* 2003), significantly reducing the influx of calcium ions to the cell. Thus, the voltage-gated calcium current described by Johnson *et al.* cannot be the major driving force behind the slow depolarization in AB when DA is added, nor can it be the prime driver for the DA-evoked oscillations. However, DA enhances calcium-dependent properties in AB, such as the increase in synaptic output (Johnson *et al.,* 1995; Harris-Warrick *et al.,* 1998) and an augmentation of $I_{K(Ca)}$ (Johnson *et al.,* 2003). Therefore, I tested the hypothesis that DA may also enhance the calcium-activated non-specific current, I_{CAN}, in the AB neuron for rhythm generation in the pyloric network.

The CAN channels are non-selective cationic channels with slow activation kinetics; they have been demonstrated to play a critical role in the generation of bistability and plateau potentials in the Dorsal Gastric neuron in the crab STG

(Zhang *et al.,* 1995). These channels are thought to be encoded by members of *trp* family of genes in both vertebrates and invertebrates (Montell, 2001; Venkatachalam and Montell, 2007; Matsuura *et al.*, 2009); however their exact structure in the lobster STNS is unknown. The I_{CAN} does not have intrinsic voltage dependence; instead it is activated by calcium ions coming from the extracellular space or from intracellular calcium stores such as the smooth endoplasmic reticulum (ER) or mitochondria. I tested the hypothesis that in the lobster pyloric pacemaker AB neuron, DA may increase $[Ca^{2+}]_{in}$ by triggering Ca^{2+} release from intracellular stores or by inhibiting the sequestration of Ca^{2+} ions, or both; this way DA may indirectly enhance I_{CAN} and generate rhythmic oscillations.

If I_{CAN} is involved in the initiation and maintenance of dopamine-induced bursting in the AB neuron, the following predictions can be made:

1. Blockade of the I_{CAN} should reduce or stop bursting, and DA should enhance the I_{CAN} as an essential step to generating bursting from a quiescent state.
2. To activate I_{CAN}, dopamine should increase the intracellular calcium concentration by some mechanism, since it does not enhance $I_{Ca(V)}$ at the membrane.
3. The most likely source of a DA-induced Ca^{2+} rise would be by release from intracellular calcium stores. Therefore, treatment with specific blockers of channels or pumps that regulate intracellular calcium handling should prevent the emergence of, or abolish an ongoing dopamine rhythm.

MATERIALS AND METHODS

Animals and preparation. Adult California spiny lobsters (*Panulirus interruptus*) were supplied by Don Tomlinson Commercial Fishing (San Diego, CA) and kept in tanks with artificial sea water. Lobsters were anesthetized in ice; the STNS was

dissected out and pinned on a Sylgard-coated Petri dish and superfused with oxygenated lobster physiological saline. The bath temperature was maintained at 16-17℃ unless otherwise specified. The STG was desheathed, and cells were identified as previously described (Selverston *et al*., 1976). All experiments in this chapter were done on the Anterior Burster neuron (AB). In current clamp (CC) experiments, the AB cell was synaptically isolated by photoablation of three pyloric motoneurons that are electrically coupled to it - the ventricular dilator (VD) and two pyloric dilator (PD) cells, as described in Miller and Selverston (1979). In some experiments (voltage clamp and imaging), to block synaptic and neuromodulatory input to AB neuron I added TTX and PTX to the saline instead of photoablation; this did not make any difference in DA-induced bursting (also see Harris-Warrick and Flamm, 1987); therefore, all results were pooled for data analysis.

Electrophysiology. Conventional current clamp (CC) and two-electrode voltage clamp (TEVC) recordings were performed using an Axoclamp-2B amplifier, DigiData 1440 data acquisition board and pCLAMP10 software (all from Molecular Devices, Sunnyvale, CA). For voltage clamp protocols see the Materials and Methods section of Chapter 2 of this thesis. Leak subtraction was done either on-line (P/N=6 leak subtraction protocol during data acquisition in Clampex) or off-line (direct measurement of the leak current during experiment with digital leak subtraction afterward); both methods gave similar results.

Solutions. *Panulirus* physiological saline had the following composition (in mM): 479 NaCl, 12.8 KCl, 13.7 $CaCl_2$, 3.9 Na2SO4, 10.0 MgSO4, 2 Glucose, and 11.1 Tris base, pH 7.4 (Mulloney and Selverston, 1974). The descending input to the STG from the oesophageal ganglion and the paired commissural ganglia via the stomatogastric nerve (STN) was blocked by application of isotonic

sucrose solution with 10^{-7}M TTX into a small Vaseline well built around the STN. To block all other currents I used the following blockers: 50 mM tetraethylammonium chloride (TEA) and 4 mM 4-aminopyridine (4-AP) to block potassium currents, 5 mM CsCl to block the hyperpolarization-activated current, 0.1 uM TTX to block sodium currents and $5 \cdot 10^{-6}$ M picrotoxin (PTX) to block glutamatergic synapses within the STG. In addition to the bath-applied blockers, I loaded the cell body with internal blockers by injecting small negative current steps (1-4 nA) through an electrode loaded with 2M TEA and 2M CsCl for 1-1.5 hours; the blockers were allowed to diffuse through the cell for 1-2 hours before starting the experiment. I used 100 μM Nifedipine (Nif) to block the L-type $I_{Ca(V)}$, 30 μM Flufenamic acid (FFA) to block the I_{CAN}, 30μM BAPTA-AM to chelate intracellular calcium ions, 10-100 nM Ryanodine (Ry) to block Ryanodine receptor-channels, 1-10 μM Xestospongin (Xe) C or D to block IP_3-receptor channels, and 10 μM Thapsigargin (Tg) to block the SERCA pump. The chemicals were purchased from Sigma, Tocris, or Cayman Chemical.

Two-photon calcium imaging. Fluorescent dyes were injected into the AB neuron using an ionophoresis procedure described above and elsewhere (Kloppenburg *et al*., 2000). Only AB neurons that at about half an hour following iontophoresis maintained rhythmic activity and showed labeling in fine neurites were retained for analysis. We have successfully labeled the AB neuron with combinations of dextran-conjugated Cascade Blue and potassium salts of Calcium Green-1 or Indo-1 (all from Invitrogen). The two-photon microscope is based on an upright Olympus BX50WI unit (Kwan *et al*., 2009; Diaz-Rios *et al*., 2007). The excitation, generated by a Ti:Sapphire laser (Tsunami, Spectra-Physics), was scanned by a modified Bio-Rad Radiance scan head and focused onto the sample by a water immersion 40X/NA 0.80 objective (Olympus). The laser intensity was

controlled by a Pockels cell (350-80LA, Conoptics). The typical after-objective laser power used in our experiments was 5-10 mW. For Calcium Green-1, the specimen was excited at 800 nm and the fluorescence was collected by a GaAsP photomultiplier tube (H7422, Hamamatsu) after a bandpass filter between 500-650 nm (Chroma). For Indo-1, the specimen was excited at 720 nm and the fluorescence was separated by a DCLP440 dichroic mirror into two detection channels, 360-430 nm with a bialkali photomultiplier tube (HC125-02, Hamamatsu) and 485-505 nm with a GaAsP photomultiplier tube. The line scans were synchronized to the electrophysiological recordings by connecting the voltage output of the amplifier to the image acquisition system and recording membrane potential on a third detection channel (Kloppenburg *et al*., 2000).

For the emission ratiometric calcium indicator Indo-1, we estimated the absolute calcium concentration, $[Ca^{2+}]_{in}$, by calculating the ratio between fluorescence detected at the two emission channels, $R = F_{395}/F_{495}$, and using the equation, $[Ca^{2+}] = K_{eff} \cdot (R - R_o) / (R_1 - R)$, where K_{eff} is the in situ dissociation constant of Indo-1, and R_o and R_1 are the fluorescence ratios at zero and saturating calcium concentrations. Background fluorescence was estimated from a region without neurites and subtracted from the actual fluorescence signals. Because the dissociation constant within fine neurites of STG neurons is not known, we assumed that it is similar to the value measured in salt solution, so $K_{eff} \sim K_d = 250$ nM (Grynkiewiecz *et al*., 1985). To measure R_1, we topically applied a calcium ionophore, 4-Bromo A23187 (Invitrogen) to equilibrate the intra- and extra-cellular calcium concentrations. We also tried to measure R_0 by washing in saline with zero Ca^{2+} and 100 μM BAPTA-AM, but the fluorescence signals at both detection channels decreased rapidly and precluded a meaningful measurement of R_0. We observed this rapid loss of fluorescence in three different AB neuron

preparations, and the effect also occurs frequently in other STG neurons (Warren Zipfel, personal communication). Instead of measuring R_0, we assumed that $[Ca^{2+}]_{in}$ in saline is 97 nM as previously measured in STG neurons (Kloppenburg *et al*., 2001) and used K_{eff}, R_1, and R_{saline} to calculate R_o and then used these calibration parameters to calculate $[Ca^{2+}]_{in}$ under other conditions.

Data analysis. Electrophysiological data analysis was performed using Clampfit10 (Molecular devices). The Calcium imaging data were analyzed with ImageJ (NIH, USA). Synchronization of imaging and physiology was done with custom-written MATLAB software. Statistical analyses were performed with JMP 7 (SAS systems Inc., USA). Graphs and figures were made in Excel, Origin 6 (OriginLab Corporation, Northampton, MA) and Adobe Illustrator CS3 (Adobe Systems Inc., USA).

RESULTS

Dopamine-Induced Bursting in AB is Blocked by FFA, a Blocker of the Calcium-Activated Non-Selective Current

I tested the involvement of the I_{CAN} in rhythmogenesis by application of a specific blocker of this current, Flufenamic acid (FFA), to the oscillating AB neuron. When FFA was applied at 16℃, the AB neuron ceased bursting and fell quiescent within 30 minutes at FFA concentrations of 30-70 μM (Fig. 3.1A, a synaptically isolated AB; Fig. 3.1B, another AB neuron in the presence of TTX+PTX+DA). Unfortunately, at this lower temperature, FFA was poorly soluble in lobster saline (with 0.1 % DMSO), and tended to come out of solution during the experiment. At higher bath temperatures (21℃), the FFA dissolved completely, and its blockade of AB bursting was much more powerful: 1-3μM was enough to block the ongoing dopamine bursting (Fig. 3.1C, AB in TTX+PTX+DA at 21℃). Notably, as the rhythm ceased, the oscillation's trough potential depolarized until

Figure 3.1. Low concentrations of FFA abolished DA oscillations in a synaptically isolated AB; the effective dose varies with temperature.

A, The AB neuron was isolated by photoablation.
B and C, AB neuron was isolated by application of TTX+PTX. Low temperatures require higher FFA concentration to stop oscillations: A and B, at 16℃ the effective concentration of FFA was 30μM; C, at 21℃ 3 μM FFA was sufficient to block DA oscillations.

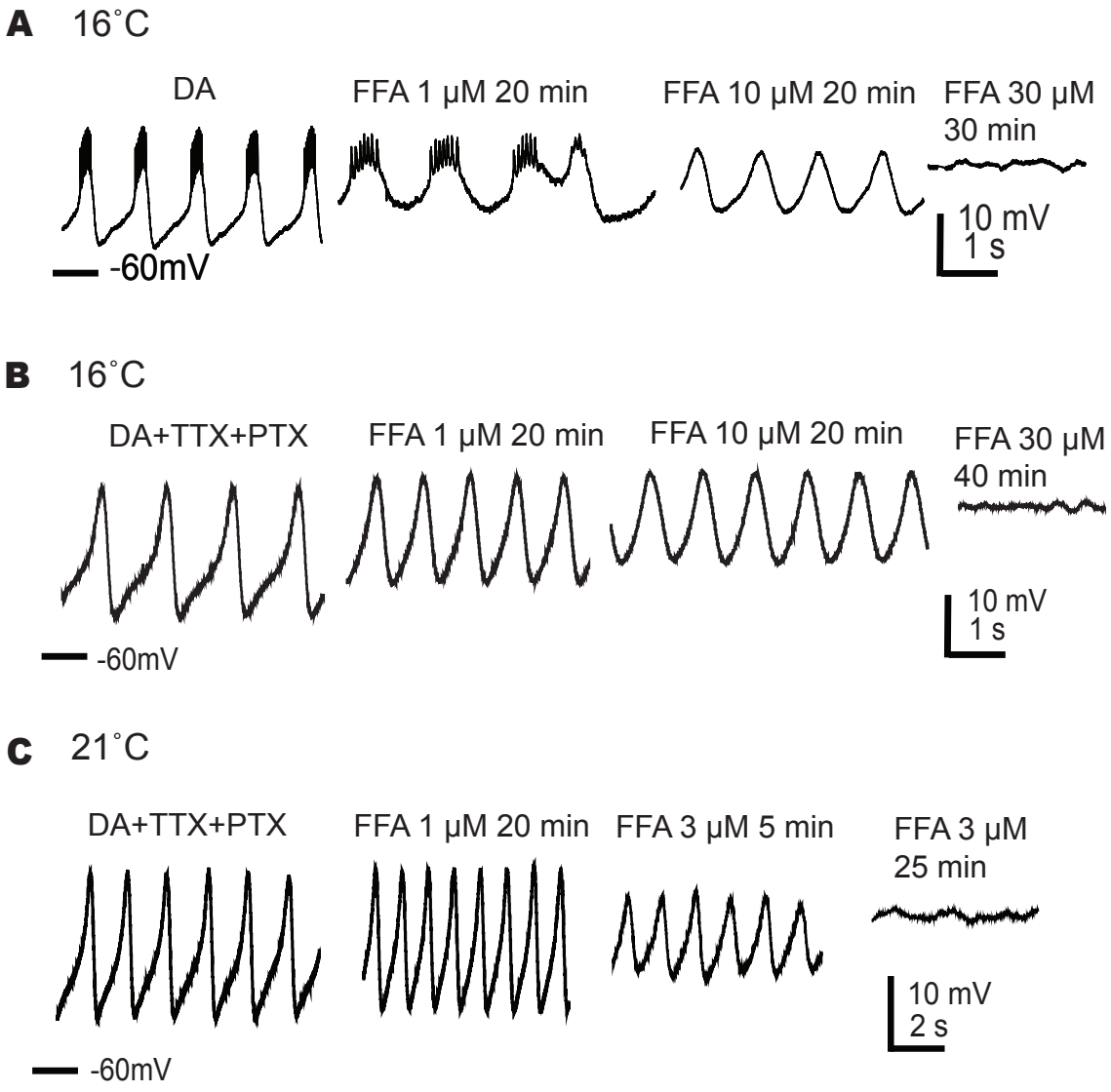
A 16˚C
DA
FFA 1 μM 20 min
FFA 10 μM 20 min
FFA 30 μM
30 min
10 mV
1 s
-60mV
B 16˚C
DA+TTX+PTX
FFA 1 μM 20 min
FFA 10 μM 20 min
FFA 30 μM
40 min
10 mV
1 s
-60mV
C 21˚C
DA+TTX+PTX
FFA 1 μM 20 min
FFA 3 μM 5 min
FFA 3 μM
25 min
10 mV
2 s
-60mV

the cell fell silent at -40-42 mV, near where the slow voltage wave peaked before FFA application during DA oscillations. This depolarization may be caused by an indirect block of $I_{K(Ca)}$ by FFA and subsequent depolarization of the V_m. To rule out the possibility that this depolarization was responsible for the cessation of bursting, I injected small negative current (usually 1-5 nA) to bring the V_m down to its pre-blocker trough values of -55-60 mV. Although early during FFA application, AB bursting could be rescued by hyperpolarizing the V_m, after 5-7 more minutes of FFA application, the cell became completely unable to burst or oscillate, even when hyperpolarized. This suggests that it is the FFA block of the inward current and not the possible secondary effect of depolarization that causes disruption of the rhythm.

Dopamine Enhances I_{CAN} despite its Inhibition of $I_{Ca(V)}$ in the AB

To further study the possible role of the I_{CAN} in pacemaker bursting, I looked at its modulation by DA. The general biophysical and pharmacological properties of the I_{CAN} have been described in Chapter 2 of this thesis.

Amplitude of I_{CAN}. I compared the peak amplitude of the CAN current before and during application of dopamine. The I_{CAN} amplitude was measured as the amplitude of the slow tail current after a depolarizing pre-step to 0 mV to activate the $I_{Ca(V)}$ (Fig. 3.2A, $I_{Ca(V)}$ is marked by an arrow and I_{CAN} by an arrowhead; voltage protocol shown in the small inset). In agreement with the previous results in our lab (Johnson *et al.* 2003), DA significantly reduced the amplitude of $I_{Ca(V)}$ (Fig. 3.2A, red trace, arrow). Despite this, the mean peak amplitude of I_{CAN} was larger in the presence of DA (Fig. 3.2A, red trace, arrowhead). For all 8 neurons tested, this effect of DA was statistically significant at voltages more hyperpolarized than -45 mV ($p<0.05$, Fig. 3.2B). For instance, at -65 mV, the

peak amplitude of I_{CAN} in DA was almost twice its amplitude under control conditions (Fig. 3.2C).

Voltage-dependent deactivation of I_{CAN}. I studied the rate at which I_{CAN} deactivates by measuring the time constant of decay of the current at different voltages following an activating pre-step to 0 mV (Fig. 3.3A, voltage clamp protocol; current traces from top to bottom: control, DA and washout). The decay of I_{CAN} most likely reflects the availability of calcium ions in the intracellular space near CAN channels. Within each treatment (control, DA and washout) there was no voltage-dependence of the time constants of decay (Fig. 3.3B; student's t-test, $p>0.05$, $n=7$ for each treatment). However, when I compared the mean time constants between treatments (control and DA), the time constant in DA was significantly slower compared to control at each voltage step. The difference became statistically significant (student's t-test, $p<0.05$, $n=7$) at -65 mV and more depolarized voltages (Fig. 3.3B, asterisks mark the steps where τ in DA was statistically different from the τ in control). Thus, despite the fact that DA inhibits most of the voltage-gated calcium current, the I_{CAN} in DA deactivates more slowly than before DA application.

Time-dependent inactivation of I_{CAN}. With prolonged voltage steps to 0 mV under control conditions, the voltage-dependent calcium currents inactivate, leading to a drop in amplitude of I_{CAN} when measured as the slow tail current at the end of the depolarizing step. The peak amplitude of I_{CAN} was measured from a series of depolarizing steps of increasing duration (Fig. 3.3C, series of current traces in control, upper panel, in DA, middle panel, and after DA washout, lower panel). Under control conditions, the mean peak amplitude of I_{CAN} decreased from -7.7±2 nA after a 100 ms pre-step to -3.7±2.1 nA after a 450 ms pre-step. This reduction in I_{CAN} amplitude with longer pre-steps most likely reflects inactivation of $I_{Ca(V)}$

Figure 3.2. DA enhances the amplitude of I_{CAN} while inhibiting $I_{Ca(v)}$.

A. Voltage clamp current traces under control conditions (black), DA (red) and after 30 minutes of washout (gray). Dopamine inhibited $I_{Ca(v)}$ (arrows), while enhancing the I_{CAN} amplitude (arrowheads). Data are not leak-subtracted. The voltage protocol used to measure I_{CAN} is shown in the small inset.

B. I_{CAN} current-tail step voltage relationship under control conditions (open squares), in 0.1 mM DA (closed circles) and after washout (gray triangles). All data points are mean+/-SE (n=8). Asterisks mark the voltage steps where the difference between control and DA was statistically significant ($p<0.05$, student's t-test).

C. Current amplitude at -65mV in DA and after washout as % of control amplitude. Double asterisk: significantly different from control ($p<0.05$, student's t-test).

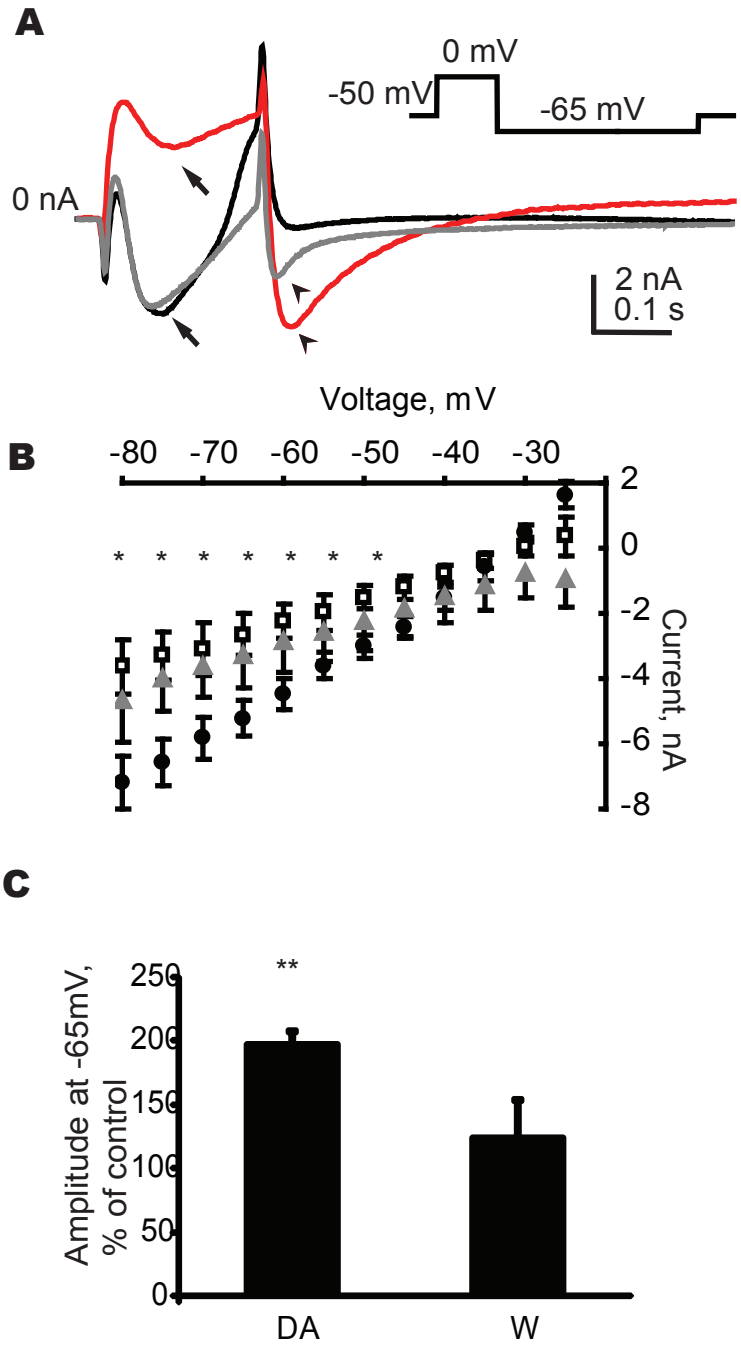
A
0 mV
-50 mV
-65 mV
0 nA
2 nA
0.1 s
Voltage, mV
B
-80
-70
-60
-50
-40
-30
2
0
-2
-4
-6
-8
Current, nA
C
Amplitude at -65mV,
% of control
250
200
150
100
50
0
**
DA
W

with time. Dopamine practically eliminated the time-dependent inactivation of I_{CAN} at longer depolarizing pre-steps; the mean peak amplitude of I_{CAN} stayed above 7.5 nA at all steps (Fig. 3.3D, open squares, under control conditions; closed circles, in the presence of DA; gray triangles, after washout). This effect was statistically significant for pre-steps of 200 ms duration and longer ($p<0.05$, n=7). For example, at the 350 ms pre-step, the mean peak amplitude of the tail current was 230±32% of the control value in DA and recovered to 144±43% after washout of DA. Thus, despite the clear inactivation of $I_{Ca(V)}$ with time, and dopamine's direct reduction of $I_{Ca(V)}$, I_{CAN} was enhanced by dopamine and became independent of the amplitude of $I_{Ca(V)}$.

The leak current amplitude. In addition to its enhancement of I_{CAN}, DA simultaneously inhibited the leak current. The leak current was measured at the end of 5 mV hyperpolarizing steps from a holding potential of -60mV or -55mV (Fig. 3.4A, current traces, arrowhead; voltage clamp protocol shown in the small inset). Under our experimental conditions, the mean conductance of the leak current measured at -65mV was 45±17 pS in control, 11±8 pS in dopamine and 41±23 pS after DA washout (Fig. 3.4B). This ~70% reduction in leak current in the presence of DA is larger than the 10% reduction previously reported in the AB (Peck *et al*. 2001, 2006).

Release of Calcium from Intracellular Stores is Essential for the Dopamine-Induced Bursting in AB

I hypothesized that in the presence of DA, I_{CAN} is activated by an increase in intracellular calcium concentration. This increase may occur as a result of either release of Ca^{2+} from intracellular stores such as the endoplasmic reticulum (ER) or mitochondria, or inhibiting Ca^{2+} sequestration and buffering in intracellular compartments, or both.

I initially assessed the involvement of the calcium stores in induction of bursting by disturbing the intracellular calcium balance in the oscillating AB. This was achieved in two ways: by chelating the intracellular calcium with BAPTA-AM and by blocking some of the calcium-handling proteins (channels and pumps) located on the ER membrane.

The endoplasmic reticulum membrane expresses two types of intracellular calcium release channels, Ryanodine receptor channels (RyR) and IP_3 receptor channels (IP_3R). The latter are activated by binding of the IP_3, a soluble product of the phospholipase C-mediated PIP_2 hydrolysis that occurs as a result of activation of GPCRs in the plasma membrane. RyR channels have an inverted U-shaped dose response activation curve: they are activated by low to medium and inhibited by high concentrations of cytoplasmic calcium. Ryanodine receptor channels also release calcium from the ER lumen to the cytoplasm upon binding of calcium ions to the receptor; high cytoplasmic calcium concentrations inhibit RyR. Free cytoplasmic calcium ions are taken up by the sarco-endoplasmic reticular ATP-ase, or SERCA, that pumps calcium back into the ER lumen. Thus either type of the ER calcium channel can activate first and potentiate the other type of calcium channel on the ER, creating a local calcium increase that can lead to the global rise in intracellular calcium.

To test the importance of an intracellular calcium rise during DA-induced bursting, I first applied BAPTA-AM, a membrane-soluble form of the fast calcium chelator. Bath application of 30 μM BAPTA-AM blocked ongoing dopamine oscillations in AB within 40 minutes. Fig. 3.5A shows a synaptically isolated AB that was induced to burst by DA; BAPTA effectively turned this bursting into tonic spiking (n=4).

Figure 3.3. DA un-couples the I_{CAN} deactivation from the $I_{Ca(v)}$.

A. The tail current (I_{CAN}) traces under control conditions (top), during 0.1 mM DA (middle) and after washout (bottom). Voltage clamp protocol is shown in the small inset.
B. Time constant of deactivation of the tail current vs. voltage steps. Under control conditions (open squares), there was no significant voltage-dependence of deactivation of the tail current. In 0.1 mM DA the time constant of deactivation of the tail current was significantly slower at -65 mV and more depolarized voltages (closed circles); the effect was reversible (gray triangles). Asterisks: significantly different from control ($p<0.05$, student's t-test).
C. I_{CAN} amplitude as a function of the duration of the activating pre-step to 0 mV. The pre-step duration was varied from 100 to 550 ms (small inset) followed by a step to -80 mV to measure the slow tail current. I_{CAN} traces under control conditions (top), 0.1 mM DA (middle) and after washout (bottom).
D. Under control conditions, the I_{CAN} amplitude decreased with longer pre-steps (open squares) reflecting the inactivation of $I_{Ca(V)}$ during the pre-step. In contrast, in DA the amplitude remained at the same level at all pre-step durations (closed circles). The difference between current amplitude in control and DA was significant for pre-steps longer than 200 ms (marked by asterisks).

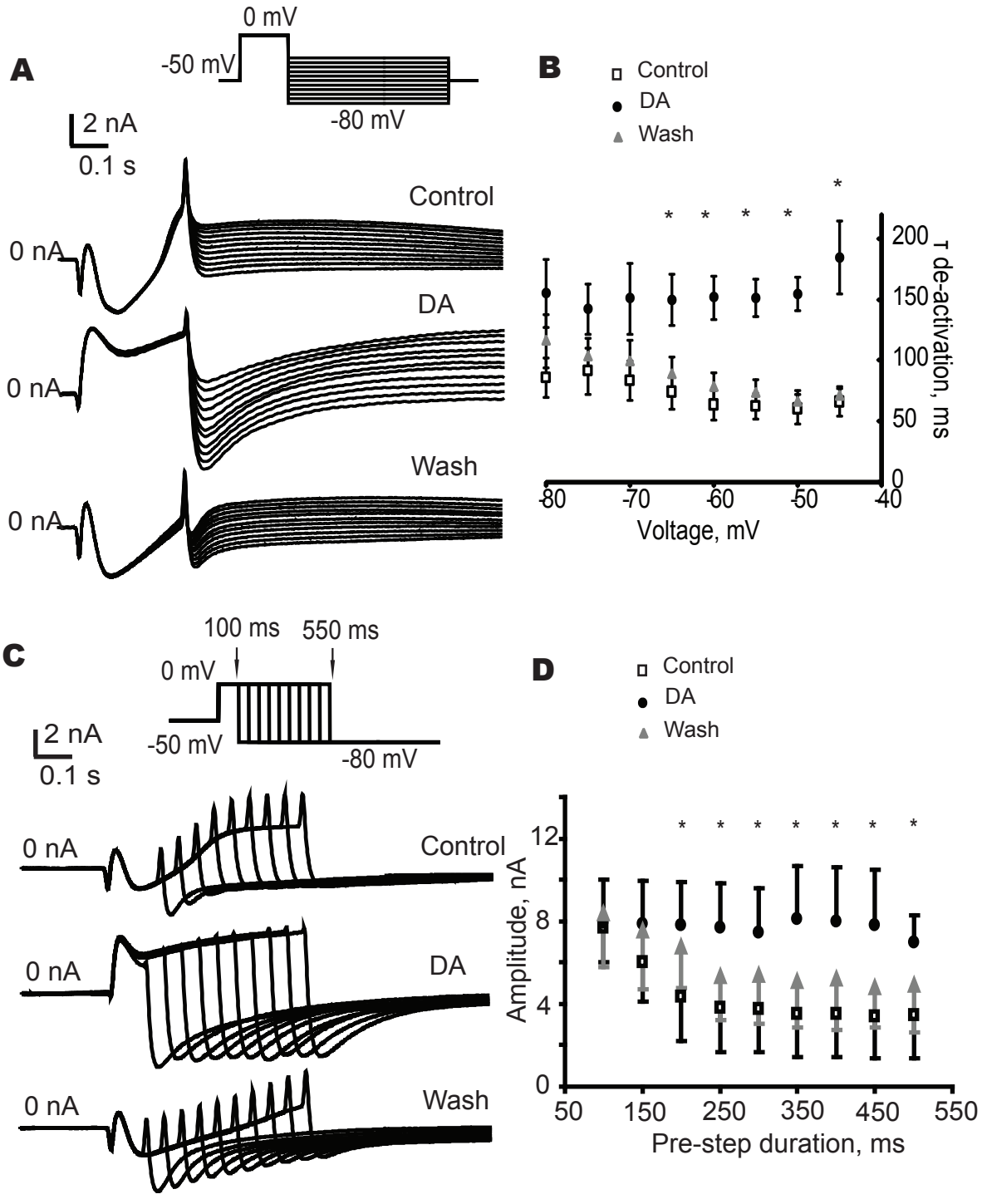
A
0 mV
-50 mV
-80 mV
2 nA
0.1 s
Control
0 nA
DA
0 nA
Wash
0 nA
B
Control
DA
Wash
τ de-activation, ms
200
150
100
50
0
-80
-70
-60
-50
-40
Voltage, mV
C
100 ms
550 ms
0 mV
-50 mV
-80 mV
2 nA
0.1 s
0 nA
Control
0 nA
DA
0 nA
Wash
D
Control
DA
Wash
Amplitude, nA
12
8
4
0
50
150
250
350
450
550
Pre-step duration, ms

Next, I applied Ryanodine, a specific blocker of the RyR, to the DA-induced oscillating AB neuron (in this and the following examples, TTX and PTX were applied to block synaptic transmission as another way to isolate the AB from all inputs). DA-induced AB bursting was highly sensitive to Ryanodine; 1nM stopped oscillations within an an hour and a half, while 1nM or higher blocked took around 40 minutes to block the rhythm. (n=7, Fig. 3.5B). Xestospongin C (XeC) is a specific IP_3R blocker (Gafni et al., 1997); 10μM XeC effectively halted DA rhythm in AB neuron (n=3, Fig. 3.5C). Finally, application of 1μM Thapsigargin, a specific blocker of SERCA pump, stopped an on-going DA oscillation within 40-50 minutes (n=3, Fig. 3.5D). In sum, these data suggest that release of intracellular calcium via RyRs and IP_3Rs is essential for dopamine-induced oscillations in the AB neuron.

Calcium Imaging Reveals an Increase of Intracellular Calcium Concentration in Fine Neurites in the Presence of Dopamine

To directly test the possibility that dopamine induces an increase in the intracellular Ca^{2+} concentration, I collaborated with Alex Kwan (Dept of Biophysics, Cornell) to carry out two-photon laser confocal microscopic imaging of intracellular calcium activity in the AB neuron, using calcium-sensitive indicator dyes. Briefly, we loaded the AB neuron with a calcium indicator dye (Calcium Green-1 or Indo-1, both in potassium salt form), let the dye diffuse for 30 min to 1hr, and performed synchronized imaging and electrophysiological recordings. For Calcium Green-1, the preparation was excited at 800 nm and the fluorescence was collected between 500-650 nm. For the emission ratiometric calcium indicator Indo-1, the preparation was excited at 720 nm and the fluorescence was separated into two detection channels, 360-430 nm and 485-505 nm. The absolute calcium concentration could be calculated from the ratio of

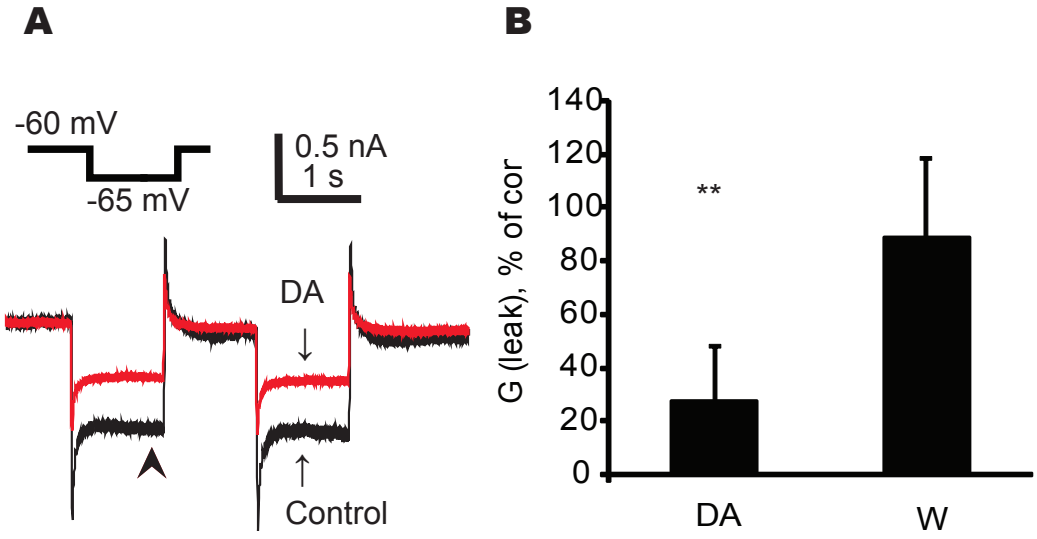

Figure 3.4. DA reduces the leak current in the AB neuron.

A. Current traces under control conditions (black) and during 0.1 mM DA (red) in response to step hyperpolarizations from -60 to -65 mV. Measurements were taken at the end of the step (arrowhead).

B. Leak conductance is significantly lower in the presence of DA ($p<0.05$, $n=5$, studet's t-test)

fluorescence $R=F_{395}/F_{495}$, as described in the Materials and Methods of this Chapter.

Distribution and strength of the calcium signal in the AB neuron

The dye-filled cell body and neurites showed clear calcium fluorescence in both oscillating intact and DA-stimulated AB neurons. The signal from the cell body and primary neurites was mostly saturated and we were unable to detect any oscillation-related fluorescence changes there; this is consistent with previous results suggesting that the oscillations arise outside the soma, in the neuropil. As a consequence all our measurements were done in small neurites with diameter less than 5μM, at distances from the soma of more than 500 μm.

We performed time-lapse measurements of fluorescence in fine neurites before and during dopamine wash-in, combined with simultaneous V_m recordings from the cell soma. Fig. 3.6 shows an example of the AB soma and its extensive dendritic tree filled with Indo-1 (A, fluorescence from 395 channel), where yellow arrowheads show approximate regions of calcium imaging and the dashed line demarcates the region enlarged in B and C). The calcium signals from 19 regions of interest were measured in this fragment; some of the ROIs are highlighted by different colors in Fig.3.6B. The fluorescence was separated into two detection channels, 395 nm and 495 nm (Fig. 3.6C upper and lower panels respectively) for determination of the calcium concentration.

Base level of intracellular calcium rises during DA application

Upon dopamine application, all small neurites visible under control conditions (pre-DA), displayed increases in calcium fluorescence of varying amplitude. From the total of 27 neurites from three different AB neurons, fluorescence measurements were taken at five time points: 1) when the neuron was spontaneously bursting in the physiological saline; 2) in the synaptically isolated

Figure 3.5. Release of calcium from intracellular stores is essential for DA-induced AB bursting.

A. 30 µM BAPTA-AM (BAP) blocked DA-induced bursting in a synaptically isolated AB. In this experiment, the AB neuron was isolated from all synaptic and descending neuromodulatory inputs by photoablation of the PD and VD neurons and local application of TTX to the STN.

B, C and D. 10 nM Ryanodine (Ry), 10 µM Xestospongin C (XeC) and 1µM Thapsigargin (Tg) blocked DA-induced oscillations in the AB. In these experiments, the AB was isolated by application of TTX and PTX.

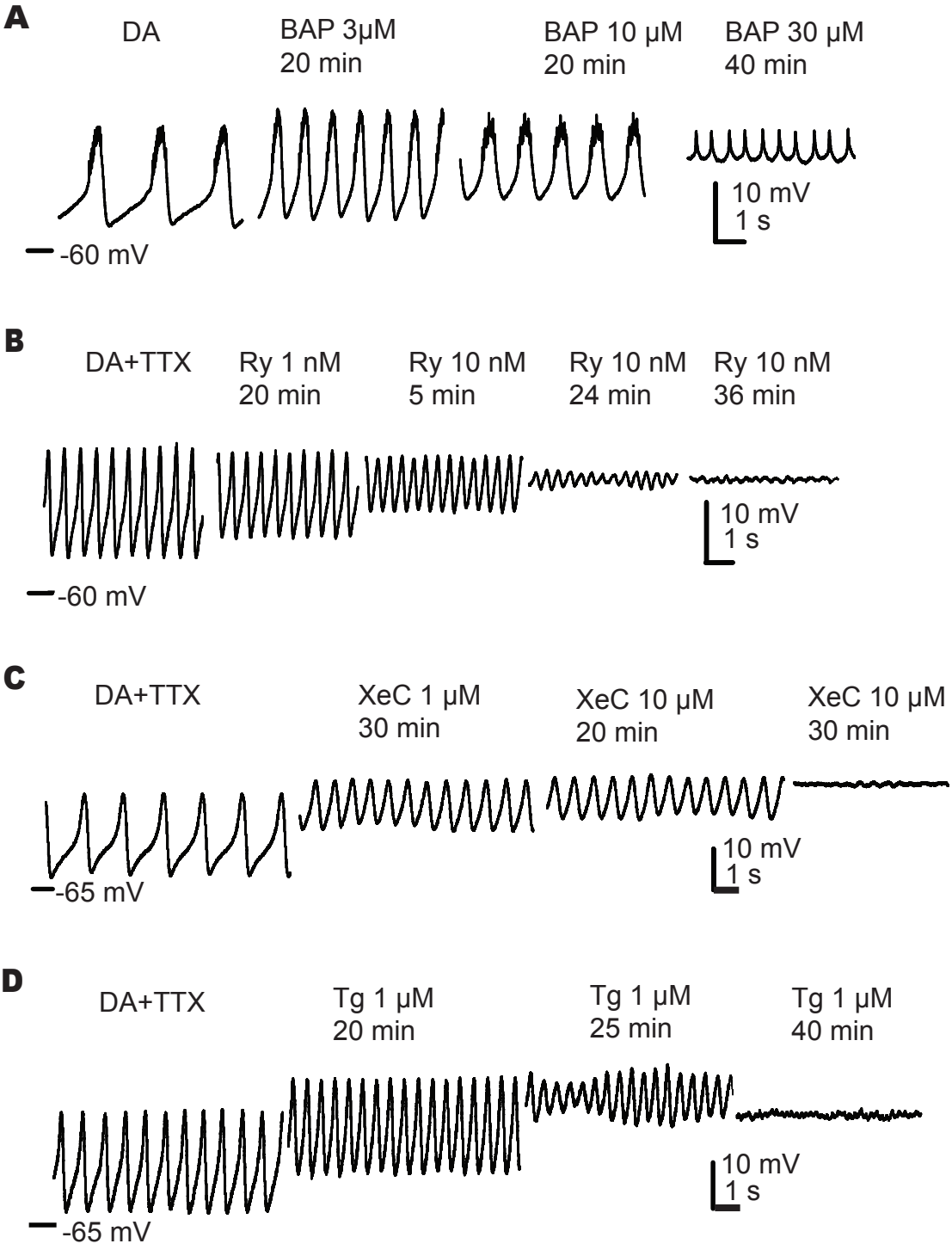
A
DA
BAP 3μM
20 min
BAP 10 μM
20 min
BAP 30 μM
40 min
10 mV
1 s
-60 mV
B
DA+TTX
Ry 1 nM
20 min
Ry 10 nM
5 min
Ry 10 nM
24 min
Ry 10 nM
36 min
10 mV
1 s
-60 mV
C
DA+TTX
XeC 1 μM
30 min
XeC 10 μM
20 min
XeC 10 μM
30 min
10 mV
1 s
-65 mV
D
DA+TTX
Tg 1 μM
20 min
Tg 1 μM
25 min
Tg 1 μM
40 min
10 mV
1 s
-65 mV

quiescent AB in TTX; 3) at the start of the first burst during DA wash-in; 4) during stable bursting in dopamine; 5) in a quiescent AB after DA was washed out of the bath saline (Fig.3.7A, Saline, TTX, DAstart, DAosc, Wash, respectively).

Variability in calcium handling in different neurites

For individual neurites, when averaged calcium measurements were taken at slow speed (6-10 images/sec) the DA-induced increase in calcium concentration ranged from 136% to 555% of the pre-DA TTX+PTX control, with an average of 302% (n=27 ROIs, three AB neurons). Fig. 3.7B shows an example of measurements from 10 different neurites (labeled with different colors) in a single cell. The changes in $[Ca^{2+}]_{in}$ were monitored in parallel with voltage recordings; DA was added to the bath solution at the first arrowhead, labeled "DA in"); DA wash out started the second arrowhead, labeled "DA out"). The values of $[Ca^{2+}]_{in}$ were plotted for each of 10 neurites at three time points: under control conditions, during DA oscillations near the end of the DA perfusion period, after washout when DA oscillations stopped (white, black and gray bars, respectively, Fig. 3.7 B and C). The different dendrites showed variable rises in Ca^{2+} before the neuron started to oscillate; once stable oscillations were established, all the neurites showed a significant increase of $[Ca^{2+}]_{in}$ levels. Thus, different neurites of a single neuron showed marked variability in calcium handling both under control conditions and in the presence of dopamine.

The onset of $[Ca^{2+}]_{in}$ rise precedes the onset of bursting

For the large majority of neurites (25 out of 27), the rise in $[Ca^{2+}]_{in}$ started before the emergence of voltage oscillations and bursting. Fig. 3.8A shows synchronized V_m and $[Ca^{2+}]_{in}$ recordings during the onset of DA application. Calcium started rising about 3 minutes from the moment DA was added to the

Figure 3.6. Anterior Burster neuron filled with calcium indicator Indo-1.

A. Z-stack of the AB neuron labeled with Indo-1, showing fluorescence from the 395 channel. Cell body with a bright nucleus is in the lower left corner. The primary and secondary neurites along with an extensive dendritic tree is clearly labeled throughout. The yellow arrowheads mark the approximate regions of fine neuropil where calcium measurements were typically taken. The bar is 100 μm. The region in the yellow square is shown enlarged in B and C.

B. Fragment of the fine neuropil with some of the regions of interest (ROIs) traced and filled with different colors. The calcium signals from 19 regions of interest were measured in this fragment; the red square is the RIO where the background signal was detected and subtracted before the 395/495 ratios were calculated (for the level of background signal for each channel see B).

C. The same fragment of the fine neuropil where calcium signal was detected from two channels – 395 nm (top) and 495 nm (bottom). The bar is 25 μm. Changes are seen primarily in the 395 nm channel after blockade of synaptic input with TTX, and again after adding 0.1 mM DA.

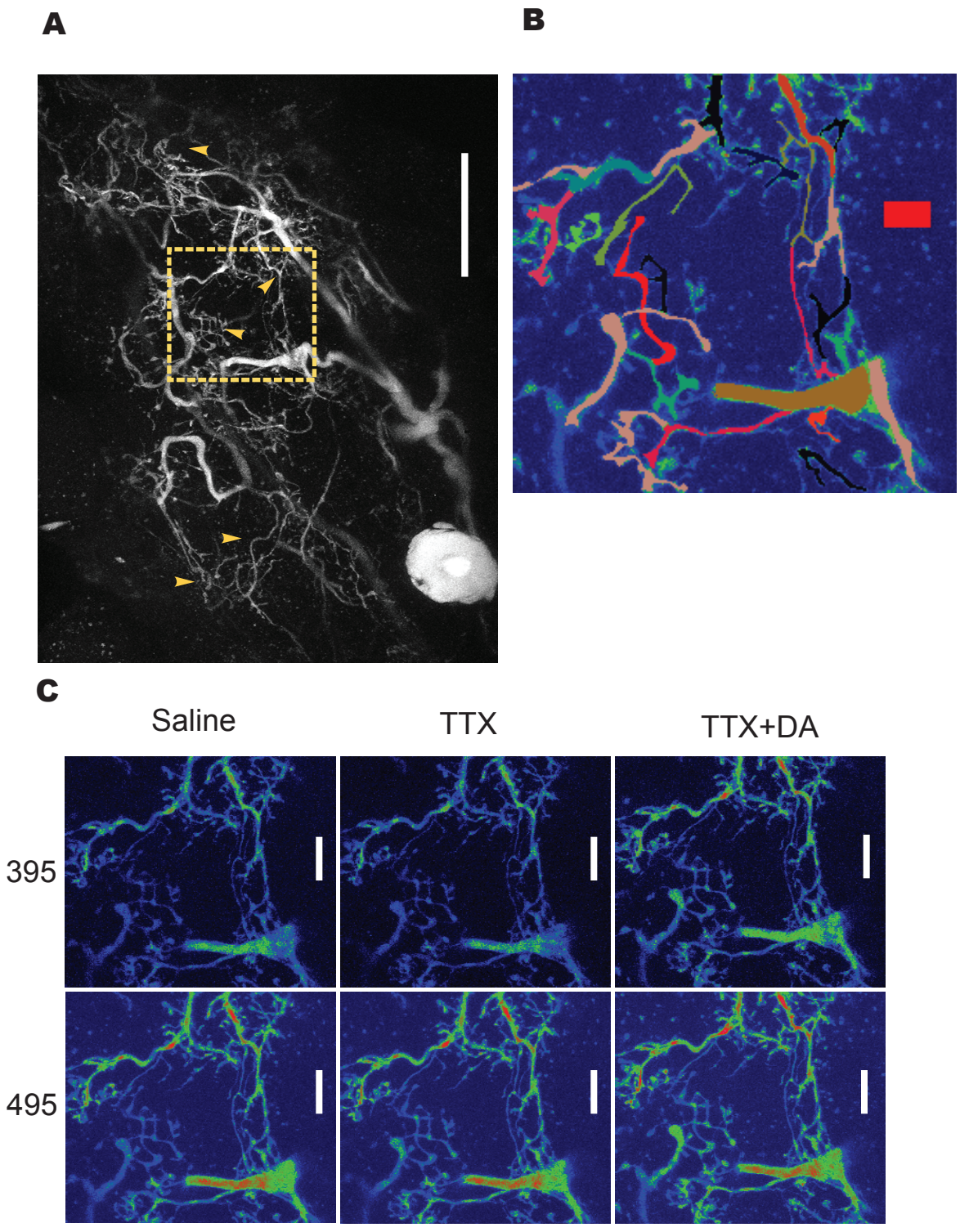
A
B
C
Saline
TTX
TTX+DA
395
495

Figure 3.7. DA induces intracellular Ca^{2+} accumulation in fine neurites.

A. Calcium concentrations calculated from the total of 27 neurites from three different AB neurons (nM). From each of three AB neurons, fluorescence measurements were taken at five time points: 1) when the neuron was spontaneously bursting in the physiological saline (Saline); 2) in the synaptically isolated quiescent AB (TTX); 3) at the start of the first burst during DA wash-in (DAstart); 4) during stable bursting in dopamine (DAosc); 5) in a quiescent AB after DA was washed out of the bath saline (Wash). Asterisks, statistically significant difference, $p<0.05$.

B. The time course of the calcium signal detected from 10 neurites of a single neuron is displayed: before DA (white bar), in 0.1 mM DA during stable oscillations (black bar) and after washout (gray bar). First arrow marks the time when DA was added to the bath (DA in) and the second arrow marks the time when DA was removed from the saline (DA out). Calculated calcium concentrations from each neurite are represented by a different color. Some neurites (for ex, the dark blue marker) showed a steeper and larger response to DA than others (for ex, the brown marker).

C. For each of the 10 neurites, the $[Ca^{2+}]_{jn}$ is plotted at three time points: before DA (white bars), during DA oscillations (black bars) and after washout (gray bars). Note the differences in $[Ca^{2+}]_{jn}$ both in control and in DA and the full reversal of the DA effect.

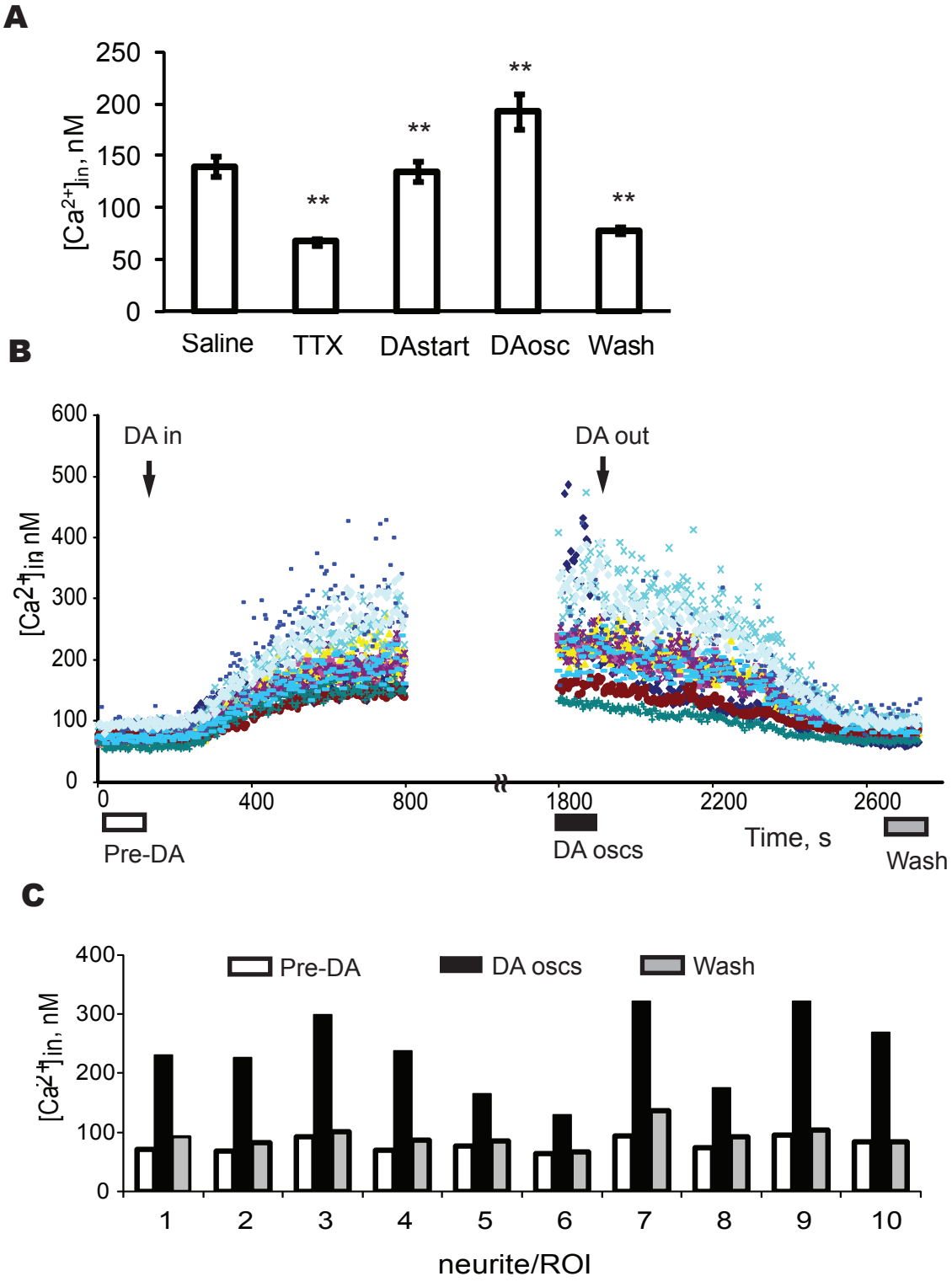
A
250
200
150
100
50
0
[Ca2+]in, nM
**
**
**
**
Saline
TTX
DAstart
DAosc
Wash
B
600
500
400
300
200
100
0
[Ca2+]in nM
DA in
DA out
0
400
800
1800
2200
2600
Time, s
Pre-DA
DA oscs
Wash
C
400
300
200
100
0
[Ca2+]in, nM
Pre-DA
DA oscs
Wash
1
2
3
4
5
6
7
8
9
10
neurite/ROI

bath. The interval between the start of the calcium increase and the onset of bursting is highlighted with a light gray bar. On average, bursting started 108±12 s after the onset of calcium rise in fine neurites (n=27 neurites, three AB neurons). The earlier onset of calcium rise in fine neurites – more than 1.5 minutes before emergence of bursting, suggests that the rise in the intracellular calcium concentration might bring about depolarization and rhythmic oscillations of the membrane potential. Dopamine's effect was completely reversible: washing DA out of the bath solution abolishes the membrane potential oscillations and brings the levels of $[Ca^{2+}]_{in}$ back to pre-DA levels (Fig. 3.8D). Notably, the degree of DA-induced calcium increase increased with the frequency of bursting: more neurites exhibited higher calcium increase during stable oscillations (Fig 3.9).

Effect of pre-treatment with Ryanodine and Xestospongin C on dopamine bursting

Our model for AB bursting predicts that pre-treatment with a cocktail of intracellular calcium channel blockers (Ryanodine and Xestospongin C) would prevent the dopamine-induced increase in calcium levels and subsequent bursting. In two cells that were pre-treated with a cocktail of 10 μM Ryanodine and 10 μM Xestospongin C for 30 min, DA elicited a modest calcium increase and voltage oscillations that were somewhat slower than usual (frequency about 0.1-0.5Hz). With continued application of the blockers and DA for an hour, the DA-evoked oscillations stopped and the calcium concentration levels decreased to 113±40 nM (Fig. 3.10A, B). In our next experiment (Fig. 3.10C) we incubated the ganglion with Ryanodine and Xestospongin for one hour before applying dopamine. This longer pre-treatment abolished the DA-evoked increase in intracellular calcium: the mean calcium concentration was 82±11 nM before DA

Figure 3.8. The onset of the DA-induced calcium rise precedes the onset of membrane potential oscillations.

A. The time course of the voltage (top) and $[Ca^{2+}]_{in}$ change during DA application. 0.1 mM DA was added to the bath at zero time. Note that in the region highlighted with light gray, calcium concentration started rising before emergence of bursting. Voltage oscillations initially are slower and later the rhythm picks up (shown in B on a faster time scale).

B. Voltage oscillations from A on a faster time scale (fragment corresponds to the horizontal bar above the voltage trace in A).

C. Fragment of the fine neuropil of the cell from A, where the calcium measurements were taken. Top is the fluorescence from the 395 channel; bottom is the same image with the neurites color labeled: these correspond to the calcium markers on the calcium plots in A and B. In this cell, the red RIO showed the steepest and the fastest rise in calcium signal; the red line is a sigmoidal fit of the data points from the red neurite.

D. As DA was washed out of the bath solution, the voltage oscillations and calcium signal gradually decreased back to their pre-DA levels.

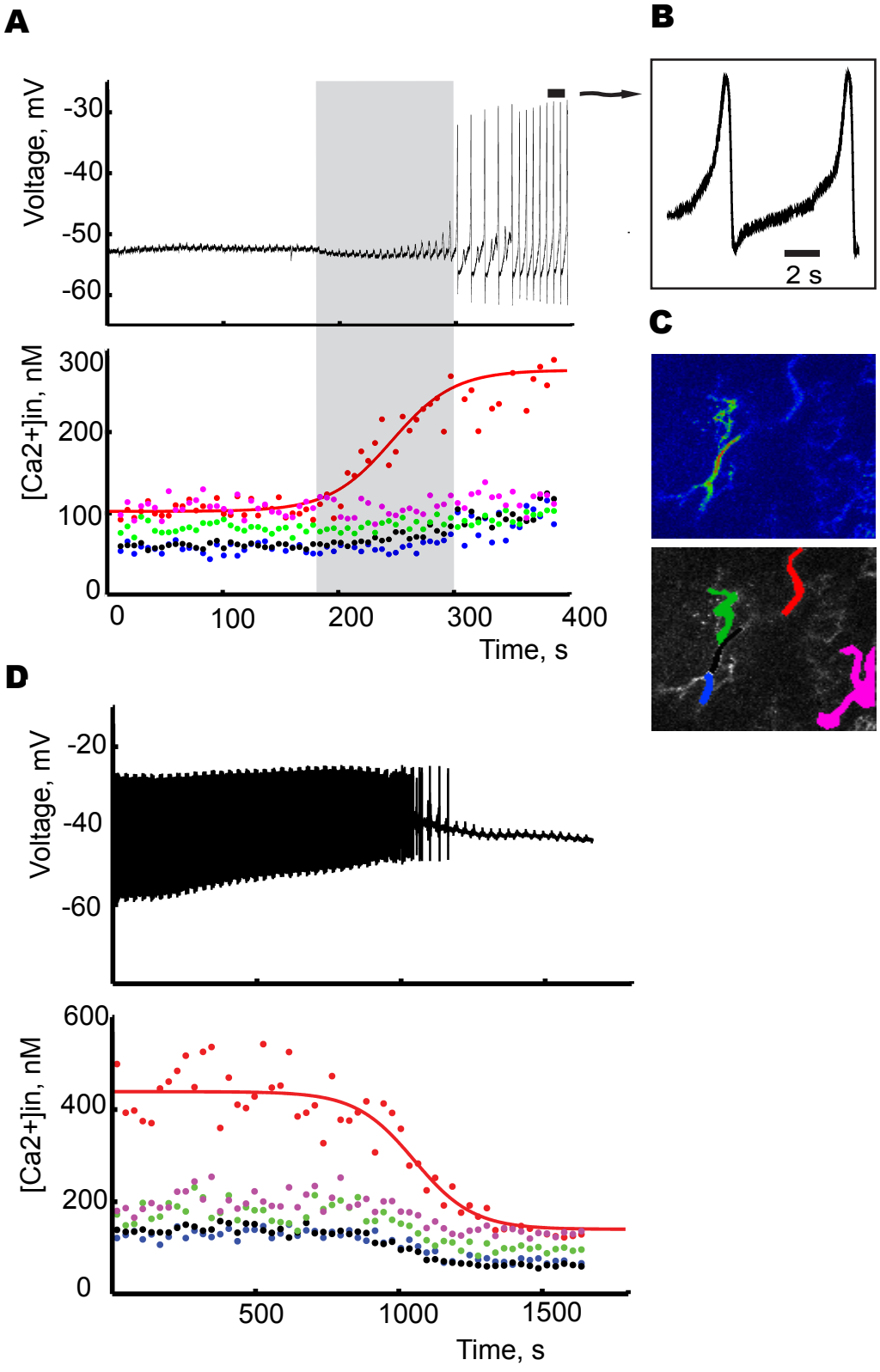
A
B
C
D
Voltage, mV
-30
-40
-50
-60
[Ca2+]in, nM
300
200
100
0
0
100
200
300
400
Time, s
2 s
Voltage, mV
-20
-40
-60
[Ca2+]in, nM
600
400
200
0
500
1000
1500
Time, s

and 87±17 nM in the presence of DA ($p>0.05$, n=10 RIOs, one neuron). DA failed to evoke voltage oscillations in this AB neuron, although the V_m slightly depolarized from -58 mV before DA to -50 mV in dopamine, possibly because of dopamine's effect on other ionic currents (Fig. 3.10B).

High temporal resolution imaging of intracellular calcium levels with simultaneous recording of membrane potential in the bursting AB

We used Calcium Green (CG) -1 to track calcium changes on a faster time scale (cycle-by-cycle) during spontaneous and DA-evoked AB oscillations. As above, we did not detect any calcium oscillations in the cell soma or primary neurites, but the fluorescence signal in fine neurites revealed clear oscillatory behavior with a frequency identical to that of the membrane potential oscillations.

To look at the calcium changes on a finer time scale, we used a fast line scan (frequency 164 Hz) to monitor calcium activity in the fine neurites along with synchronized recordings of voltage membrane in the soma. We have found that the change in fluorescence level dF/F in the spontaneously bursting AB oscillated with the same frequency as the voltage did (Fig. 3.11A). Application of TTX and PTX to eliminate descending modulatory inputs effectively blocked both voltage and calcium oscillations within less than 10 minutes (Fig. 3.11B). Addition of DA restored rhythmic bursting of voltage along with calcium oscillations (Fig. 3.11C). Notably, the peaks (i.e. maxima) of the calcium oscillations were phase-delayed by 150 ms relative to the peaks of the membrane potential oscillations. This was true for both spontaneous physiological bursting (Fig. 3.11A) and DA-induced bursting in the presence of TTX and PTX (Fig. 3.11C) and is summarized in Fig. 3.12. Ryanodine treatment of the bursting pacemaker in the continued presence of DA halted both calcium and voltage oscillations within 40 minutes (Fig. 3.11D). Calcium oscillations had a similar delayed time course and

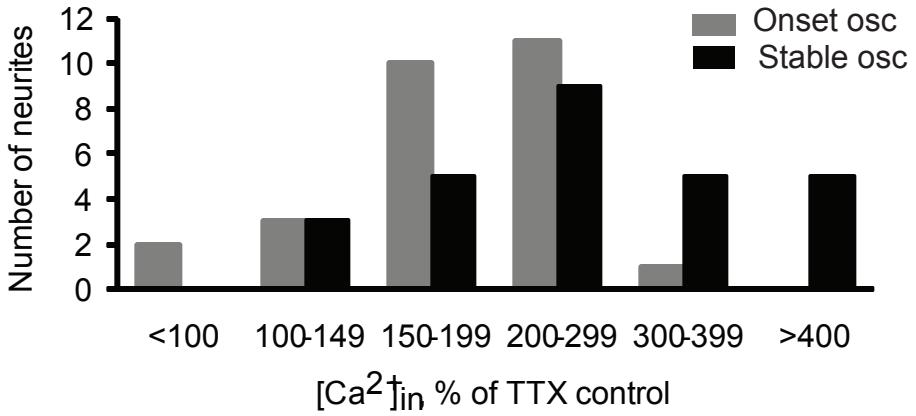

Figure 3.9. Degree of calcium rise increases with bursting intensity. Histogram view of [Ca2+]in in dopamine, at the onset of oscillations (gray bars) and during stable oscillations (black bars). At the start of bursting, the calcium signal from majority of neurites reached 150-300% of calcium levels in TTX; two neurites showed a decrease in calcium levels while only 1 increased calcium levels by more than 300%. 30 minutes after the onset of bursting, after DA oscillations stabilized, all neurites showed an increase in calcium signal, and 10 had increases above 300% of calcium levels in TTX. Measurements were taken from 27 neurites, three different AB neurons.

amplitude in both a spontaneously bursting AB neuron and a synaptically isolated AB in the presence of DA (Fig. 3.12, spontaneous bursting and DA-induced oscillations, red and black traces, respectively)

DISCUSSION

I studied dopamine's induction of bursting and oscillations in the pyloric pacemaker AB neuron, and explored the possible mechanisms of this effect. The CAN current is thought to be important in pacemaker bursting because of its biophysical properties of slow activation by accumulation of intracellular calcium and voltage-independence. I_{CAN} is permeable to cations including calcium and thus is capable of positive feedback and self-activation (Partridge *et al,* 1994). To test the involvement of I_{CAN} and intracellular stores in DA bursting, I first looked at dopamine's effects on biophysical properties of this current. Next I explored the sources of calcium accumulation necessary for I_{CAN} activation by chelating intracellular Ca^{2+} or blocking the intracellular calcium release channels, and tested whether these actions disrupt or prevent DA bursting. Finally, to directly measure dopamine's effects on levels of intracellular calcium, I collaborated with Alex Kwan to carry out two-photon calcium imaging and electrophysiological recordings of the AB neuron before and during dopamine application.

The FFA-sensitive I_{CAN} is essential in pacemaking and is enhanced by DA

There are two lines of evidence that I_{CAN} is a potential dopamine target in generating bursting in the AB neuron. First, FFA terminated ongoing dopamine-evoked oscillations in the AB neuron, suggesting that the CAN current contributes to membrane depolarization and rhythmogenesis (Fig. 3.1). I showed in Chapter 2 that FFA blocks I_{CAN} with an IC_{50} of 16±7 μM (Fig. 2.1E). The concentration of FFA needed to block the ongoing DA oscillations (3-10 μM) is sufficient to block at least one third of the peak amplitude of I_{CAN}. Thus, in spite

Figure 3.10. Pre-treatment with intracellular calcium channel blockers dampens or prevents the rise in $[Ca^{2+}]_{in}$ and voltage oscillations during DA application.

A. Dopamine-induced voltage and calcium changes in a neuron pre-incubated with 10 μM Ryanodine and 10 μM Xestospongin C for 30 minutes before DA application. Upon application of DA, $[Ca^{2+}]_{in}$ increased and the neuron began to burst, but with continued application of the blockers, DA-induced bursting stopped and the calcium signal decreased to its pre-DA levels (10 neurites from 2 AB neurons). DA was added at time 0.
B. Another AB neuron was incubated in the same blocker cocktail for 60 minutes. After this longer pre-incubation, calcium levels did not differ from the levels under control conditions (in TTX) and application of dopamine did not induce an increase of calcium or any voltage oscillations. Note the small depolarization of V_m in DA, probably due to direct effects of DA on other ionic currents (n=10 neurites from a single neuron). DA was added at time 0.
C. Mean calcium concentration in nM under control conditions (TTX, 20 neurites from 3 neurons); after 60 min pretreatment in Ryanodine and Xestospongin C (RyXe, 10 neurites from one neuron, shown in B); in DA (and Ry+Xe) while the cells were oscillating (DAo1, n=10, 2 neurons); 40 min later in DA (and Ry+Xe), oscillations and $[Ca^{2+}]_{in}$ decreased (DAo2, 10 neurites from 2 neurons); in DA and Ry+Xe when AB was quiescent (DAq, n=20, 3 neurons). Asterisks, statistically significant change ($p<0.05$): DAo1 was different from RyXe, DAq was different from DAo2. Note that DAo1 and DAo2 were not statistically different ($p>0.05$).

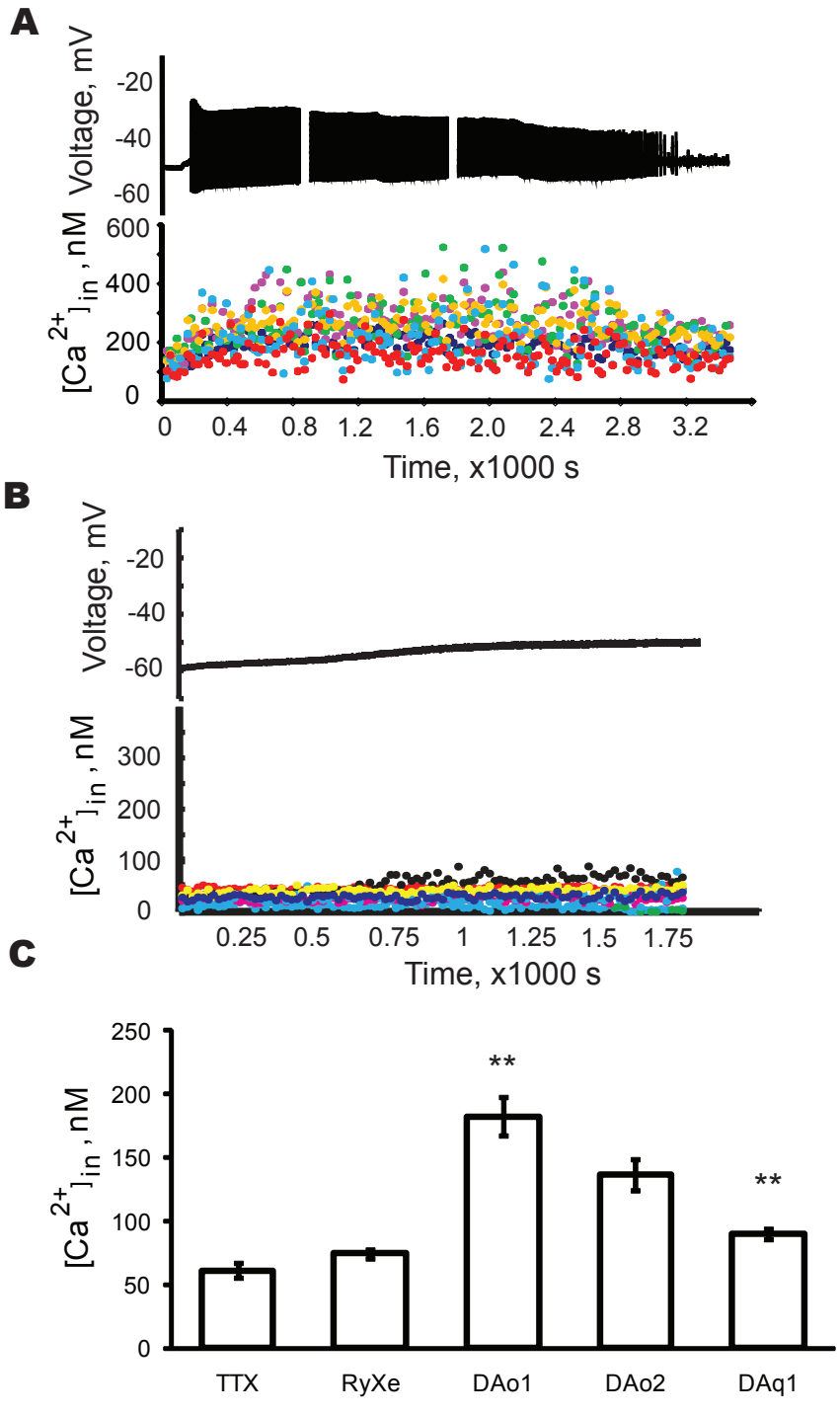
A
Voltage, mV
-20
-40
-60
[Ca2+]in, nM
600
400
200
0
0
0.4
0.8
1.2
1.6
2.0
2.4
2.8
3.2
Time, x1000 s
B
Voltage, mV
-20
-40
-60
[Ca2+]in, nM
300
200
100
0
0.25
0.5
0.75
1
1.25
1.5
1.75
Time, x1000 s
C
[Ca2+]in, nM
250
200
150
100
50
0
**
**
TTX
RyXe
DAo1
DAo2
DAq1

of small amplitude of this current in AB neuron (about -3nA on average), its partial block by FFA was sufficient to halt the dopamine rhythm.

FFA specificity. In both invertebrates and vertebrates FFA is routinely used at 100–500 μM (Derjean et al. 2005; Ghamari-Langroudi and Bourque 2002; Green and Cottrell 1997; Morisset and Nagy 1999; Partridge and Valenzuela 2000; Shaw et al.1995). However, at higher concentrations FFA has multiple side effects. For instance, in the lamprey spinal cord, FFA partially inhibited calcium channels and NMDA receptors at the concentration of 100-200 uM (Wang et al., 2006). In cultured kidney cells, it affected the K(Ca) channels with a U-shaped dose response: in enhanced the conductance at concentrations below 10 uM and above 50 uM, and inhibited the activity in the intermediate range (Kochetkov et al., 2000). FFA appears to induce release from calcium stores in *Aplysia* bag neurons at 300 uM (Gardam et al., 2008) and in circumesophageal ganglion *of Helix aspers* at 500uM, but not at 100uM (Shaw et al., 1995; Lee at el., 1996). At 85uM, FFA triggered calcium release from isolated mouse brain mitochondria (Tu *et al.,* 2009). I attempted to avoid these non-specific effects by using much lower FFA concentration (10-30 uM).

Notably, after bursting was terminated by FFA, the neuron's membrane potential hung up at around -40-42 mV (Fig. 3.1), which is the upper voltage limit of the slow oscillatory wave under normal conditions. This raises the possibility that the real cause of the rhythm block by FFA may be a lack of calcium supply to the $I_{K(Ca)}$ that would normally repolarize the potential to its resting state. This end-point depolarization was also seen, although to varying degrees, in all the experiments where I blocked AB bursting by blocking release of calcium from intracellular stores (Fig. 3.5 A-D). It is possible that when I_{CAN} was blocked by FFA, the threshold potential and the level of $[Ca^{2+}]_{in}$ necessary for activation of

$I_{K(Ca)}$ were not reached. Everything that blocks accumulation of intracellular Ca seems to block $I_{K(Ca)}$, and the FFA effect may be via that common need for Ca, so the two may be secondary to the level of the intracellular calcium. If FFA's indirect block of $I_{K(Ca)}$ was the real cause of its block of the AB oscillations, then repolarization of the AB neuron would restore oscillations. This did indeed occur when hyperpolarizing current was injected at the time the neuron had just stopped oscillating. However, within 5-10 minutes, when the FFA block was more complete, the cell failed to burst even when hyperpolarized. This suggests that the main cause of the FFA blocking effect was not the block of a calcium-activated outward current, but the block of I_{CAN}.

A second line of evidence for the important role of I_{CAN} in DA-induced AB bursting comes from the fact that DA significantly enhanced the I_{CAN} amplitude (Fig. 3.2) and slowed down its deactivation (Fig. 3.3). Interestingly, the I_{CAN} peak amplitude almost doubled during DA application, in spite of dopamine's inhibition of the voltage-gated calcium current in AB (Johnson *et al*. 2003). Monoamine-induced modulation of the CAN channels were observed in Aplysia neuron R15 (Lotshaw *et al.,* 1986) and Helix bursting neurons (Partridge *et al.,* 1990). This may occur due to GPCR-mediated channel phosphorylation which can directly target the gating particle of the channel or result in changes in the Hill coefficient of the calcium-binding sites similar to K(Ca) channels, altering the calcium-dependence of the channel function (Reinhart *et al.,* 1991; Golowasch *et al.,* 1986). In the AB neuron, the larger amplitude and significantly slower deactivation kinetics of I_{CAN} in DA suggest that dopamine basically un-coupled I_{CAN} from its normal activation by $I_{Ca(V)}$, making its functional state less dependent on the voltage-gated calcium entry.

Dopamine-induced Rise in Intracellular Calcium is Central for Pacemaker Bursting

Several bursters rely on intracellular calcium stores as a source of calcium ions necessary for I_{CAN} activation in both invertebrates (Swandulla and Lux, 1985, Partridge and Swandulla, 1987, Yazenian and Bayerly 1989, Partridge & Valenzuela 1999, Levy 1992, Sawada *et al* 1990) and vertebrates (Pena *et al.*, 2004, Pace *et al.,* 2007, Del Negro *et al.*, 2008; Rubin *et al.*, 2009).

In the AB neuron, application of the calcium chelator (BAPTA-AM) or intracellular calcium channel blockers (Ry, Xe, Tg) blocked DA oscillations. Although low concentrations of Ry and Tg initially increased the amplitude and frequency of bursting, possibly due to a brief increase in $[Ca^{2+}]_{in}$, with longer treatment or higher dose they ultimately blocked DA oscillations in the AB. Direct evidence of the importance of intracellular calcium stores came from calcium imaging of the AB neuron in its two states – quiescent and bursting. In a spontaneously bursting AB (with all synaptic and neuromodulatory inputs intact) the calcium levels in fine neurites were on average around 150 nM as estimated by our Indo-1 experiments. Application of TTX lowered calcium levels by blocking this descending modulatory transmission, and abolished rhythmic oscillations; this resulted in decreased calcium levels below 100 nM. Application of dopamine to a quiescent TTX-blocked AB reliably and reversibly induced an increase in the average level of calcium in fine dendrites, along with stable voltage oscillations. Generally, in any rhythmically oscillating AB (bursting in physiological saline with intact modulatory inputs, or DA-induced bursting in TTX), the average calcium levels were at least twofold higher than in a quiescent neuron.

Strikingly, this DA-induced increase in $[Ca^{2+}]_{in}$ started almost two minutes before the emergence of voltage oscillations (Fig. 3.8A and C) and even before the neuron started to depolarize. At the start of the first burst in DA, the mean calcium concentrations was around 150 nM; this seems to be the average concentration of intracellular calcium needed for emergence of bursting (i.e. "threshold" calcium level).

Our estimated base calcium concentrations at rest and in a rhythmic AB interneuron are in agreement with values in lamprey spinal cord motoneurons and hippoglossal motoneurons (Backsai *et al.* 1995; Lev-Tov and O'Donovan 1995, Ladewig and Keller 2000; Di Prisco and Alford 2004). The magnitude of calcium oscillations during fictive locomotion in these preparations were close to our values in the AB neuron, despite the fact that in these motoneurons, calcium signal changes were due influx of calcium during action potentials, while in AB, they were observed in the presence of TTX.

In pyloric cells, the majority of ion channels and monoamine receptors are located in the fine neuropil (Clark and Baro 2006, 2007, Clark *et al.,* 2008). Moreover, in many neurons the fine neurites, including dendritic spines and synaptic boutons, contain smooth endoplasmic reticulum (Blaustein and Golovina, 2001; Verkhratsky, 2005) which can store calcium ions and release them to the cytoplasm via intracellular calcium receptor-channels (IP_3R and RyR). Presumably, in the AB fine neuropil, dopamine receptors activate secondary messenger mechanisms which can interact with nearby IP_3R and RyR. If Ryanodine and IP_3 receptors play a part in the dopamine effect, then pre-treatment with a cocktail of their blockers (Ryanodine and Xestospongin C) should prevent the emergence of bursting and calcium rise upon application of DA. This was observed provided that the blockers were applied for a long

enough time (Fig. 3.11). The DA-induced small depolarization seen in the presence of Ryanodine and Xestospongin C is the result of the other effects of DA on other channels: enhancement of the hyperpolarization-activated current I_h (Peck et al., 2006), reduction of the transient potassium current (Peck et al., 2001), and decrease in the leak (Peck et al., 2001 and this chapter).

Ry and Tg application have been reported to augment the calcium signal and I_{CAN} in rat hippocampal neurons (Partridge and Valenzuela, 1999). While this is in apparent disagreement with my results, it can be explained by the complex mechanisms of action of Tg and Ry. Initially, Tg blocks the uptake of calcium into the ER lumen, while low doses of Ry make its receptors leakier; both these processes cause a temporary increase in the local $[Ca^{2+}]_{in}$. However, with time in the presence of the blockers, ER stores are depleted and a long-term decrease in $[Ca^{2+}]_{in}$ is observed. When I used the brief pre-treatment (30 min) with Ry and Xe, application of DA initially induced a $[Ca^{2+}]_{in}$ increase and V_m oscillations, probably due to the temporary increase in RyR open time probability. After 50 minutes of continuous application of the blockers and DA, when Ry block was more complete and the calcium stores were depleted, both calcium signal and V_m returned to resting levels. After a longer pre-treatment (60 min) with Ry and Xe, addition of DA failed to increase in $[Ca^{2+}]_{in}$ or induce bursting.

In Bursting AB Neurons Intracellular Calcium Oscillates in Parallel with Voltage

Our high speed calcium imaging studies with Calcium-Green-1 showed that when the AB neuron was stably oscillating, the intracellular calcium fluorescence signal also stably oscillated. The amplitude and the time course of calcium oscillations were similar both in a spontaneously bursting AB

Figure 3.11. The AB neuron calcium signal oscillates in phase but with a delay compared with voltage oscillations

A. Spontaneously bursting AB neuron in physiological saline. Simultaneous recordings (from top to bottom): fluorescence signal (Fluo) and membrane potential (V_m, blue trace); the sync channel was used to synchronize imaging and voltage traces; dF/F is the relative change in fluorescence. Note that the peak of calcium signal follows the voltage peak. Time markers, in sec, are below the voltage trace.
B. TTX+PTX blocked both voltage and calcium oscillations in less than 10 minutes.
C. DA-induced membrane potential and calcium signal oscillations. Both had the same frequency but the calcium signal is delayed relative to the voltage oscillation.
D. Application of 10 μM of Ryanodine stopped both voltage and calcium oscillations.

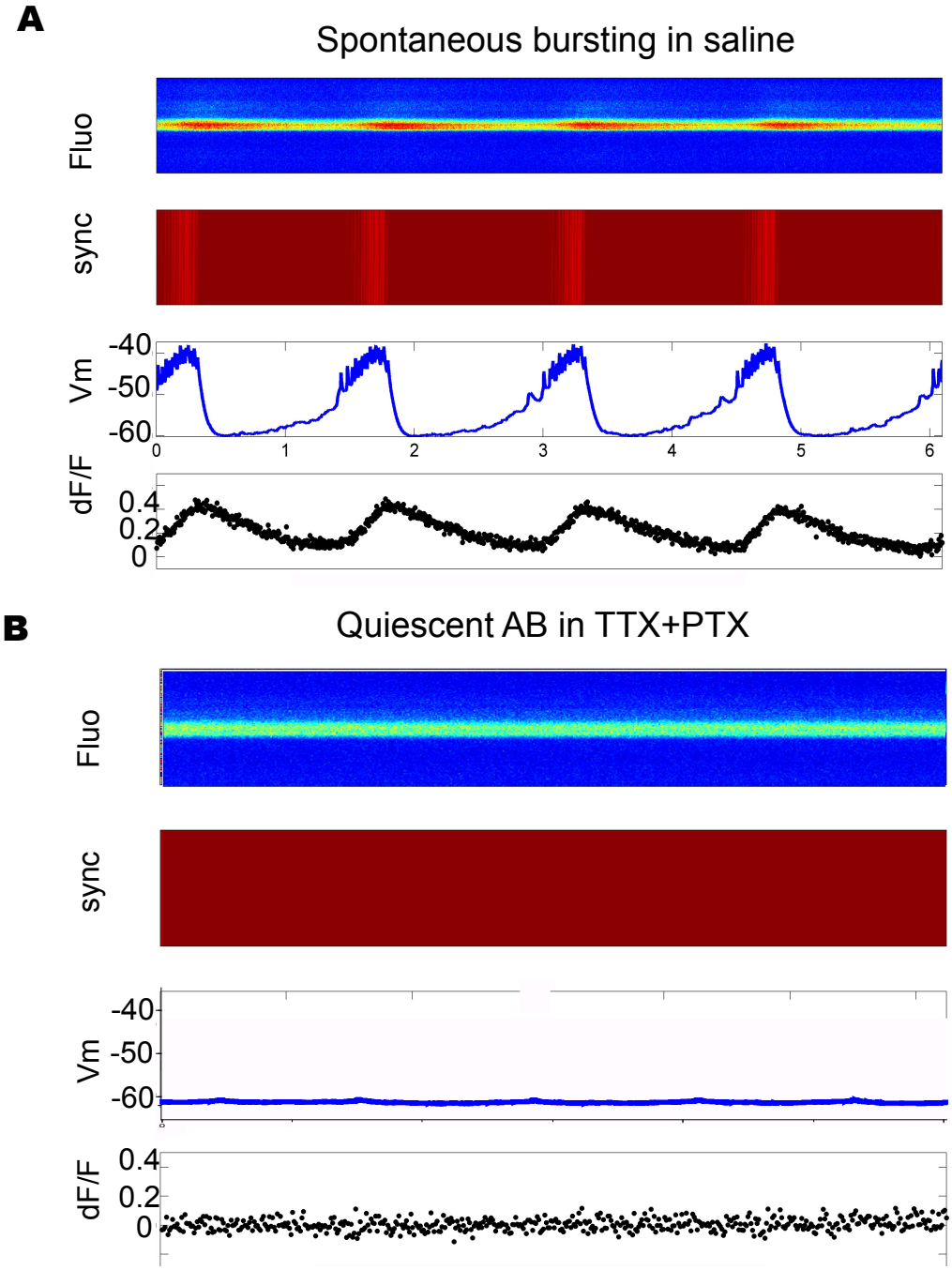
A
Spontaneous bursting in saline
Fluo
sync
Vm
-40
-50
-60
0
1
2
3
4
5
6
dF/F
0.4
0.2
0
B
Quiescent AB in TTX+PTX
Fluo
sync
Vm
-40
-50
-60
dF/F
0.4
0.2
0

Figure 3.11 (Continued)

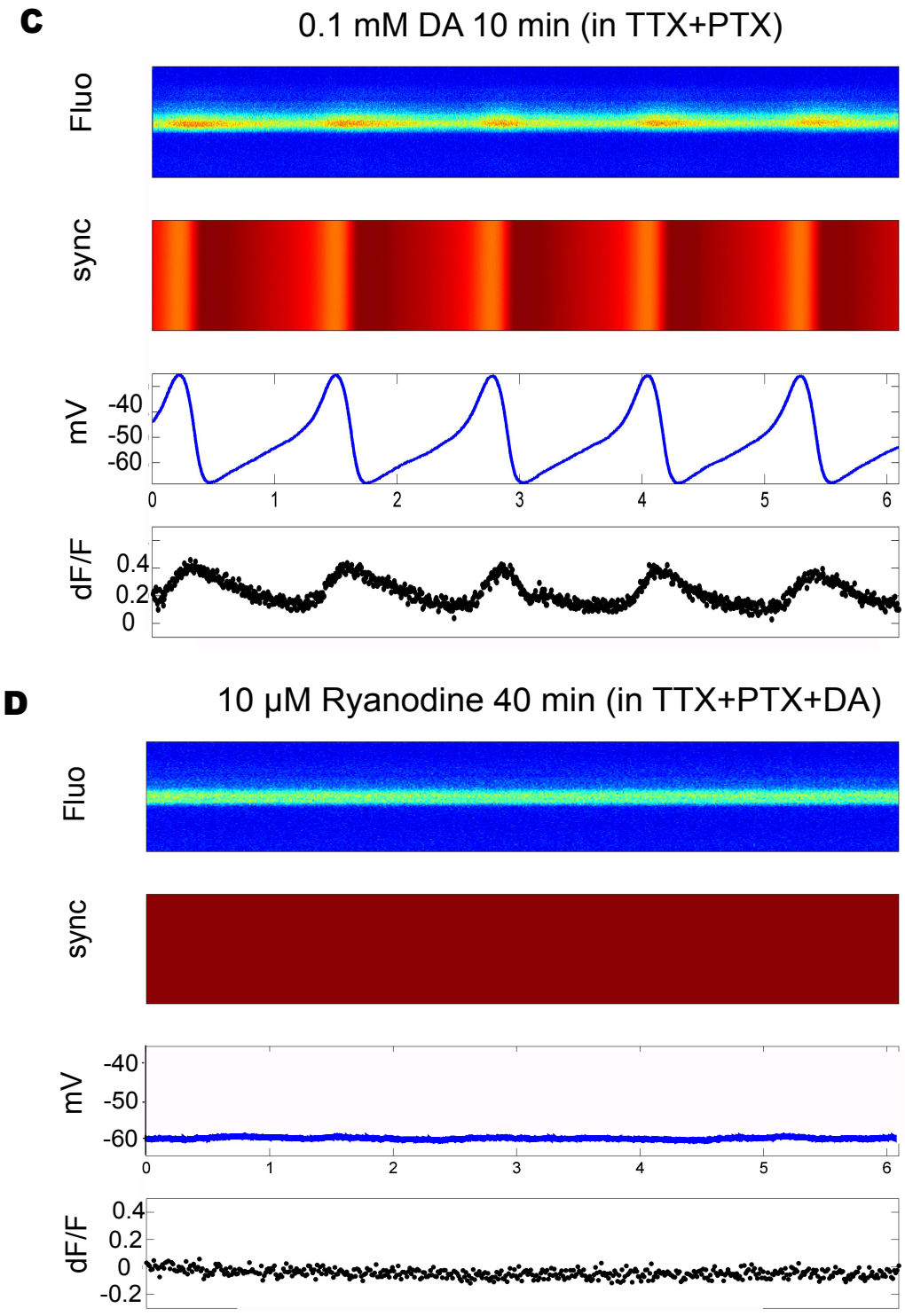

(receiving neuromodulatory input from higher ganglia), and in a dopamine-induced bursting AB, with a fluorescence range of about 20-40% above the base level (Fig. 3.12). The calcium signal oscillated with the same frequency as the membrane potential, but the calcium oscillations were phase-delayed by about 0.08 of the period, relative to the voltage oscillations (Figs 3.11 and 3.12). Calcium increased during the fast upstroke (depolarization) of the V_m, with the mean threshold -55 mV. One way to interpret these data is that the tonic release of calcium from intracellular stores activates I_{CAN} , which acts as a tonic ramp current to depolarize the neuron; above a voltage threshold, the depolarization activates voltage-dependent calcium current $I_{Ca(V)}$ which participates in the rapid rise of the oscillation. This voltage-dependent calcium influx would bring about fast Vm depolarization to the maximum of the voltage wave, activation of $I_{K(Ca)}$ and subsequent repolarization, finishing the cycle.

The essential role of calcium release from intracellular stores is maintained even after the neuron starts to oscillate since application of Ryanodine blocked these ongoing calcium oscillations along with potential oscillations in the AB (Fig. 3.11). One way Ryanodine receptors may participate in maintenance of bursting could be calcium-induced calcium release (CICR) and further amplification of the cytoplasmic calcium rise (see next section). It could also just be uptake into the ER of the calcium coming in from the oscillation, and then being released again.

One would expect that the $[Ca^{2+}]_{in}$ would decline from its peak just like its rise, in parallel with the fall in membrane potential and with a similar delay. We found that the calcium concentration kept slowly declining even as voltage reached its trough (minimum) and started a new depolarization cycle (Fig.

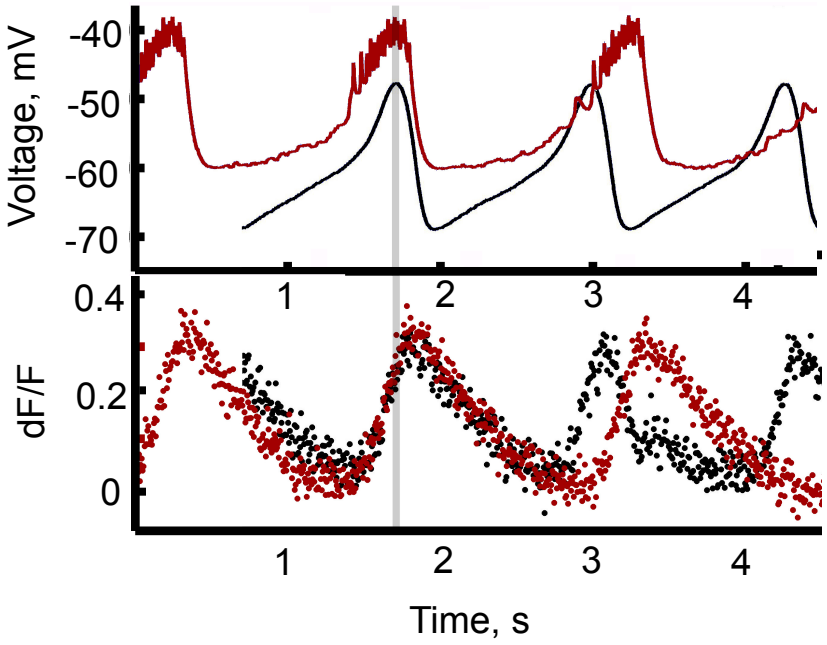

Figure 3.12. Overlay of voltage and calcium traces. Calcium oscillations had similar delayed time course and amplitude both in a spontaneously bursting AB neuron (red traces) and in a synaptically isolated AB in the presence of DA (black traces). Top is the voltage trace and bottom is the calcium signal change (dF/F).

3.12). In lamprey spinal cord CPG (Di Prisco *et al.,* 2004) the calcium signal also decayed slower than the voltage and kept decreasing even during V_m depolarization. This discrepancy between decay time courses of V_m and calcium could be due to a slow buffering of the calcium dye, so that the fluorescent signal could not follow the sharp drop of V_m at the end of the burst (see also Friel and Tsien, 1992; Li et al., 1995; Koshiya and Smith, 1999). In this case we would unable to accurately capture the kinetics of calcium decrease at the end of the bursting cycle. The delay in Ca^{2+} rise probably reflects the time required to reach the voltage threshold for activation of $I_{Ca(V)}$, as described above.

Cross-Talk between IP_3 and Ryanodine Receptors and Their Respective Pathways

The ER appears to play a critical role in DA-induced AB bursting, since blockade of Ryanodine receptors and IP_3 receptors prevented or abolished ongoing dopamine bursting in the pyloric pacemaker neuron. My data demonstrated that induction of bursting is dependent on at least one of the intracellular calcium channels: IP_3-sensitive or Ryanodine-sensitive receptor-channels (Fig. 3.10, Ry and Xe pre-treatment). Maintaining the bursting requires the normal function of both types, and presumably the SERCA pump (Fig. 3.5). DA is not synthesized by neurons within the STG; it is produced by the neurons that are located in the COG and the brain, and send their axons via the stomatogastric nerve down to the STG (Kushner and Maynard 1977; Sullivan *et al.* 1977; Barker *et al.* 1979; Kushner and Barker 1983). DA is also present as a neurohormone in the hemolymph surrounding the STG (Sullivan *et al.,* 1977), though in the lobster the concentrations in the blood are probably too low to affect the STG DA receptors.

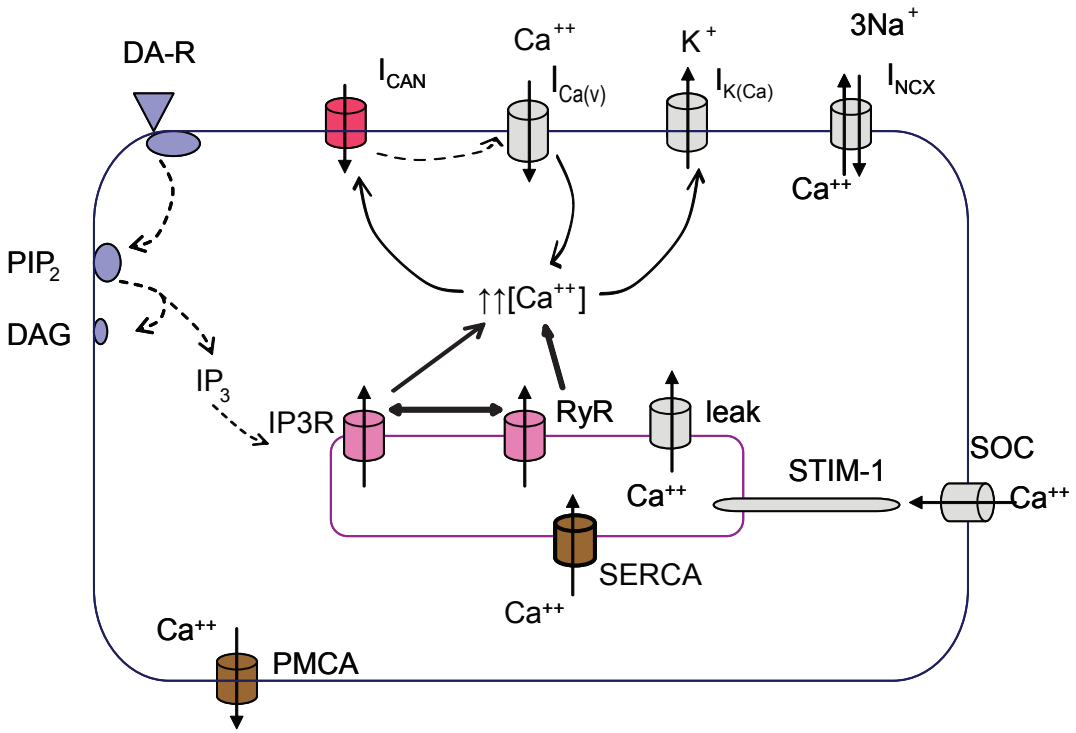

Figure 3.13. Intracellular calcium dynamics.

DA-R, dopamine receptor; PIP2, Phosphatidylinositol 4,5-bisphosphate; DAG, diacylglycerol; IP3, Inositol trisphosphate; IP3R, Inositol trisphosphate receptor; RyR, ryanodine receptor; SERCA, sarco-endoplasmic reticulum calcium ATPase; PMCA, plasma membrane calcium APTase; [Ca2+]in, intracellular calcium concentration; ICAN, calcium-activated non-selective current; ICa(v), voltage-gated calcium current; IK(Ca), calcium-activated potassium current; leak, leak current; INCX, sodium-calcium exchanger current; STIM-1, stromal interaction molecule 1; SOC, store-operated channel.

Three types of DA receptors that belong to the superfamily of G-protein coupled receptors (GPCRs) have so far been identified in the lobster STG: $D_{1alphaPan}$, $D_{1betaPan}$ and $D_{2alphaPan}$ (Clark and Baro 2006, 2007). The $D_{1alphaPan}$ receptor couples with G_s and G_q, the $D_{1betaPan}$ receptor couples with Gs, and the $D_{2alphaPan}$ receptor couples with G_i (Clark *et al.,* 2008). All three receptors are localized exclusively to the synaptic neuropil, but the pyloric cell type specific distribution of the DA receptors is currently unknown. The effect of DA on the intrinsic properties of the individual pyloric cell types varies greatly (Flamm and Harris-Warrick, 1986a,b; Harris-Warrick and Flamm, 1987; Ayali and Harris-Warrick, 1999; Kloppenburg et al.,2000, 2007; Peck *et al.,* 2001, 2006; Johnson *et al.,* 2003; Gruhn *et al.,* 2005); it is expected that each cell type will have its own unique set of DA receptors, second messengers, and complement of effector proteins (Clark *et al.,* 2008). It would be interesting to see in the lobster STNS how DA receptor types are expressed in different types of pyloric cells and how the expression pattern correlates with cell identity and physiological function.

In vertebrate preparations, DA can trigger mobilization of intracellular calcium through concurrent activation of the D1 and the D2 receptors or the D1-D2 heteromer, via activation of G_q, phospholipase C (PLC), and the inositol trisphosphate (IP_3) cascade (Undie *et al.,* 1994, Lee *et al.,* 2004, Hasbi *et al.,* 2009a, 2009b). In Drosophila photoreceptors, activation of this signaling cascade leads to calcium release from IP_3R and calcium influx via two types of TRP channels (Hardie and Minke, 1993) that are located in close proximity to IP_3-sensitive calcium stores (Pollock *et al.,* 1995). In AB neuron, DA most likely acts on the $D_{1\alpha Pan}$ receptor or its heteromer with a D_2-like receptor to activate the G_q-PLC-IP_3 pathway.

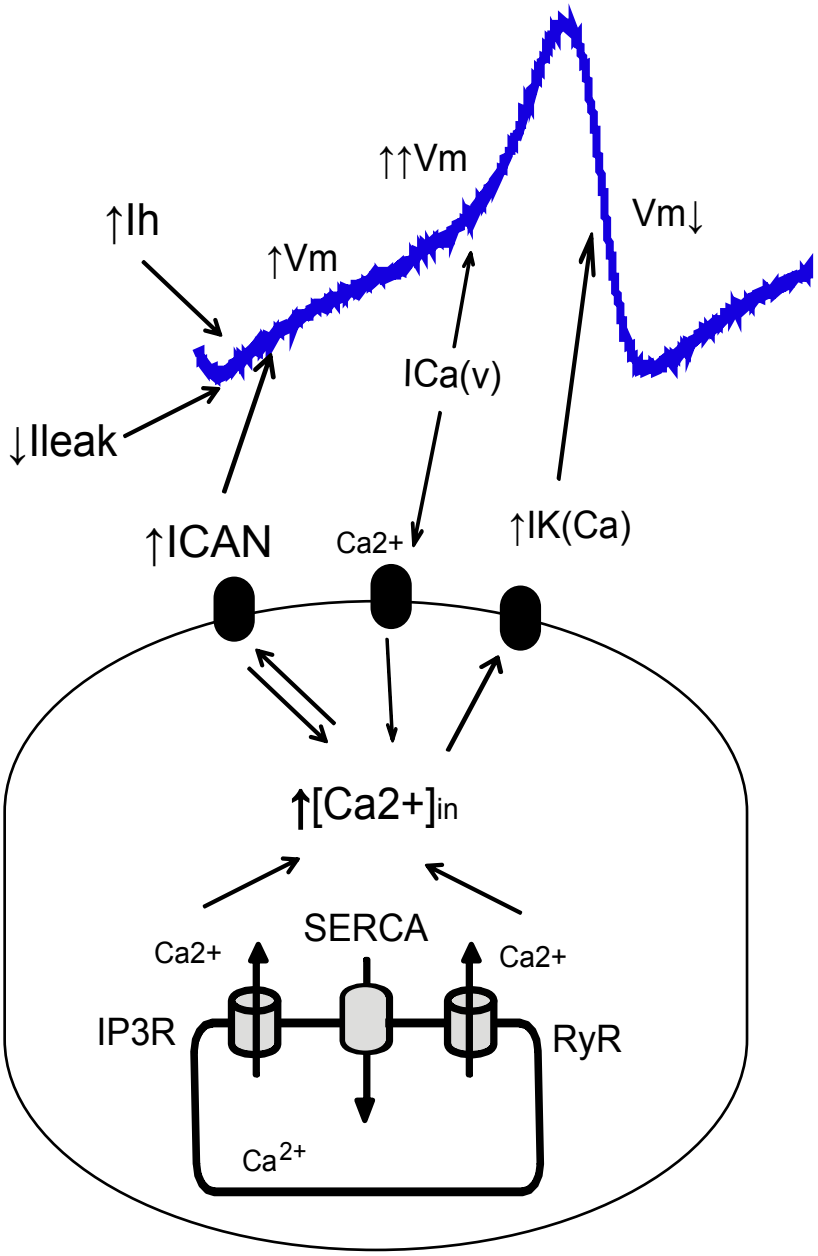

Figure 3.14. Model of DA-induced bursting in the AB neuron. Dopamine modulates multiple currents in the AB neuron: enhancement of ICAN and Ih, reduction of ICa(v), Ileak, IA. DA increases intracellular calcium concentration by triggering calcium release from IP3R and RyR.

In addition, DA could also activate $D_{1\alpha Pan}$ or $D_{1\beta Pan}$ coupled to the G_s-cAMP-PKA-pathway (Clark et al., 2008) leading to an increased phosphorylation of RyR protein and augmentation of calcium release from ER, as demonstrated in the heart pacemaker (sino-atrial node cells) (Vinogradova *et al.,* 2006). Since both ER receptor channels are sensitive to calcium, they are subject to positive autofeedback, leading to a regenerative opening of RyRs and/or $InsP_3Rs$ beyond a certain threshold of $[Ca^{2+}]_i$ and amplification and globalization of the initial calcium signal (Verkhratski, 2005). Whether it is the IP_3Rs or the RyRs that are first activated by dopamine is impossible to say without the knowledge of the exact types of the dopamine receptors expressed in AB neuron. In any case, the initial calcium release from intracellular calcium channels leads to the massive self-amplification of the calcium signal and activation of I_{CAN} throughout the dendritic tree. The replenishment of the intracellular calcium stores is critically important to the DA bursting and it may occur in part *via* I_{CAN}, in part *via* $I_{Ca(v)}$ and in part *via* store-operated calcium entry (SOCE). Although I did not test this directly in the AB neuron, SOCE appears to be a more effective way of refilling the stores than calcium influx via CAN channels in rat hepatocytes (Gregory *et al.,* 2003).

Model of Dopamine-induced Bursting of the Pyloric Pacemaker Neuron

Based on the previous work in the STG and my data, I suggest the following model of the dopamine-induced bursting in the lobster pyloric pacemaker (Fig. 3.13):

1. DA binding to $D_{1\alpha Pan}$ or $D_{1\beta Pan}$ receptors increases the intracellular calcium concentration in the fine neuropil, with the ER calcium channels and the SERCA pump playing a major part in this process. Most likely the IP_3R is

activated first via the G_q-PLC-PIP_2 pathway with a subsequent activation of more IP_3R as well as RyRs as calcium is released from the ER.

2. This rise in intracellular calcium activates and enhances I_{CAN}. DA increases the peak current amplitude and slows the rate of deactivation of the current, probably due to high base levels of calcium.

3. I_{CAN} activation acts as a ramp current via the influx of cations (mostly Na^+ and Ca^{2+}, as well as weaker efflux of K^+) to depolarize the cell after the termination of the previous burst, bringing the cell to threshold to activate other inward currents including $I_{Ca(V)}$ to initiate the full burst.

4. Depolarization and high intracellular calcium activate $I_{K(Ca)}$, which must have either slower activation kinetics or a higher calcium concentration dependence for its activation than I_{CAN}. $I_{K(Ca)}$ at some point prevails over I_{CAN} and additional currents underlying the depolarization; this repolarizes the cell, ending the cycle.

5. Extracellular calcium is essential for replenishment of the intracellular calcium stores, and is carried inside in part via I_{CAN} and in part via remaining voltage-gated calcium channels. In addition, store-operated calcium channels may play a role in the replenishment of intracellular stores as well. Once free calcium ions enter the cytoplasm, they are partially pumped into the ER lumen by SERCA or into the mitochondria or buffered by special proteins.

6. In addition to these effects, previous work in our laboratory (Peck et al., 2001, 2006), as well as my additional measurements, have shown that DA also reduces the tonic leak current, which will make the neuron electrically tighter and more compact, enhancing the effects of the rather small I_{CAN} and other subthreshold currents. DA also reduces the transient outward potassium current (Peck *et al.,* 2001, 2006), which would normally try to counteract the ramp I_{CAN} current, so its blockade also enhances the ability of I_{CAN} to depolarize the

the neurons. Finally, DA enhances the hyperpolarization-activated inward current, I_h (Peck et al., 2006), which will also contribute to the depolarizing ramp, further contributing to V_m depolarization and regenerative oscillations in AB (Fig.3.14).

Multiple Pacemaking Mechanisms

There are multiple possible mechanisms to generate bursting within neurons, and relative contribution of each may vary under different conditions (Harris-Warrick and Flamm, 1987; Pena *et al.,* 2004). It has been proposed that in rhythmogenic CPGs, there may exist different groups of pacemaker neurons, each with a distinct rhythmogenic mechanism – either sodium-dependent (Pace 2007b, Tazerart *et al.*, 2007; Zhong *et al.*, 2007) or calcium-dependent (Del Negro *et al.*, 2002; Pena et al, 2004, Pace 2007a). In this chapter I have looked at the ionic currents underlying DA- induced bursting in the pyloric pacemaker that earlier had been shown to be calcium-dependent (Harris-Warrick and Flamm, 1987). My data suggest that DA generates rhythmic oscillations by triggering calcium release from the ER, leading to a rise of intracellular calcium concentration and activating various ionic currents in succession – first I_{CAN} to depolarize membrane potential, next $I_{Ca(V)}$ to further depolarize and trigger additional calcium influx and finally, $I_{K(Ca)}$ to repolarize the potential. This process is regenerative and self-sustaining due to involvement of two intracellular calcium pathways (IP_3R and RyR) and a constant replenishment of calcium stores via CAN and voltage-dependent calcium channels with possible involvement of store-operated calcium channels. In the next chapter I will show that the same pyloric pacemaker AB neuron uses a completely different mechanism of bursting in the presence of serotonin (5HT), a neurohormone in the lobster. Thus, if in the respiratory CPG there may be different groups of pacemaker neurons in the same CPG, in the pyloric CPG, the same pacemaker

neuron can employ two quite distinct mechanisms based on different ionic currents for rhythmogenesis in the pyloric network.

REFERENCES

Barker D. L., Kushner P. D. and Hooper N. K. (1979) Synthesis of dopamine and octopamine in the crustacean stomatogastric nervous system. *Brain Res.* 161, 99–113.

Berridge, M.J. (2006) Calcium microdomains: organization and function. *Cell Calcium* 40(5-6):405-12.

Blaustein MP, Golovina VA (2001) Structural complexity and functional diversity of endoplasmic reticulum Ca^{2+} stores. *Trends Neurosci*. 24(10):602-8.

Buschges, A., Wikström, M.A, Grillner, S. and El Manira, A. (2000) Roles of high-voltage-activated calcium channel subtypes in a vertebrate spinal locomotor network. *J Neurophysiol* 84**:** 2758–2766

Clark M.C., Khan R., Baro D.J. (2008) Crustacean dopamine receptors: localization and G protein coupling in the stomatogastric ganglion. *Journal of Neurochemistry* 104(4):1006-19.

Clark, M.C. and Baro, D.J. (2006) Molecular cloning and characterization of crustacean type-one dopamine receptors: D1alphaPan and D1betaPan. *Comp Biochem Physiol B Biochem Mol Biol.* 143(3):294-301

Clark, M.C. and Baro, D.J. (2007) Arthropod D2 receptors positively couple with cAMP through the Gi/o protein family. *Comp Biochem Physiol B Biochem Mol Biol.* 146(1):9-19

Cramer NP, Li Y, Keller A. (2007) The whisking rhythm generator: a novel mammalian network for the generation of movement. *J Neurophysiol.* 97(3):2148-58.

Crowder EA, Saha MS, Pace RW, Zhang H, Prestwich GD, Del Negro CA. (2007) Phosphatidylinositol 4,5-bisphosphate regulates inspiratory burst activity in the neonatal mouse preBötzinger complex. *J Physiol*. 582(Pt 3):1047-58

Di Prisco, V. and Alford, S. (2004) Quantitative Investigation of Calcium Signals for Locomotor Pattern Generation in the Lamprey Spinal Cord. *J Neurophysiol* 92: 1796-1806

Díaz-Ríos, M., Dombeck, D.A. Webb, W.W. and Harris-Warrick, R.M. (2007) Serotonin Modulates Dendritic Calcium Influx in Commissural Interneurons in the Mouse Spinal Locomotor Network. *J Neurophysiol* 98: 2157-2167.

Friel, D. D. & Tsien, R. W. (1992) Phase-dependent contributions from Ca2+ entry and Ca2+ release to caffeine-induced [Ca2+]i oscillations in bullfrog sympathetic neurons. *Neuron* 8, 1109–1125.

Gafni J, Munsch J.A., Lam T.H., Catlin M.C., Costa L.G., Molinski T.F., Pessah I.N. (1997) Xestospongins: potent membrane permeable blockers of the inositol 1,4,5-trisphosphate receptor. *Neuron* 19(3):723-33.

Garaschuk O, Yaari Y, Konnerth A. (1997). Release and sequestration of calcium by ryanodine-sensitive stores in rat hippocampal neurones. *J Physiol.* 502(Pt 1):13-30.

Goldberg JH, Yuste R. (2005) Space matters: local and global dendritic Ca2+ compartmentalization in cortical interneurons. *Trends Neurosci*. 28(3):158-67.

Graubard, K. and Ross, W.N. (1985) Regional distribution of calcium influx into bursting neurons detected with arsenazo III. *Proc Natl Acad Sci U S A* 82: 5565-5569.

Gruhn M, Guckenheimer J, Land B, Harris-Warrick RM (2005) Dopamine modulation of two delayed rectifier potassium currents in a small neural network. *J Neurophysiol.* 94(4):2888-900

Grynkiewiecz GM, Poenie M, Tsien RY (1985) A new generation of Ca^{2+} indicators with greatly improved fluorescence properties. *Journal of Biological Chemistry* 260:3440-3450

Guckenheimer J, Gueron S, Harris-Warrick RM. (1993) Mapping the dynamics of a bursting neuron. *Philos Trans R Soc Lond B Biol Sci*. 341(1298):345-59.

Han, P., Nakanishi S.T., Tran M.A., and Whelan, P. J. (2007). Dopaminergic Modulation of Spinal Neuronal Excitability. *J Neurosci* 27(48):13192-13204

Hardie R.C., Minke B. (1993) Novel Ca2+ channels underlying transduction in Drosophila photoreceptors: implications for phosphoinositide-mediated Ca2+ mobilization. *Trends Neurosci*. 16(9):371-6.

Harris-Warrick, R. M. and Flamm, R. E. (1987) Multiple mechanisms of bursting in a conditional bursting neuron. *Journal of Neuroscience* **7:**2113-2128.

Harris-Warrick, R. M. and Johnson, B.R. (1987) Potassium channel blockade induces rhythmic activity in a conditional burster neuron. *Brain Research 416:381*-386.

Harris-Warrick, R.M., Johnson, B.R., Peck, J.H., Kloppenburg, P., Ayali, A., and Skarbinski, J. (1998) Distributed Effects of Dopamine Modulation in the Crustacean Pyloric Network. *Ann N Y Acad Sci*. 860:155-67.

Hasbi A, Fan T, Alijaniaram M, Nguyen T, Perreault ML, O'Dowd BF, George SR 2009b. Calcium signaling cascade links dopamine D1-D2 receptor heteromer to striatal BDNF production and neuronal growth. *Proc Natl Acad Sci U S A*. Nov 30

Hasbi A, O'Dowd BF, George SR. 2009a Heteromerization of dopamine D2 receptors with dopamine D1 or D5 receptors generates intracellular calcium signaling by different mechanisms. *Curr Opin Pharmacol*. Nov 6.

Hernandez-Lopez S., Tkatch T., Perez-Garci E., Galarraga E., Bargas J., Hamm H. and Surmeier D. J. (2000) D2 dopamine receptors in striatal medium spiny neurons reduce L-type Ca2+ currents and excitability via a novel Plc[Beta]1-Ip3-calcineurin-signaling cascade. *J. Neurosci*. 20, 8987–8995.

Jin LQ, Goswami S, Cai G, Zhen X, Friedman E.(2003). *J Neurochem*. 85:378–386.

Johnson BR, Kloppenburg P, Harris-Warrick RM. (2003) Dopamine modulation of calcium currents in pyloric neurons of the lobster stomatogastric ganglion. *J Neurophysiol*. 90(2):631-43

Johnson BR, Peck JH, Harris-Warrick RM. (1995) Distributed amine modulation of graded chemical transmission in the pyloric network of the lobster stomatogastric ganglion. *J Neurophysiol.* 74(1):437-52.

Johnson BR, Schneider LR, Nadim F, Harris-Warrick RM. (2005) Dopamine modulation of phasing of activity in a rhythmic motor network: contribution of synaptic and intrinsic modulatory actions. *J Neurophysiol.* 94(5):3101-11

Johnson, B.R., Kloppenburg, P. and Harris-Warrick, R. M. (2003) Dopamine Modulation of Calcium Currents in Pyloric Neurons of the Lobster Stomatogastric Ganglion. *Journal of Neurophysiology* 90: 631–643.

Johnson, B.R., Peck, J.H. and Harris-Warrick, R. M. (1992) Elevated temperature alters the ionic dependence of amine-induced pacemaker activity in a conditional burster neuron. *Journal of Comparative Physiology A* 170:201-209.

Johnson, B.R., Peck, J.H. and Harris-Warrick, R. M. (1995) Distributed Amine Modulation of Graded Chemical Transmission in the Pyloric Network of the Lobster Stomatogastric Ganglion. *Journal of Neurophysiology* 74(1): 437-452.

Kemnitz CP. (1997) Dopaminergic modulation of spinal neurons and synaptic potentials in the lamprey spinal cord. *J Neurophysiol*. 77(1):289-98.

Kloppenburg P, Zipfel WR, Webb WW, Harris-Warrick RM (2000) Highly localized Ca2+ accumulation revealed by multiphoton microscopy in an identified motoneuron and its modulation by dopamine. *Journal of Neuroscience* 20:2523-2533.

Kloppenburg P, Zipfel WR, Webb WW, Harris-Warrick RM (2007) Heterogeneous effects of dopamine on highly localized, voltage-induced Ca2+ accumulation in identified motoneurons. *Journal of Neurophysiology* 98:2910-2917.

Koshiya N, Smith JC. (1999) Neuronal pacemaker for breathing visualized in vitro. *Nature.* 400(6742):360-3.Kushner P. D. and Barker D. L. (1983) A neurochemical description of the dopaminergic innervation of the stomatogastric ganglion of the spiny lobster. J.Neurobiol. 14, 17–28. Kushner P. D. and Maynard E. A. (1977) Localization of monoamine fluorescence in the stomatogastric nervous system of lobsters. Brain Res. 129, 13–28.

Kwan AC, Dietz SB, Webb WW, Harris-Warrick RM (2009) Activity of Hb9 interneurons during fictive locomotion in mouse spinal cord. *J Neurosci* 29:11601-11613.

Ladewig T and Keller BU. (2000) Simultaneous patch-clamp recording and calcium imaging in rhythmically active neuronal network in the brain stem slice preparation from mouse. *Pflügers Arch* 440: 322–332,

Ladewig T, Kloppenberg P, Lalley PM, Zipfel WR, Webb WW, Keller BU (2003) Spatial profiles of store-dependent calcium release in motoneurons of the nucleus hypoglossus from newborn mouse. *Journal of Physiology* 547.3:775-787

Lee SP, So CH, Rashid AJ, Varghese G, Cheng R, Lança AJ, O'Dowd BF, George SR. (2004). Dopamine D1 and D2 receptor Co-activation generates a novel phospholipase C-mediated calcium signal. *J Biol Chem* 279(34):35671-8.

Levi R, Samoilova M, Selverston AI (2003) Calcium signaling components of oscillating invertebrate neurons in vitro. *Neuroscience* 118:283-296.

Lev-Tov A and O'Donovan MP. (1995) Calcium imaging of motoneuron activity in the en bloc spinal cord preparation of the neonatal rat. *J Neurophysiol* 74: 1324–1334.

Li, Y. X., Keizer, J., Stojilkovic, S. S. & Rinzel, J. (1995) Ca2+ excitability of the ER membrane: an explanation for IP3-induced Ca2+ oscillations. *Am. J. Physiol.* 269, 1079–1092.

Matsuura H, Sokabe T, Kohno K, Tominaga M, Kadowaki T. (2009) Evolutionary conservation and changes in insect TRP channels. *BMC Evol Biol*. 9:228.

Miller JP, Selverston A. (1979) Rapid killing of single neurons by irradiation of intracellularly injected dye. *Science* 206(4419):702-4.

Miller, J. P. and Selverston, A. I. (1982a) Mechanisms underlying pattern generation in lobster stomatogastric ganglion as determined by selective inactivation of identified neurons. II. Oscillatory properties of pyloric neurons. *Journal of Neurophysiology* 48**:**1378-1391.

Miller, J. P. and Selverston, A. I. (1982b) Mechanisms underlying pattern generation in lobster stomatogastric ganglion as determined by selective inactivation of identified neurons. IV. Network properties of pyloric system. *Journal of Neurophysiology* 48**:**1416-1432.

Montell, C. (2001) Physiology, phylogeny, and functions of the TRP superfamily of cation channels. *Sci STKE*. (90):re1.

Mulloney B, Selverston A. (1972) Antidromic action potentials fail to demonstrate known interactions between neurons. *Science* 177(43):69-72

Okamoto H, Unno T, Arima D, Suzuki M, Yan HD, Matsuyama H, Nishimura M, Komori S. (2004). Phospholipase C involvement in activation of the muscarinic

receptor-operated cationic current in Guinea pig ileal smooth muscle cells. *Journal of pharmacol Sci*. 95(2):203-13.

Pace, R. W., Mackay, D. D., Feldman, J. L. and Del Negro, C. A. (2007a) Inspiratory bursts in the preBotzinger complex depend on a calcium-activated non-specific cation current linked to glutamate receptors in neonatal mice. *Journal of Physiology* 582: 113-125.

Pace, R. W., Mackay, D. D., Feldman, J. L. and Del Negro, C. A. (2007b) Role of persistent sodium current in mouse preBotzinger Complex neurons and respiratory rhythm generation. *J Physiol* 580:485-496.

Partridge, L.D. and Swandulla, D. (1987) Single Ca-activated cation channels in bursting neurons of Helix. *Pflugers Arch*. 410(6):627-31.

Partridge, L.D. and Valenzuela, C.F. (1999) Ca2+ store-dependent potentiation of Ca2+-activated non-selective cation channels in rat hippocampal neurones in vitro. *J Physiol*. 521 Pt 3:617-27.

Partridge, L.D. and Valenzuela, C.F. (2000) Block of hippocampal CAN channels by flufenamate. *Brain Res.* 867(1-2):143-8.

Partridge, L.D.(1990) Modulation of calcium-activated non-specific cation currents by cyclic AMP-dependent phosphorylation in neurones of Helix

Partridge, L.D., Miller, T.H., Swandulla D. (1994) Calcium-activated non-selective channels in the nervous system. *Brain Research Reviews* 19:319-325

Peck JH, Gaier E, Stevens E, Repicky S, Harris-Warrick RM. (2006) Amine modulation of Ih in a small neural network. *J Neurophysiol*. 96(6):2931-40

Peck JH, Nakanishi ST, Yaple R, Harris-Warrick RM (2001) Amine modulation of the transient potassium current in identified cells of the lobster stomatogastric ganglion. *J Neurophysiol*. 86(6):2957-65

Pena, F., Parkis, M. A., Tryba, A. K. and Ramirez, J. M. (2004) Differential contribution of pacemaker properties to the generation of respiratory rhythms during normoxia and hypoxia. *Neuron* 43, pp. 105-117.

Perrier, J.-F., Mejia-Gervacio, S. and Hounsgaard, J. (2000) Facilitation of plateau potentials in turtle motoneurones by a pathway dependent on calcium and calmodulin. *J Physiol* 528.1: 107–113

Pollock JA, Assaf A, Peretz A, Nichols CD, Mojet MH, Hardie RC, Minke B. (1995) TRP, a protein essential for inositide-mediated Ca2+ influx is localized adjacent to the calcium stores in Drosophila photoreceptors. *J Neurosci*. 15(5 Pt 2):3747-60.

Rabbah P, Nadim F. (2005) Synaptic dynamics do not determine proper phase of activity in a central pattern generator. *J Neurosci*. 25(49):11269-78.

Ramirez, J.M., Tryba, A.K., Peña, F. (2004) Pacemaker neurons and neuronal networks: an integrative view. *Curr Opin Neurobiol*. 14(6):665-74

Ross, W.N. and Graubard, K. (1989) Spatially and temporally resolved calcium concentration changes in oscillating neurons of crab stomatogastric ganglion. *Proc Natl Acad Sci USA* 86:1679-1683.

Rubin, J. E., Hayes, J. A., Mendenhall, J. L. and Del Negro, C. A. (2009) Calcium-activated nonspecific cation current and synaptic depression promote network-dependent burst oscillations. *Proc Natl Acad Sci USA* 106**:**2939-2944.

Selverston AI, Russell DF, Miller JP (1976) The stomatogastric nervous system: structure and function of a small neural network. *Prog Neurobiol*. 7(3):215-90

Smith, T.G., Barker, J.L. and Gainer, H. (1975) Requirements for bursting pacemaker potential activity in molluscan neurons. *Nature.* 253:450-452

Soto-Treviño C, Rabbah P, Marder E, Nadim F. (2005) Computational model of electrically coupled, intrinsically distinct pacemaker neurons. *J Neurophysiol.*

94(1):590-604.Sullivan R. E., Friend B. J. and Barker D. L. (1977) Structure and function of spiny lobster ligamental nerve plexuses: evidence for synthesis, storage, and secretion of biogenic amines. J. Neurobiol. 8, 581–605.

Tang TS, Bezprozvanny I. (2004) Dopamine receptor-mediated Ca(2+) signaling in striatal medium spiny neurons. *J Biol Chem*. 279:42082–42094.

Tazerart S, Viemari JC, Darbon P, Vinay L, Brocard F (2007) Contribution of persistent sodium current to locomotor pattern generation in neonatal rats. *J Neurophysiol*. 98(2):613-28.

Undie AS, Weinstock J, Sarau HM, Friedman E. (1994) Evidence for a distinct D1-like dopamine receptor that couples to activation of phosphoinositide metabolism in brain. *J Neurochem*. 62(5):2045-8

Vázquez-Martínez O, Cañedo-Merino R, Díaz-Muñoz M, Riesgo-Escovar JR. (2003) Biochemical characterization, distribution and phylogenetic analysis of Drosophila melanogaster ryanodine and IP3 receptors, and thapsigargin-sensitive Ca2+ ATPase. *J Cell Sci*. 116(Pt 12):2483-94.

Venkatachalam, K. and Montell, C. (2007) TRP channels. *Annu Rev Biochem.*76:387-417.

Verkhratsky A. (2005) Physiology and pathophysiology of the calcium store in the endoplasmic reticulum of neurons. *Physiol Rev.* 85(1):201-79.

Vinogradova T.M., Lyashkov A.E., Zhu W, Ruknudin A.M., Sirenko S,. Yang D. et al. (2006) High basal protein kinase A-dependent phosphorylation drives rhythmic internal Ca^{2+} store oscillations and spontaneous beating of cardiac pacemaker cells. *Circ Res* 98:505–514.

Wang D., Grillner S, Wallén P. (2006). Effects of flufenamic acid on fictive locomotion, plateau potentials, calcium channels and NMDA receptors in the lamprey spinal cord. *Neuropharmacology.* 51(6):1038-46.

Wang H.Y., Undie A.S., Friedman E. (1995) Evidence for the coupling of Gq protein to D1-like dopamine sites in rat striatum: possible role in dopamine-mediated inositol phosphate formation. *Mol Pharmacol*. 48:988–994.

Wray S, Burdyga T, Noble K. (2005) Calcium signaling in smooth muscle. *Cell Calcium*. 38(3-4):397-407.

Wu N., Enomoto A., Tanaka S, Hsiao C.F., Nykamp D.Q., Izhikevich E., Chandler S.H. (2005) Persistent sodium currents in mesencephalic v neurons participate in burst generation and control of membrane excitability. *J Neurophysiol*. 93(5):2710-22.

Zhang Y, Golowasch J. (2007) Modeling Recovery of Rhythmic Activity: Hypothesis for the role of a calcium pump. *Neurocomputing* 70(10-12):1657-1662.

Zhang, B., Wooton, J. F. and Harris-Warrick, R. M. (1995) Calcium-dependent plateau potentials in a crab stomatogastric ganglion motoneuron. II. Calcium-activated slow inward current. *Journal of Neurophysiology* 74:1938-1946.

Zholos, A.V. (2006). Regulation of TRP-like muscarinic cation current in gastrointestinal smooth muscle with special reference to PLC/InsP3/Ca2+ system. *Acta Pharmacol Sin* 27(7):833-42.

Zhong G., Masino M.A., Harris-Warrick R.M. (2007) Persistent sodium currents participate in fictive locomotion generation in neonatal mouse spinal cord. *J Neurosci*. 27(17):4507-18.

Ziskind-Conhaim L., Wu L., Wiesner E.P. (2008) Persistent sodium current contributes to induced voltage oscillations in locomotor-related hb9 interneurons in the mouse spinal cord. *J Neurophysiol*. 100(4):2254-64.

CHAPTER 4

SEROTONIN-INDUCED BURSTING OF THE PYLORIC PACEMAKER

INTRODUCTION

Properties of Serotonin-Induced AB Bursting

Serotonin-induced AB bursting, unlike that evoked by dopamine, is critically dependent on the concentration of external sodium (Harris-Warrick and Flamm, 1987). Low external sodium prevents bursting: the cell remains hyperpolarized, near the previous trough of the oscillation. Low external calcium however, only slows down the 5HT bursting without completely blocking it. In agreement with its sensitivity to low external sodium, 5HT-induced bursting is blocked by 10^{-7}M TTX, a specific blocker of sodium channels (Harris-Warrick and Flamm, 1987). Intrinsic conductances responsible for the oscillatory bursting behavior in the AB neuron have not yet been identified experimentally. Generally, slow oscillatory behavior can arise from two major mechanisms, slow activation and inactivation of inward current and/or slow activation and inactivation of outward current, for "type I bursting" described by the minimal models of bursting (Bertram et al., 1995; Rinzel and Lee, 1987). Based on the previous work in the lobster pyloric pacemaker neuron (Flamm and Harris-Warrick 1986; Harris-Warrick and Flamm, 1987), I investigated a possible involvement of a subthreshold sodium inward current with slow kinetics in serotonin-induced AB bursting.

Properties and function of $I_{Na(P)}$ in cell excitability

The molecular mechanisms that cause the persistent openings of the sodium channels are not well understood. One hypothesis is that it originates from the classical Hodgkin-Huxley type transient sodium channels as a “window current” (Attwell *et al.,* 1979) but this cannot explain the current under study here (see Chapter 2). Another explanation is that persistent activity results from periodic

transition of conventional transient sodium channels to a persistent gating mode (Alzheimer *et al.,* 1993; Crill, 1996). The transition from transient to persistent gating can occur randomly, or as a result of channel phosphorylation by PKC (Numann *et al.,* 1991) or G-protein interaction (Ma *et al.,* 1997). A persistent sodium current ($I_{Na(P)}$) was found in both vertebrates and invertebrates, which suggests an evolutionary conservation of this channel type. This current was described in cockroach (Christensen *et al.,* 1988; Lapied *et al.,*1989) and *Drosophila* (Saito and Wu, 1991) neurons, followed by reports of this current in the mushroom body of the honeybee (Schäfer *et al.,* 1994), the heart interneurons of the medicinal leech (Opdyke and Calabrese, 1994), squid giant axons (Rakowski *et al.,* 2002; Clay *et al.,* 2003), and snail interneurons (Nikitin *et al*., 2006, 2008; Kiss *et al.,* 2009). Recent molecular cloning revealed that biophysical properties, pharmacology, gene organization, and even intron splice sites of invertebrate sodium channels are largely homologous to those of mammalian sodium channels (Goldin, 2002; Plummer and Meisler, 1999). The pore forming α-subunit can be encoded by multiple genes and some of them may be more likely to switch to the persistent mode (Raman *et al.,* 1997; Smith *et al.,* 1998). The auxiliary β-subunits may also modulate gating properties of the sodium channels favoring incomplete inactivation (Paton *et al.,* 1994; Morgan *et al.,* 2000). $I_{Na(P)}$ is implicated in both synaptic and cellular plasticity and learning (Nikitin *et al*., 2008; Kiss *et al.,* 2009), while in the leech heart interneurons it underlies plateau potentials (Opdyke and Calabrese, 1994).

The functional role of $I_{Na(P)}$ was more extensively investigated in vertebrate CPGs. It was first postulated and tested in a model that $I_{Na(P)}$ can function as a primary voltage-dependent burst-generating mechanism in the inspiratory neurons of the pre-Bötzinger complex (pre-BötC) of neonatal rat (Butera et al. 1999a,b;

Del Negro et al., 2001). Later it was confirmed experimentally in the *in vitro* brainstem slice preparation, that bursting behavior depends on the balance between the persistent sodium and the leak conductances (Smith et al., 2000; Del Negro, 2001, 2002, 2005; Koizumi and Smith, 2008). Likewise, in the locomotor CPG, $I_{Na(P)}$ is critical to the pacemaker function, as Riluzole application, at concentrations which partially block $I_{Na(P)}$, stops rhythmic bursting in the neurons of neonatal mouse spinal cord (Tazerart *et al*., 2007; Ziskind-Conhaim *et al.*,2008). In masticatory CPG, subthreshold sodium currents, including $I_{Na(P)}$ and resurgent sodium current, are essential for rhythmic burst generation in rat mesencephalic trigeminal neurons (Wu et al., 2005; Enomoto et al., 2006).

$I_{Na(P)}$ is a common target of 5HT modulation in CPGs

Serotonin potently facilitates the persistent sodium current in numerous mammalian neurons, modulating (Hsiao et al., 1998; Harvey et al., 2006a, b) and generating (Cramer et al., 2005) rhythmic firing. In pre-BötC neurons of neonatal mice, 5HT augmented $I_{Na(P)}$ via activation of 5-HT_{2A} receptors (Peña and Ramirez, 2002) which contribute to the bursting of inspiratory neurons. However, in rat medullary preparations, Ptak and colleagues (2009) did not find such an enhancing effect on the persistent sodium current, although application of 5HT transformed non-intrinsic bursters into intrinsic bursters, at least in part by reducing the leak conductances in respiratory neurons.

Here, I test the hypothesis that serotonin induces bursting in the lobster AB neuron, by shifting the balance between persistent sodium and outward currents. 5HT could do this by either enhancing the persistent sodium current, and/or inhibiting the leak current.

MATERIALS AND METHODS

Animals and preparation. Adult California spiny lobsters (*Panulirus interruptus*) were supplied by Don Tomlinson Commercial Fishing (San Diego, CA) and kept in tanks with artificial sea water. Lobsters were anesthetized in ice; the STNS was dissected out and pinned on a Sylgard-coated Petri dish and superfused with oxygenated lobster physiological saline. The bath temperature was maintained at 16-17℃ unless otherwise specified. The STG was desheathed, and cells were identified as previously described (Selverston *et al*. 1976). All experiments in this chapter were performed on the pyloric pacemaker neuron, the Anterior Burster (AB). In current clamp (CC) experiments, the AB cell was synaptically isolated by photoablation of the three pyloric motoneurons that are electrically coupled to it - the Ventricular Dilator (VD) and two Pyloric Dilator (PD) cells, as described by Miller and Selverston (1979).

Electrophysiology. Conventional current clamp (CC) and two-electrode voltage clamp (TEVC) recordings were performed using sharp microelectrodes, an Axoclamp-2B amplifier, DD 1440 data acquisition board and pCLAMP10 software (all from Molecular Devices, Sunnyvale, CA). The command voltage was set as a slow depolarizing ramp (100 mV/sec) from -90 mV to 10 mV. Leak subtraction was done either on-line (P/N=6 protocol) or off-line (direct measure of the leak current and digital leak subtraction); both methods gave similar results.

Solutions. *Panulirus* physiological saline had the following composition (in mM): 479 NaCl, 12.8 KCl, 13.7 $CaCl_2$, 3.9 Na2SO4, 10.0 MgSO4, 2 Glucose, and 11.1 Tris base, pH 7.4 (Mulloney and Selverston 1974). The descending input to the STG from the oesophageal ganglion and the paired commissural ganglia via the stomatogastric nerve (STN) was blocked by application of isotonic sucrose solution with 10^{-7}M TTX into a small Vaseline well built around the

STN. When measuring the persistent sodium current, all other currents were blocked with the following blockers: 50 mM tetraethyl-ammonium chloride (TEA) and 4 mM 4-aminopyridine (4-AP) to block potassium currents, 5 mM CsCl to block the hyperpolarization-activated current, 0.6 mM $CdCl_2$ to block calcium and calcium-activated potassium currents, and $5 \cdot 10^{-6}$ M picrotoxin (PTX) to block glutamatergic synapses within the STG. In addition to the bath-applied blockers, I loaded the cell body with internal blockers of potassium channels by injecting small negative current steps (1-4 nA) for 1-1.5 hours to an electrode loaded with 2M TEACl and 2M CsCl; the cell was allowed to recover for 1-2 hours before start of the experiment. I used Tetrodotoxin (TTX) (0.1μM) and Riluzole (Ril) (3-10 μM) to block the persistent sodium current. When measuring the total outward current, I used the cocktail of 10^{-4}M TTX, 5μM PTX and 5mM CsCl. I added 0.6mM $CdCl_2$ to this cocktail to isolate I_A which was calculated as a difference between the currents with and without $CdCl_2$. I added 2 mM 4-AP to TTX, PTX, CsCl mix to isolate the sum of $I_{K(Ca)}$ and $I_{K(V)}$; finally, to separate the last two currents, I added 0.6mM $CdCl_2$ to the TTX, PTX, CsCl, 4-AP blocker cocktail. The chemicals were purchased from Sigma, Tocris, or Cayman Chemical.

RESULTS

The Persistent Sodium Current is Essential for Serotonin-Induced Oscillations

TTX-sensitive serotonin bursting activity could involve the transient sodium current or the resurgent sodium current along with persistent sodium current (Raman and Bean 1997, Enomoto *et al.,* 2006). To test the hypothesis that $I_{Na(P)}$ is involved in the serotonin-induced bursting, I applied Riluzole, a fairly specific blocker of this current (Urbani and Belluzzi, 2000; Miles *et al.,* 2005; Wu *et al.,* 2005, Kuo *et al.,* 2006) to an AB oscillating in the presence of 5HT.

Figure 4.1. Serotonin-induced oscillations in a synaptically isolated AB are highly sensitive to blockers of sodium currents

A. Riluzole blocks serotonin-induced oscillations in the AB. Intact AB in physiological saline was spontaneously bursting. The synaptically isolated AB became quiescent. 5HT application (10 μM) induced regular bursting, which was abolished by 3-10 μM Riluzole.

B. Time course of Riluzole block: during early wash-in of Riluzole, the AB neuron "skipped" full-sized bursts (180 s); subthreshold oscillations (STO) were still regularly occurring at the same frequency as before, but some of these failed to reach the threshold for bursting (350 s). With further washing, the STO amplitude kept decreasing with no change in frequency (600 s), until oscillations finally completely stopped (1020 s).

C. and D. Frequency (C, closed circles) and amplitude (D, open squares) of oscillatory events as plotted from B. C, The frequency of the events (including both full-sized bursts and STOs) stayed relatively constant until the oscillations completely stopped at the time point around 1020 s. D, Amplitude of the bursts stayed relatively constant, while amplitude of STOs decreased continuously with time. An event was labeled as a "burst" if there was at least one action potential and the amplitude of the voltage "envelope" was larger than 4 mV (marked by a red oval), and as an "STO" when the amplitude was between 2 and 4 mV and lacked action potentials (marked by a blue oval). For clarity, only every 20^{th} event is plotted.

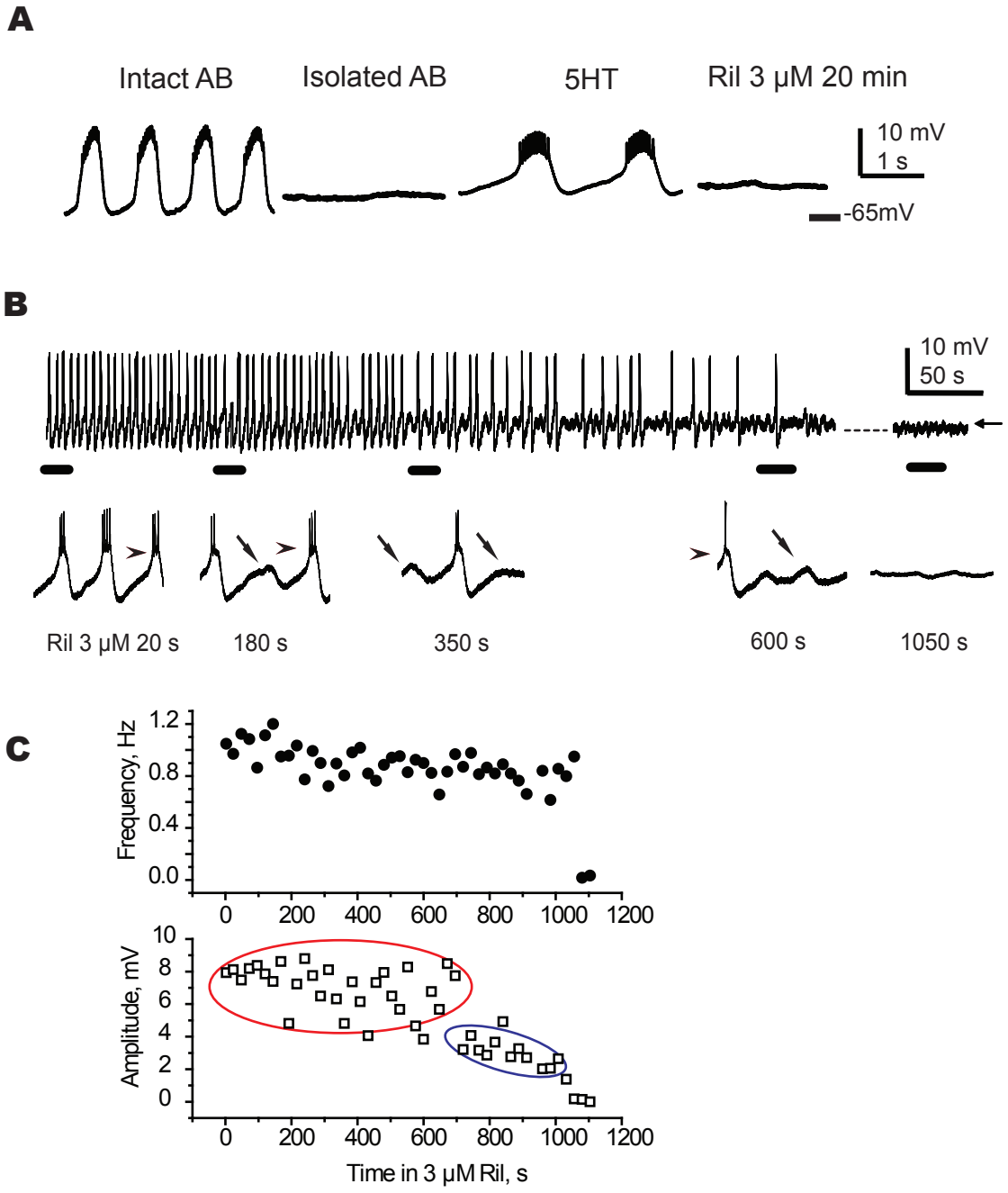
A
Intact AB
Isolated AB
5HT
Ril 3 μM 20 min
10 mV
1 s
-65mV
B
10 mV
50 s
Ril 3 μM 20 s
180 s
350 s
600 s
1050 s
C
Frequency, Hz
1.2
0.8
0.4
0.0
0
200
400
600
800
1000
1200
Amplitude, mV
10
8
6
4
2
0
Time in 3 μM Ril, s

In physiological saline, the spontaneously bursting AB neuron typically stopped oscillating after all synaptic and neuromodulatory input was removed by a TTX block on the STN (Fig 4.1A). Application of 10 μM 5HT usually restored bursting, which in turn was blocked by low micromolar concentrations of Riluzole in all neurons tested (Fig.4.1A, n=8). As Riluzole (3-10 μM) exerted its effect, the frequency of all oscillatory events stayed relatively constant till the very end, when it sharply dropped to zero (at the time point 1050 s in Fig. 4.1C, closed circles). An oscillatory event was considered a burst if it had a least one action potential and a slow wave amplitude of more than 4 mV; it was considered a subthreshold oscillation (STO) if it lacked APs and had a slow wave amplitude below 4 mV (Fig. 4.1B, full bursts are labeled by arrowheads and STOs are labeled by arrows). In the course of Riluzole application, some subthreshold oscillations (STOs) developed into full bursts, while others failed to come to full size. The amplitude of full bursts stayed about the same (in Fig. 4.1D open squares inside the red oval), while the STOs were getting smaller and smaller in amplitude till they disappeared and the rhythm terminated (Figure 4.1D, open squares inside the blue oval). Thus, Riluzole changed the shape of the burst envelope and sequentially decreased the number of action potentials per burst in a bursting AB as it washed in. With time in Riluzole, the neuron stopped firing action potentials, leaving subthreshold oscillations; the depolarizing slope became smaller and eventually flattened out when AB became quiescent. This suggested that a likely mechanism for the Riluzole block of serotonin-induced bursting might be blocking the neuron from getting to threshold for spike initiation, perhaps by slowing down the rate of depolarization during the rising phase of the oscillation (Kuo et al., 2006; Theiss et al., 2007).

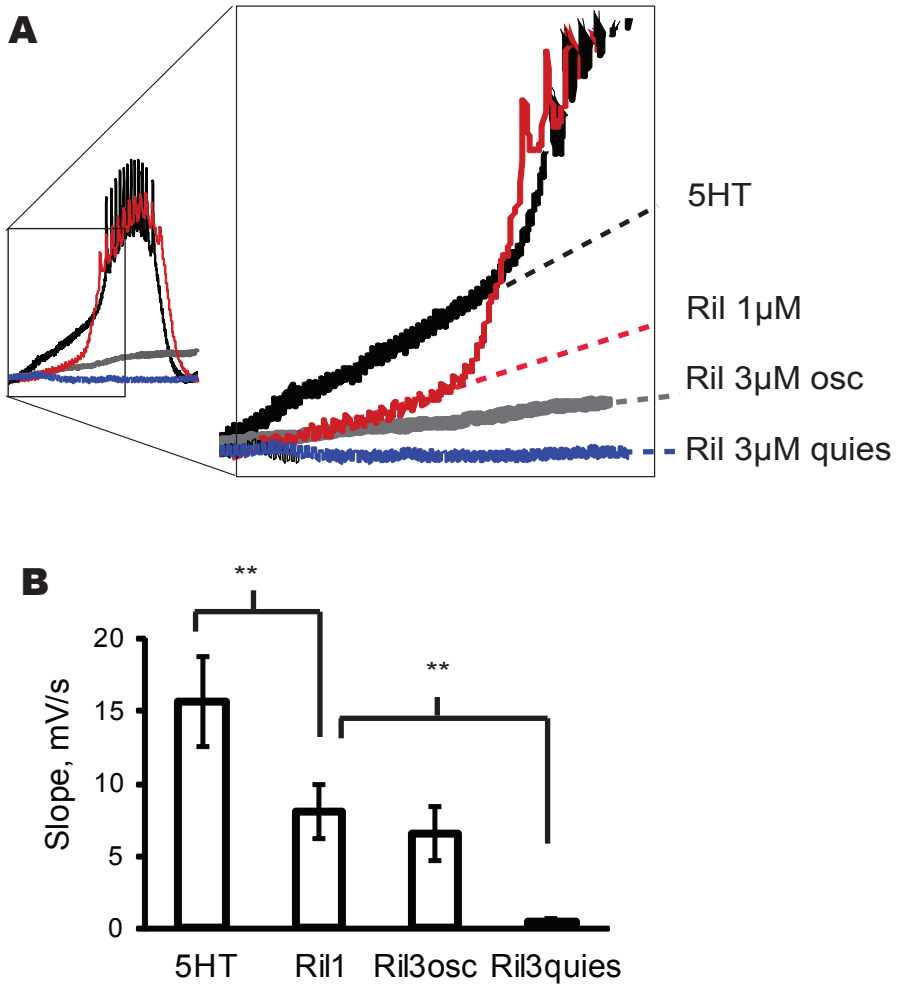

Figure 4.2 . Riluzole blocked the AB rhythm by reducing the rate of depolarization preceding the oscillation.

A. The depolarizing slope decreased in the presence of Riluzole, as shown by overlapping voltage traces during 5HT bursting (black voltage trace), in the presence of 1 μM Ril (red trace), after 12 minutes in 3 μM Riluzole, when the neuron was still oscillating (Ril3osc, gray trace), and after 20 min in 3 μM Riluzole, when oscillations stopped (Ril3quies, blue trace).

B. Summary of the depolarizing slope measurements from 2 neurons at four time points: during 5HT bursting (correspond to the black trace in A) and in the presence of different concentrations of Riluzole (Ril1, Ril3osc and Ril3quies correspond to the red, gray and blue traces in A). Asterisks mark statistically significant difference ($p<0.05$, n=30 bursts per treatment, two AB neurons).

I have measured and compared the slope of the rising phase of the oscillation under control conditions and at different time points during Riluzole treatment. Figure 4.2A shows an overlay of voltage traces in the presence of 5HT (black), in the presence of 1 and 3 μM Riluzole (red and gray traces), while the neuron was still oscillating, and after 20 min in 3 μM Riluzole, when oscillations had stopped (blue trace). The rise slope of each trace is indicated by a dashed line of matching color in an enlarged fragment on the right. During Riluzole treatment the rate of depolarization kept decreasing in parallel with loss of bursting: the mean slope was 16±3mV/s in 5HT, 8±2 mV/s in 1μM Riluzole, 7±2 mV/s at the start of 3μM Riluzole treatment (when the AB is still oscillating) and close to 0 mV/s at the end of Riluzole treatment (silent AB) ($p<0.05$, n=30 bursts per treatment, 2 different AB neurons, Figure 4.2B). These data suggest that the Riluzole-sensitive $I_{Na(P)}$ determines the rate of depolarization by driving the membrane voltage to the threshold for bursting; the rate of this depolarization has to be fast enough to make the transition to bistability before other currents such as fast sodium current $I_{Na(T)}$ inactivate and block spiking (Kuo et al, 2006, Theiss et al, 2007).

Serotonin Does Not Enhance the Persistent Sodium Current in the AB

In Chapter 2, I described the biophysical and pharmacological characterization of $I_{Na(P)}$ in the AB neuron. Briefly, the current was measured in TEVC with a slowly depolarizing ramp command voltage and a P/N=6 leak subtraction protocol, after pharmacological block of most other ionic currents. The $I_{Na(P)}$ formed a region of negative slope conductance in the subthreshold voltage region (Figs. 4.3 and 2.4). It activated around -65 mV and peaked around -45mV (see Chapter 2 for details). The average peak amplitude of $I_{Na(P)}$ in the AB was around -3 nA. The persistent sodium current was blocked by Riluzole in a concentration-dependent manner

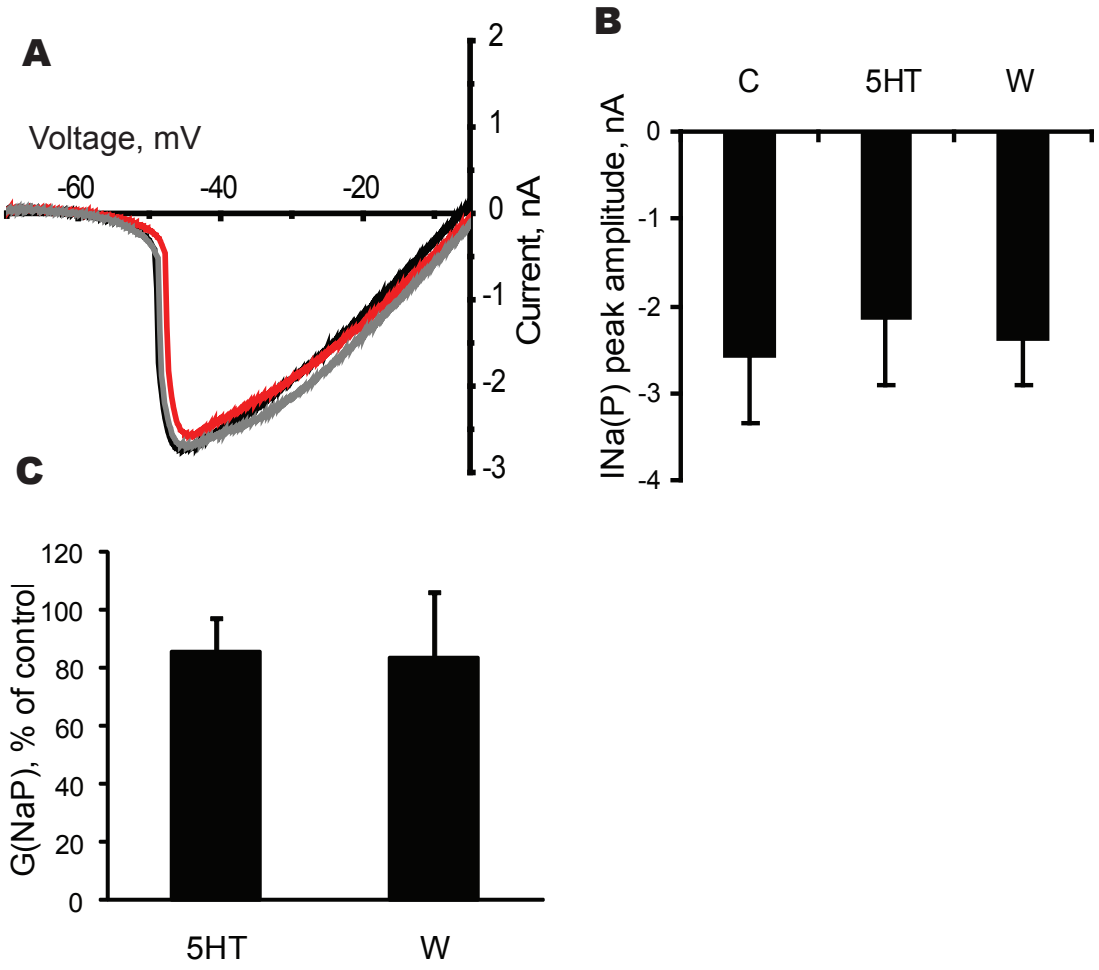

Figure 4.3. Serotonin does not modulate the persistent sodium current in the AB neuron.

A. Persistent sodium current-voltage plot under control conditions (black), during 5HT application (red) and after 40 min washout (gray) from a representative AB neuron.

B. The mean INa(P) peak amplitude in the presence of 5HT was not statistically different from mean peak amplitude under control conditions or after washout ($p>0.05$, $n=5$).

C. The mean Na(P) conductance in 5HT and after washout as a percentage of the control values. There was no significant difference between conditions ($p>0.05$, $n=4$).

with an IC_{50} of 3.2±0.2 μM, as well as by TTX with an IC_{50}= 4.4±0.2 nM. For figures and detailed description of $I_{Na(P)}$ properties, see Chapter 2.

As shown by the Riluzole block of 5HT- induced oscillations, $I_{Na(P)}$ seemed to be critical in sodium-dependent bursting, but it was not enhanced by 5HT in the AB neuron. There was no difference between I-V plots under control conditions, during 5HT application and after 30 min washout (Fig. 4.3A, black, red and gray traces respectively, from a representative AB neuron). The mean peak amplitude was - 2.6±0.8nA under control conditions, -2.2±0.8 nA in serotonin and -2.4±0.5 nA after serotonin washout (Fig. 4.3B, n=5). The mean reduction in amplitude of 0.4±0.4 nA in 5HT was not statistically significant (student's t-test, $p>0.05$, n=5). The mean peak persistent sodium conductance was 28±3.8 nS under control conditions and 22±3.7 nS in the presence of 5HT ($p>0.05$, n=4)

Serotonin Inhibits Outward Currents in the AB

An additional possible mechanism for serotonin-activated bursting is an inhibition of the outward currents which compete with $I_{Na(P)}$ to determine the ramp depolarization leading to the burst; such a reduction would then uncover the persistent sodium current and tip the membrane equilibrium towards bistability. To measure the 5HT effect on the amplitude of outward currents in the pyloric pacemaker, I used a cocktail of 10^{-4}M TTX, 5μM PTX and 5mM CsCl to block sodium currents, glutamatergic synapses and I_h, respectively (for these experiments, AB was not isolated from the PD and VD neurons). I have found that in the AB neuron, serotonin significantly inhibited two potassium currents, the leak current and $I_{K(Ca)}$, while it had no visible effect on the transient potassium current, I_A.

Transient potassium current. To block the calcium-activated potassium current, I used 0.6mM $CdCl_2$ in addition to TTX, PTX, and CsCl to block other currents. I

Figure 4.4. Serotonin effects on the outward currents in the AB

A. The leak current was measured at the end of a -5 mV step from the -55 mV holding potential (arrowhead). Leak current was reversibly reduced by serotonin: black (under control conditions), red (during 5HT) and gray (after washout).
B. Leak current in the presence of 5HT and after wash, as a percentage of control values. Asterisks show statistically significant difference ($p<0.05$, n=5, student's t-test).
C. The total outward current is a sum of $I_{K(V)}$ and $I_{K(Ca)}$. Current traces are shown during a step to +25 mV: black, under control conditions, red, during 5HT application, gray, after washout. The transient portion of the current, I_{tr}, is marked by an arrowhead; the sustained portion, I_s, is marked by an arrow.
D. Mean amplitude of the transient total outward current (I_{tr}) decreased in 5HT by 10%. Asterisks indicate a statistically significant difference ($p<0.05$, n=5, student's t-test).
E. Mean amplitude of the sustained outward current (I_s) decreased in 5HT by 1.2% ($p>0.5$, n=8, student's t-test).

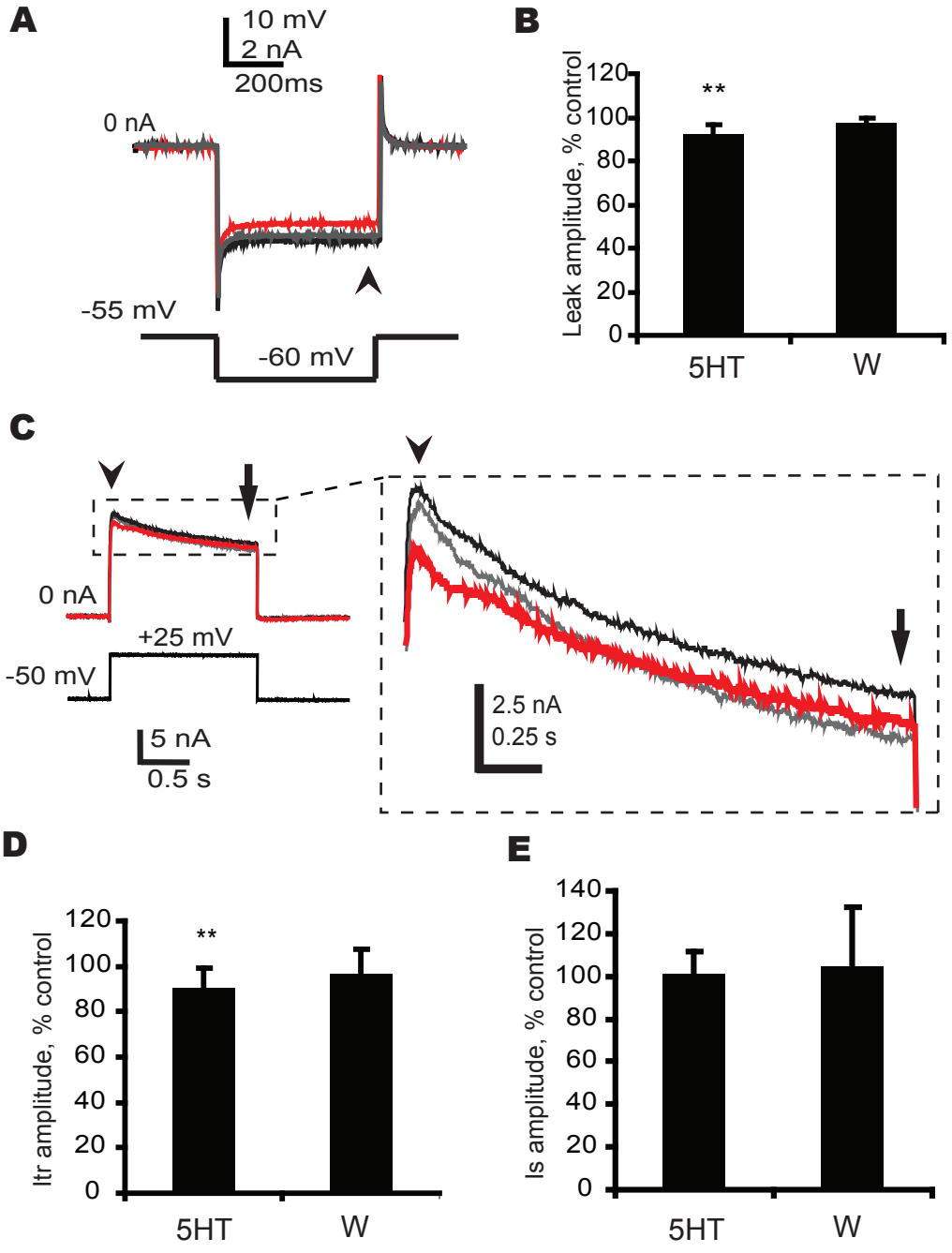
A
10 mV
2 nA
200ms
0 nA
-55 mV
-60 mV
B
Leak amplitude, % control
120
100
80
60
40
20
0
**
5HT
W
C
0 nA
+25 mV
-50 mV
5 nA
0.5 s
2.5 nA
0.25 s
D
Itr amplitude, % control
120
100
80
60
40
20
0
**
5HT
W
E
Is amplitude, % control
140
120
100
80
60
40
20
0
5HT
W

then generated two sets of depolarizing voltage steps, one of which is preceded by a long hyperpolarizing pre-step to –80 mV to de-inactivate the transient potassium channels. I_A was calculated as the difference between the current series measured with and without hyperpolarizing pre-steps. In agreement with Peck *et al* (2001), serotonin did not have any effect on the amplitude of I_A in the AB neuron (data not shown).

Leak current. I measured the leak current at the end of 5 mV hyperpolarizing steps (Fig. 4.4A, an upward arrowhead) from a holding potential of -55 mV, in the presence of all the above mentioned blockers. Upon addition of serotonin, the amplitude of the leak current on average was reversibly reduced (Fig. 4.4A, leak current traces under control conditions (black), in the presence of 5HT (red), and after 40 min washout (gray)). The mean reduction of amplitude was 8.1±4.5 % of the control value (Fig. 4.4B, asterisks, statistically significant difference, student's t-test, $p<0.02$, $n=5$).

Delayed rectifier and calcium-activated potassium currents. To measure the sum of $I_{K(V)}$ and $I_{K(Ca)}$, 2 mM 4-AP was added to the blocker cocktail to eliminate I_A; to separate the two remaining potassium currents, 0.6 mM $CdCl_2$ was applied to measure $I_{K(V)}$; $I_{K(Ca)}$ was calculated as a difference between the currents measured with and without $CdCl_2$.

Serotonin partially inhibited the total outward current measured from a holding potential of -50 mV, which constituted the sum of $I_{K(V)}$ and $I_{K(Ca)}$ (Figure 4.4C). The transient (peak) portion of this total outward current (marked by a downward arrowhead, Fig. 4.4C) showed a statistically significant decrease of 10±3.7% during serotonin application ($p<0.005$, $n=8$, Fig. 4.4D). The sustained portion of the total current (marked by a downward arrow, Fig.4.4C) decreased by 1.2% which was not statistically significant ($p>0.05$, $n=8$, Fig. 4.4E). To separate

serotonin's effects on either current, I directly measured $I_{K(V)}$ in the AB neuron after blocking $I_{K(Ca)}$ with Cd^{2+}: serotonin slightly increased $I_{K(V)}$ amplitude in two cells (Fig. 4.5A) and decreased it in two other cells (Fig. 4.5B); both effects were reversible upon washout. The mean I-V curve for all 4 neurons tested under control conditions (black), in 5HT (red) and after washout (gray) overlap (Fig 4.5C). The mean amplitude of $I_{K(V)}$ measured at 25 mV was 14.9±3 nA under control conditions and 14.1±6 nA in 5HT, ($p>0.05$; n=4, Fig. 4.5D).

To determine serotonin's effect on $I_{K(Ca)}$, I calculated the difference between the total outward current (in the presence of TTX, PTX,4-AP and CsCl) and $I_{K(V)}$ (measured in $CdCl_2$, TTX, PTX, 4-AP and CsCl) by digital subtraction (Fig. 4.5E, current traces under control conditions and in the presence of 5HT, black and red, respectively). The mean peak current amplitude was 8.3±1.3 nA under control conditions and 6.7±1.5 nA in the presence of 5HT (81% of the control value); this reduction was statistically significant (Fig.4.5F, $p<0.05$, n=4). Thus, the main effect of serotonin on the AB outward currents was an inhibition of two potassium currents, $I_{K(Ca)}$ and the leak current.

DISCUSSION

The role of the persistent sodium current in motor systems has been extensively studied, both in invertebrate (Christensen *et al.,* 1988; Lapied *et al.,*1989; Saito and Wu, 1991; Schäfer *et al.,* 1994; Opdyke and Calabrese, 1994; Rakowski *et al.,* 2002; Clay *et al.,* 2003; Nikitin *et al*., 2006, 2008) and vertebrate CPGs, including those for mastication (Wu *et al.,* 2005; Enomoto *et al.,* 2006), locomotion (Zhong et al., 2007; Tazerart et al., 2007, 2008; Ziskind-Conhaim *et al.,* 2008) and respiration, among others. Notably, in the respiratory CPG, there is still controversy about the role of $I_{Na(P)}$ in rhythmogenesis: some suggest that it is important (Rybak *et al*., 2007; Smith *et al.,* 2007; Rybak *et al.,* 2003); while

Figure 4.5. Serotonin inhibits $I_{K(Ca)}$, but not $I_{K(V)}$ in the AB

A. Serotonin had a variable, non-significant effect on the delayed rectifier potassium current $I_{K(V)}$ in the AB neuron. Examples from two different AB neurons are shown. A, slight increase of the current amplitude in 5HT; B. slight decrease of the current amplitude in 5HT.

C. Mean I-V curve for $I_{K(V)}$ from 4 AB neuron: under control conditions black), in 5HT (red) and after washout (gray).

D. Mean $I_{K(V)}$ amplitude measured during a voltage step to +25 mV in the presence of 5HT was not different from the current amplitude under control conditions ($p>0.05$, $n=4$).

E. Isolated $I_{K(Ca)}$ traces from a representative AB neuron during a voltage step to 25 mV: black, under control conditions, red, in 5HT. The current was calculated as a difference between the total outward current and $I_{K(V)}$.

F. Mean peak (transient) current amplitude of $I_{K(Ca)}$ at +25 mV in 5HT and after washout, as a percentage of control values. Asterisks indicate a statistically significant difference ($p<0.05$, $n=4$).

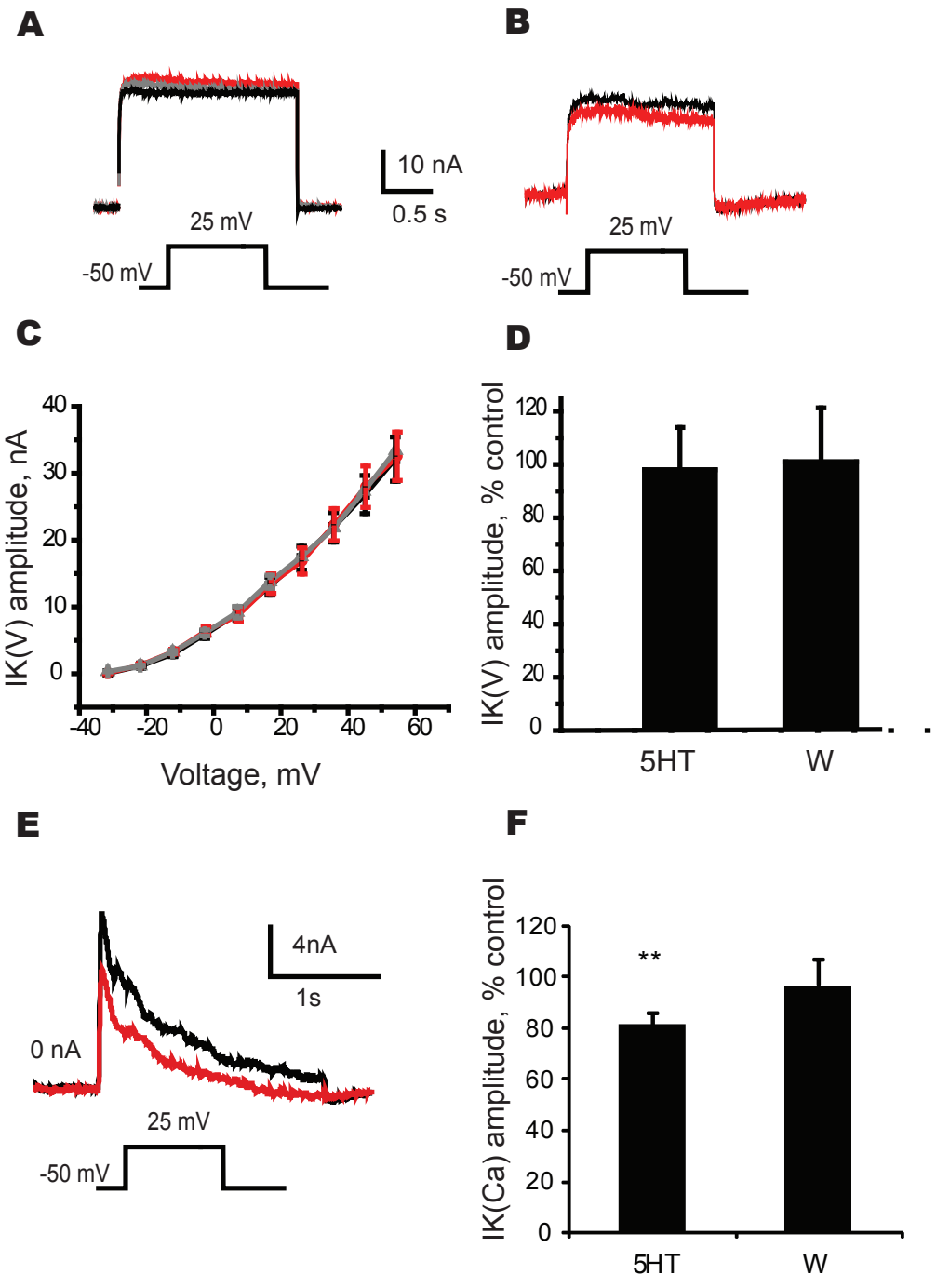
A
10 nA
0.5 s
25 mV
-50 mV
B
25 mV
-50 mV
C
IK(V) amplitude, nA
40
30
20
10
0
-40
-20
0
20
40
60
Voltage, mV
D
IK(V) amplitude, % control
120
100
80
60
40
20
0
5HT
W
E
4nA
1s
0 nA
25 mV
-50 mV
F
IK(Ca) amplitude, % control
120
100
80
60
40
20
0
**
5HT
W

others suggest it is not necessary for network rhythm generation (Del Negro *et al.*, 2002; Pace *et al*., 2007) even though $I_{Na(P)}$ clearly enables a population of respiratory neurons to burst rhythmically (Del Negro *et al.*, 2002; Pace *et al*., 2007). These differences in the results on $I_{Na(P)}$ are probably due to different experimental approaches and different preparations used in these studies.

More critical than the mere presence of $I_{Na(P)}$ in these neurons is the balance between this current and outward currents that oppose it in the subthreshold voltage range. In particular, the ratio of the persistent sodium conductance and the leak conductance was demonstrated both theoretically and experimentally to be the most reliable criterion for a neuron to be able to burst in the respiratory Pre-Bötzinger complex (Butera *et al.,* 1999a; Smith et al., 200; DelNegro, 2002, 2005; Koizumi and Smith, 2008).

Riluzole blocks 5HT bursting by slowing down the rate of V_m depolarization

Two lines of evidence suggest that the persistent sodium current is essential for serotonin-induced AB bursting. First, bursting is highly dependent on the external sodium concentration, and is blocked by TTX (Harris-Warrick and Flamm, 1987). Second, Riluzole blocks 5HT-induced bursting at 3-10 μM (Fig. 4.1), a concentration that would block 40-80% of $I_{Na(P)}$ based on the IC_{50}=3.2 μM determined in Chapter 2.

My results suggest that Riluzole blocks serotonin bursting by an inhibition of $I_{Na(P)}$ which specifically slows down the rate of depolarization in the rise to the start of each burst (Figure 4.2A and B). Riluzole changed the shape of the burst envelope and sequentially decreased the number of action potentials per burst in a bursting AB as it washed in. With time in Riluzole, the neuron stopped firing action potentials, leaving subthreshold oscillations; the depolarizing slope became smaller and eventually flattened out when AB became quiescent. The mean

depolarizing slope in the presence of 1 μM Riluzole was half of its pre-Riluzole value; the difference in slope values of bursting AB neuron before and during Riluzole application was statistically significant ($p<0.05$, n=30, Fig. 4.2C). The data suggest that $I_{Na(P)}$ determines the slope (rate) of the membrane potential depolarization making it more likely to reach the threshold for bursting. In spinal motoneurons, $I_{Na(P)}$ provides the drive for reaching the threshold for action potential generation and repetitive firing (Kuo et al, 2006, Theiss et al, 2007). Thus, in the AB neuron, the persistent sodium current activates at more hyperpolarized voltages, initiates depolarization to reach the threshold for $I_{Na(T)}$ and helps the activation of the transient sodium channel overcome its inactivation. It appears that both sodium currents are needed to generate sustained bursting in the AB. Unfortunately, there is no experimental way to selectively block $I_{Na(T)}$ without also blocking $I_{Na(P)}$ to separate the roles of each current in bursting generation. Using a mathematical model of AB or the Dynamic clamp may be useful in addressing this question.

Specificity of Riluzole effect. A critical issue is whether Riluzole stops 5HT oscillations by blocking currents other than $I_{Na(P)}$. Although 10-300 μM is routinely used as a specific blocker of $I_{Na(P)}$ in vertebrate neuronal preparations (Urbani and Belluzzi, 2000; Miles *et al.,* 2005; Kuo *et al,*. 2006; DelNegro *et al.,* 2002; Wu *at al.,* 2005; Cramer *et al.,* 2005; Zhong *et al.,* 2007; Tazerart *et al.,* 2007), Riluzole has side effects on other currents at higher concentrations. For instance, it was reported to block (Zona *et al.,* 1998; Duprat *et al.*, 2000; Cao *et al*., 2002; Ahn *et al.,* 2005) or activate (Duprat *et al.*, 2000; Beltran-Parrazal and Charles, 2003) potassium conductances at concentrations of 100 μM and above. Riluzole also blocks high voltage activated and other types of calcium channels at 100-300 μM (Huang *et al*., 1997; Siniscalchi *et al.*, 1997; Stefani

et al., 1997). In addition, Riluzole also inhibits the synaptic release of GABA and glycine (Umemiya & Berger, 1995; Mohammadi *et al.,* 2001; He *et al*., 2002; Lamanauskas and Nistri, 2008). Moreover, Riluzole directly inhibits PKC at 10-30 μM in cultured cortical and endothelial cells (Noh *et al.,* 2000; Yoo *et al.,* 2005).

To avoid these and other possible side effects, I used low micromolar concentrations (1-5μM) of Riluzole. It is unlikely that Riluzole's block of 5HT bursting was due to its side effects. First, all glutamatergic transmission in the STG was already blocked in the experiments, and the AB neuron does not receive GABAergic or glycinergic synapses. Second, 5HT-induced oscillations persisted in low calcium saline (Harris-Warrick and Flamm, 1987), thus making the possible partial block of calcium currents irrelevant. Finally, the effect on potassium channels was observed only at concentrations higher than 100 μM. Like its counterparts in mammalian neurons, one of the arthropod 5HT receptors cloned from the spiny lobster STNS (5-$HT_{2\beta Pan}$) couples with the G_q to PLC which activates the PKC signaling pathway (Clark et al., 2004). Moreover, this receptor was constitutively active when stably expressed in HEK cells (Clark et al., 2004). PKC has been shown to differentially modulate sodium channels, inhibiting the fast sodium and enhancing the persistent sodium currents (Numann *et al.,* 1991; Franceschetti *et al.,* 2000; Baker, 2005). Riluzole is also known to directly inhibit PKC at 10-30 μM concentration (Noh *et al.,* 2000; Yoo *et al.,* 2005), and it is possible that Riluzole blocks the persistent sodium current and hence 5HT oscillations via inhibition of the PKC pathway. However, given the much lower concentration of Ril needed to block bursting, the most likely mechanism is a direct blockade of $I_{Na(P)}$.

Model for Serotonin -induced Bursting in the AB Neuron

Figure 4.6. Ionic mechanisms of serotonin and dopamine bursting in the AB neuron.

A. Serotonin significantly increases the ratio of the persistent sodium and leak conductances in the AB. $G_{Na(P)}/G_{Leak}$ is expressed as a percentage of the ratio under control conditions ($n=4$, $p<0.05$). 5HT, in the presence of serotonin; W, after washout.
B. Serotonin induces bursting by inhibition of two outward currents, I_{leak} and $I_{K(Ca)}$. This reduction uncovers the depolarizing effect of $I_{Na(P)}$, which speeds up the rate of depolarization bringing the voltage to the threshold for bursting quickly enough to induce regenerative oscillations.
C. DA application restores the bursting of an isolated AB neuron after Riluzole blocked 5HT-induced bursting. 5HT, serotonin induced bursting in a synaptically isolated AB; 5HT+Ril, application of 3 μM Riluzole blocks bursting within 20 min; 5HT+Ril+DA, DA application restores bursting within 5 minutes. Horizontal bar corresponds to -51 mV.
D. Dopamine induces bursting by increasing the intracellular calcium concentration and enhancing I_{CAN}; DA also enhances I_h (Peck *et al.,* 2006), inhibits outward currents I_A and I_{leak} (Peck *et al.,* 2001) and considerably reduces $I_{Ca(V)}$ amplitude (Johnson *et al.,* 2003).

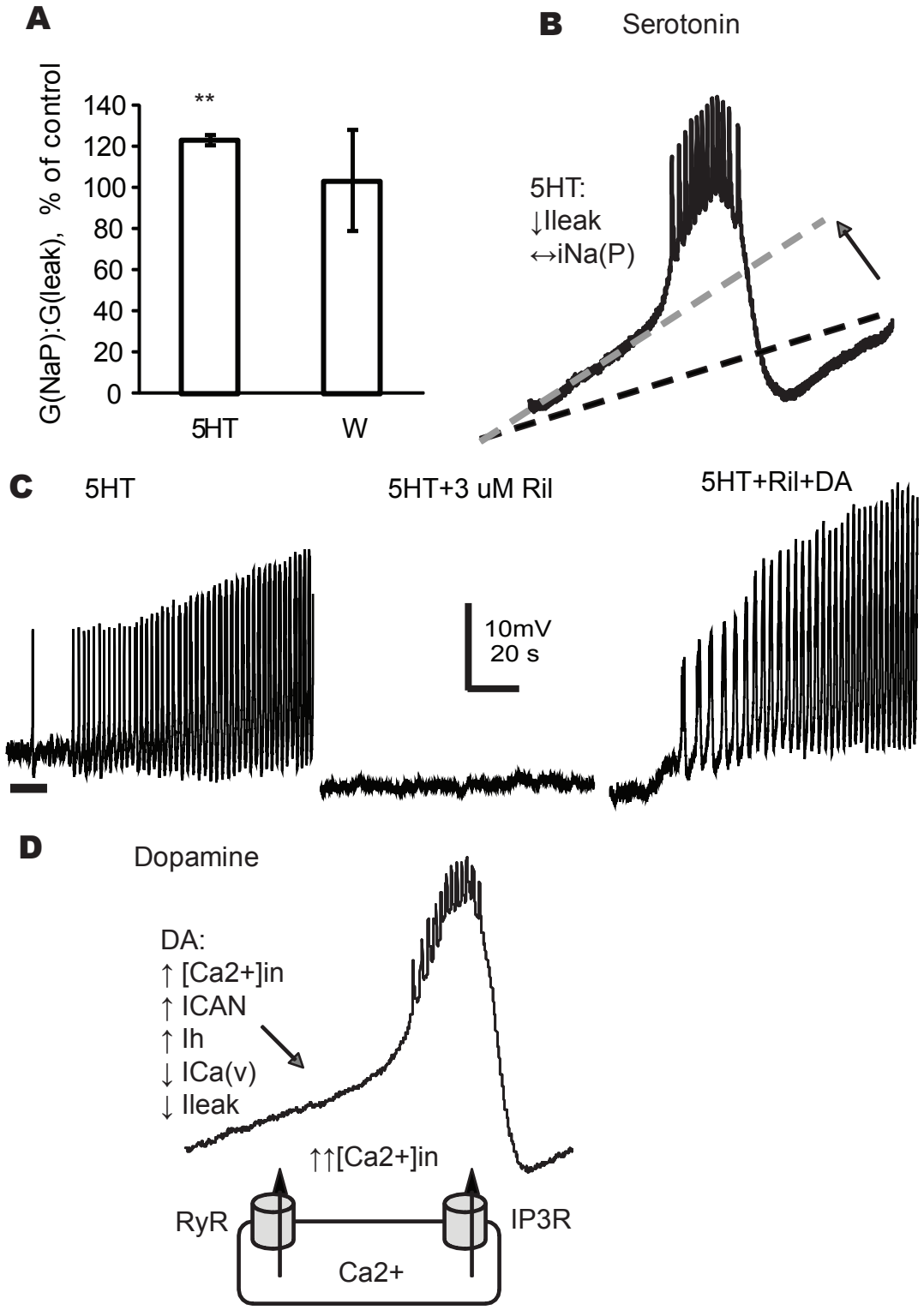
A
G(NaP):G(leak), % of control
140
120
100
80
60
40
20
0
**
5HT
W
B
Serotonin
5HT:
↓Ileak
↔iNa(P)
C
5HT
5HT+3 uM Ril
5HT+Ril+DA
10mV
20 s
D
Dopamine
DA:
↑ [Ca2+]in
↑ ICAN
↑ Ih
↓ ICa(v)
↓ Ileak
↑↑[Ca2+]in
RyR
IP3R
Ca2+

Although the persistent sodium current seems to be critical for pacemaker bursting evoked by 5HT, it was not itself enhanced by bath-applied serotonin. Instead, serotonin appears to reveal the effect on $I_{Na(P)}$ by inhibiting two competing outward currents, $I_{K(Ca)}$ (20% reduction) and the leak current (8% reduction). The inhibition was small but statistically significant and fully reversible on washout for both currents, and appears to be sufficient to uncover the depolarizing effect of the slow sodium current.

In the rodent Pre-Bötzinger complex, serotonin is critically involved in respiratory bursting, although the exact targets of serotonin vary in different species: 5HT enhanced $I_{Na(P)}$ in mouse (Pena and Ramirez, 2002) and inhibited leak currents in rat (Ptak et al., 2009). However, the common net effect of serotonin in the respiratory CPG is to increase the ratio of the persistent sodium conductance to the potassium conductances, including leak, M-current and $I_{K(Ca)}$. The importance of this balance between $I_{Na(P)}$ and outward currents in bursting pacemaker neurons was initially proposed by Butera *et al*. (1999). The ratio $G_{Na(P)}$: G_{leak} is the main difference in intrinsic properties of pacemaker and non-pacemaker neurons: the higher the ratio, the more likely for a neuron to be able to burst endogenously (Butera *et al.,* 1999a, Smith *et al.,* 2000; Del Negro *et al.,* 2002, 1998; Pace *et al,* 2007). Serotonin not only enhanced the general excitability of respiratory neurons, but transformed non-intrinsic bursters into intrinsic bursters in this CPG, although it is not clear whether 5HT inhibition of the potassium-dominated leak conductance alone is sufficient for burst generation in these neurons (Ptak et al., 2009). My own results in the pyloric pacemaker neuron provide further support for this mechanism. In the AB, the ratio of $G_{Na(P)}$ to G_{Leak} calculated at subthreshold voltage (-60 to -65 mV) significantly increased in the presence of 5HT (Fig. 4.6A); this suggests that in the AB neuron reduction

of leak conductance alone could be enough to unmask the effect of persistent sodium conductance.

It is interesting that the $5HT_{2\beta Pan}$ receptor in the spiny lobster has a one amino acid substitution that could render it constitutively active (Clark et al., 2004). Although the exact 5HT receptor profile of the AB neuron is currently unknown, it is intriguing possibility that this constitutively active receptor maintains a basal level of PKC activity, which is shown to augment $I_{Na(P)}$ (Numann *et al.,* 1991; Franceschetti *et al.,* 2000; Baker, 2005) to continuously provide the depolarizing force for AB bursting.

Dopamine and Serotonin Employ Different Strategies to Evoke Bursting in the Pacemaker AB Neuron

Building on the previous work by Harris-Warrick and Flamm in the lobster pyloric pacemaker neuron, I showed two distinct mechanisms of pacemaking – those relying on $I_{Na(P)}$ and those relying on I_{CAN}, are employed by the same AB neuron. Each of the mechanisms requires the presence of its own neuromodulator, serotonin for the $I_{Na(P)}$-based bursting and dopamine for the I_{CAN}-based bursting. Serotonin acts by a conductance decrease mechanism, similar to that in rat respiratory neurons (Ptak *et al.,* 2009): it partially inhibits two outward potassium currents to uncover the depolarizing effect of the persistent sodium current, which in turn determines the rate of membrane depolarization making it more likely to reach the threshold for bursting (Fig.4.6B). Although, I did not address this question in the current study, burst termination most likely occurs because of slow time- and voltage-dependent inactivation of $I_{Na(P)}$ in the AB, as well as activation of $I_{K(Ca)}$.

As described in Chapter 3, unlike serotonin, dopamine increases the basal levels of cytoplasmic calcium by triggering the release of calcium from internal stores.

Both types of intracellular calcium channels are critical for bursting as shown by the block of DA oscillations by Xestospongin and Ryanodine, specific blockers of IP_3 and Ryanodine receptors channels, respectively. This high intracellular calcium leads to an activation of I_{CAN} and a subsequent depolarization of the membrane potential (Fig.4.6D). This initial depolarization most likely leads to calcium influx via voltage-gated calcium channels; higher influx of calcium results in a cycle of more calcium influx via CAN channels and calcium release from RyR and IP_3R. This process of calcium –dependent depolarization is self-sustained due to several positive feedback loops: calcium-dependent activation of both I_{CAN} and ER calcium channels. At some point, the intracellular calcium concentration may reach levels at which it becomes inhibitory to the voltage-gated and intracellular calcium channels leading to the burst termination. In addition, higher $[Ca^{2+}]_{in}$ combined with depolarization trigger activation of the calcium-dependent potassium current, which overcomes the depolarizing effect of I_{CAN} and terminates bursting. Additionally, other known effect of DA, such as enhancement of I_h (Peck et al., 2006), reduction of I_A and the leak current (Peck et al., 2001) contribute to the overall excitability of the AB to facilitate rhythmic bursting.

In addition to the distinct ionic dependence, DA and 5HT bursting have dissimilar pharmacology. DA oscillations are sensitive to FFA, but not to TTX or Riluzole, while 5HT oscillations are sensitive to TTX and Riluzole, but not to FFA. Interestingly, DA application can restore oscillations in the AB neuron after Riluzole or TTX blocked 5HT bursting (Fig. 4.6C, n=5); this fact reinforces the idea that within a single neuron DA and 5HT employ two independent mechanisms for rhythm generation.

The general outcome of the burst-inducing modulators such as DA and 5HT is to trigger a non-linear response from the cellular membrane potential that is a result of interplay between ionic currents, second messenger cascades and intracellular calcium (Harris-Warrick, 2002; Ramirez *et al.,* 2004). The change that the neuromodulators introduce into this interplay need not be large to make the transition from quiescence or tonic spiking to bursting; changes of just a few percent in conductance or voltage dependence may be sufficient (Guckenheimer *et al*, 1993).

This redundancy in bursting mechanisms is not unique for the pyloric system. Many motor systems have degenerate networks or rhythmogenic mechanisms in both invertebrates and vertebrates. For example, within respiratory CPG, two different populations of pacemaker neurons with distinct pharmacology and physiological functions employ two different mechanisms of bursting, the cadmium-insensitive (sodium-dependent) and cadmium-sensitive (sodium- and calcium-dependent) (Pena et al., 2004; Viemari JC, Ramirez JM., 2006; Peña and Aguileta, 2007). However, clear evidence for multiple bursting mechanisms in a single neuron has not been presented in other systems.

Finally, it is noteworthy to remember that the pyloric pacemaker kernel consists of the AB neuron electrically coupled to the two PD neurons that have very different physiological profiles from the AB neuron. PD neurons only slow endogenous bursting in the presence of appropriate neuromodulators; they are inhibited by DA, and fire tonically when isolated from all synaptic and neuromodulatory input. The net effect of DA is different in reduced preparations of the AB alone, or the AB coupled to one or two PD neurons, compared to its effect on the more intact pyloric network (Ayali and Harris-Warrick 1999). Thus the ionic mechanisms of the AB bursting in the presence of monoamines have to

be placed into the general functional picture of the pacemaker kernel and pyloric subcircuit, as well as the whole STG.

REFERENCES

Alzheimer C, Schwindt PC, and Crill WE. (1993) Modal gating of Na^+ channels as a mechanism of persistent Na^+ current in pyramidal neurons from rat and cat sensorimotor cortex. *J Neurosci* 13: 660-673.

Attwell D, Cohen I, Eisner D, Ohba M, and Ojeda C. (1979) The steady-state-TTX-sensitive ("window") sodium current in cardiac Purkinje fibers. *Pfluegers* 379: 137-142.

Ayali A, Harris-Warrick RM. (1999) Monoamine control of the pacemaker kernel and cycle frequency in the lobster pyloric network. *J Neurosci*. 19(15):6712-22.

Baker, MD. (2005) Protein kinase C mediates up-regulation of tetrodotoxin-resistant,

persistent Na+ current in rat and mouse sensory neurones. *J Physiol.* 567(3):851-67.

Bertram, R., Butte, M. J., Kiemel, T., and Sherman, A. (1995) Topological and phenomenological classification of bursting oscillations. *Bull. Math. Biol.* 57: 413-439.

Butera RJ Jr., Rinzel J, and Smith JC. (1999a) Models of respiratory rhythm generation in the pre-Bötzinger complex. I. Bursting pacemaker neurons. *J Neurophysiol* 81: 382-397.

Butera RJ Jr., Rinzel J, and Smith JC. (1999b) Models of respiratory rhythm generation in the pre-Bötzinger complex. II. Populations of coupled pacemaker neurons. *J Neurophysiol* 81: 398-415.

Canavier CC, Baxter DA, Clark JW, Byrne JH. (1994) Multiple modes of activity in a model neuron suggest a novel mechanism for the effects of neuromodulators. *J Neurophysiol*. 72(2):872-82.

Clark MC, Dever TE, Dever JJ, Xu P, Rehder V, Sosa MA, Baro DJ. (2004) Arthropod 5-HT2 receptors: a neurohormonal receptor in decapod crustaceans that displays agonist independent activity resulting from an evolutionary alteration to the DRY motif. *J Neurosci.* 24(13):3421-35.

Clay JR. On the persistent sodium current in squid giant axons. *J Neurophysiol*. 2003 89(1):640-4.

Craelius W, Green W, Wu KM. (1993) Persistent sodium currents induced by anthopleurin-A and their relationship to early afterdepolarizations in ventricular myocytes. *Arch Int Pharmacodyn Ther.* 324:60-74.

Cramer NP, Li Y, Keller A. (2007) The whisking rhythm generator: a novel mammalian network for the generation of movement. *J Neurophysiol*. 97(3):2148-58.

Crill, WE. (1996) Persistent sodium current in mammalian central neurons. *Annu Rev Physiol*. 58:349-62. C*urr Biol* 11: R986–R996

Daun S, Rubin JE, Rybak IA. (2009) Control of oscillation periods and phase durations in half-center central pattern generators: a comparative mechanistic analysis. *J Comput Neurosci.* 27(1):3-36.

Del Negro CA, Koshiya N, Butera RJ Jr & Smith JC (2002). Persistent sodium current, membrane properties and bursting behavior of pre-botzinger complex inspiratory neurons in vitro. *J Neurophysiol* 88, 2242–5220.

Del Negro CA, Morgado-Valle C, Hayes JA, Mackay DD, Pace RW, Crowder EA & Feldman JL (2005). Sodium and calcium current-mediated pacemaker neurons and respiratory rhythm generation. *J Neurosci* 25, 446–453.

Duprat F, Lesage F, Patel AJ, Fink M, Romey G, Lazdunski M (2000) The neuroprotective agent riluzole activates the two P domain K(+) channels TREK-1 and TRAAK. *Mol Pharmacol* 57:906–912.

Enomoto A, Han JM, Hsiao CF, Chandler SH. (2007) Sodium currents in mesencephalic trigeminal neurons from Nav1.6 null mice. *J Neurophysiol*. 98(2):710-9.

Enomoto A, Han JM, Hsiao CF, Wu N, Chandler SH. (2006) Participation of sodium currents in burst generation and control of membrane excitability in mesencephalic trigeminal neurons. *J Neurosci*. 26(13):3412-22.

Franceschetti S, Taverna S, Sancini G, Panzica F, Lombardi R, Avanzini G. (2000)

Protein kinase C-dependent modulation of Na+ currents increases the excitability of rat neocortical pyramidal neurones. *J Physiol*. 528 Pt 2:291-304.

Goldin AL. (2002) Evolution of voltage-gated Na(+) channels. *J Exp Biol*. 205(Pt 5):575-84.

Golomb D, Yue C, Yaari Y. (2006) Contribution of persistent Na+ current and M-type K+ current to somatic bursting in CA1 pyramidal cells: combined experimental and modeling study. *J Neurophysiol.* 96(4):1912-26.

Guckenheimer J, Gueron S, Harris-Warrick RM. (1993) Mapping the dynamics of a bursting neuron. *Philos Trans R Soc Lond B Biol Sci*. 341(1298):345-59.

Guckenheimer J, Harris-Warrick R, Peck J, Willms A. Bifurcation, bursting, and spike frequency adaptation. *J Comput Neurosci*. (1997) 4(3):257-77.

Harris-Warrick RM. (2002). Voltage-sensitive ion channels in rhythmic motor systems. *Curr Opin Neurobiol*. 12(6):646-51.

Harvey PJ, Li X, Li Y, Bennett DJ. (2006) Endogenous monoamine receptor activation is essential for enabling persistent sodium currents and repetitive firing in rat spinal motoneurons. *J Neurophysiol.* 96(3):1171-86.

Harvey, P. J., Li X., Li, Y., and Bennett D. J. (2006a) 5-HT2 Receptor Activation Facilitates a Persistent Sodium Current and Repetitive Firing in Spinal

Motoneurons of Rats With and Without Chronic Spinal Cord Injury. *J Neurophysiol*. 96(3): 1158 - 1170.

Harvey, P. J., Li, X., Li, Y. and Bennett, D. J. (2006b) Endogenous Monoamine Receptor Activation Is Essential for Enabling Persistent Sodium Currents and Repetitive Firing in Rat Spinal Motoneurons. *J Neurophysiol*, 96(3): 1171 - 1186.

Hodgkin AL, and Huxley AF. (1952) A quantitative description of membrane current and its application to conduction and excitation in nerve. *J Physiol (Lond)* 117: 500-544.

Hsiao CF, Del Negro CA, Trueblood PR, Chandler SH. (1998) Ionic basis for serotonin-induced bistable membrane properties in guinea pig trigeminal motoneurons. *J Neurophysiol* 79: 2847–2856.

Huang CS, Song JH, Nagata K, Yeh JZ, Narahashi T (1997) Effects of the neuroprotective agent riluzole on the high voltage-activated calcium channels of rat dorsal root ganglion neurons. *J Pharmacol Exp Ther* 282:1280–1290.

Kang Y, Saito M, Sato H, Toyoda H, Maeda Y, Hirai T, Bae YC. (2007) Involvement of persistent Na+ current in spike initiation in primary sensory neurons of the rat mesencephalic trigeminal nucleus. *J Neurophysiol*. 97(3):2385-93.

Kiss T, Pirger Z, Kemenes G. (2009) Food-aversive classical conditioning increases a persistent sodium current in molluscan withdrawal interneurons in a transcription dependent manner. *Neurobiol Learn Mem*. 92(1):114-9.

Kiss, T. (2003) Evidence for a persistent Na-conductance in identified command neurones of the snail, Helix pomatia. *Brain Res.* 989(1):16-25.

Koizumi H, Smith JC. (2008) Persistent Na^+ and K^+-dominated leak currents contribute to respiratory rhythm generation in the pre-Bötzinger complex in vitro. *J Neurosci* 28: 1773–1785.

Kuo JJ, Lee RH, Zhang L, Heckman CJ (2006) Essential role of the persistent sodium current in spike initiation during slowly rising inputs in mouse spinal neurones. *J Physiol (Lond)* 574:819–834.

Kuo JJ, Siddique T, Fu R, Heckman CJ. (2005) Increased persistent Na(+) current and its effect on excitability in motoneurones cultured from mutant SOD1 mice. *J Physiol.* 563(Pt 3):843-54.

Lamanauskas N, Nistri A. (2008) Riluzole blocks persistent Na+ and Ca2+ currents and modulates release of glutamate via presynaptic NMDA receptors on neonatal rat hypoglossal motoneurons in vitro. *Eur J Neurosci*. 27(10):2501-14.

Lamanauskas N, Nistri A. (2008) Riluzole blocks persistent Na+ and Ca2+ currents and modulates release of glutamate via presynaptic NMDA receptors on neonatal rat hypoglossal motoneurons in vitro. *Eur J Neurosci.* 27(10):2501-14

Lamas JA, Romero M, Reboreda A, Sánchez E, Ribeiro SJ. (2009) A riluzole- and valproate-sensitive persistent sodium current contributes to the resting membrane potential and increases the excitability of sympathetic neurones. *Pflugers Arch*. 458(3):589-99.

Ma, J.Y., Catterall, W.A., and Scheuer, T. (1997) Persistent sodium currents through brain sodium channels induced by G protein betagamma subunits. *Neuron* 19: 443–452.

Marder E. and Bucher, D. (2001) Central pattern generators and the control of rhythmic movements. *Curr Biol.*11(23):R986-96.

Marder E. and Calabrese R.L. (1996) Principles of rhythmic motor pattern generation, *Physiol Rev* 76: 687–717

Morgan, K., Stevens, E.B., Shah, B., Cox, P.J., Dixon, A.K., Lee, K., Pinnock, R.D. (2000) J. Hughes, P.J. Richardson, K. Mizuguchi and A.P. Jackson, Beta-3: an additional auxiliary subunit of the voltage-sensitive sodium

channel that modulates channel gating with distinct kinetics. *Proc. natn. Acad. Sci.USA* 97: 2308–2313

Nikitin ES, Kiss T, Staras K, O'shea M, Benjamin PR, Kemenes G. (2006) Persistent sodium current is a target for cAMP-induced neuronal plasticity in a state-setting modulatory interneuron. *J Neurophysiol.* 95(1):453-63.

Nikitin ES, Vavoulis DV, Kemenes I, Marra V, Pirger Z, Michel M, Feng J, O'Shea M, Benjamin PR, Kemenes G. (2008) Persistent sodium current is a nonsynaptic substrate for long-term associative memory. *Curr Biol*. 18(16):1221-6.

Noh KM, Hwang JY, Shin HC, Koh JY. (2000) A novel neuroprotective mechanism of riluzole: direct inhibition of protein kinase C. *Neurobiol Dis*. 7(4):375-83

Numann R, Catterall WA, Scheuer T. (1991) Functional modulation of brain sodium channels by protein kinase C phosphorylation. *Science.* 254(5028):115-8.

Opdyke CA, Calabrese RL. (1994) A persistent sodium current contributes to oscillatory activity in heart interneurons of the medicinal leech. *J Comp Physiol A*. 175(6):781-9.

Pace RW, Mackay DD, Feldman JL & Del Negro CA (2007). Role of persistent sodium current in mouse preB¨otzinger complex neurons and respiratory rhythm generation. *J Physiol* 580, 485–496.

Patton, D.E., Isom, L.L., Catterall, W.A. and Goldin, A.L. (1994) The adult rat brain beta 1 subunit modifies activation and inactivation gating of multiple sodium channel alpha subunits. *J. biol. Chem.* 269: 17,649–17,655.

Peck JH, Nakanishi ST, Yaple R, Harris-Warrick RM. (2001) Amine modulation of the transient potassium current in identified cells of the lobster stomatogastric ganglion. *J Neurophysiol*. 86(6):2957-65

Peña F, Aguileta MA. (2007) Effects of riluzole and flufenamic acid on eupnea and gasping of neonatal mice in vivo. *Neurosci Lett*. 415(3):288-93.

Peña F, Parkis MA, Tryba AK, Ramirez JM. (2004) Differential contribution of pacemaker properties to the generation of respiratory rhythms during normoxia and hypoxia. *Neuron*. 43(1):105-17.

Peña F, Ramirez JM. (2002) Endogenous activation of serotonin-2A receptors is required for respiratory rhythm generation *in vitro*. *J Neurosci* 22:11055–11064.

Peña F, Ramirez JM. (2004) Substance P-mediated modulation of pacemaker properties in the mammalian respiratory network. *J Neurosci* 24:7549–7556.

Plummer NW, Meisler MH. (1999) Evolution and diversity of mammalian sodium channel genes. *Genomics*. 57(2):323-31.

Ptak K, Yamanishi T, Aungst J, Milescu LS, Zhang R, Richerson GB, Smith JC. (2009) Raphé neurons stimulate respiratory circuit activity by multiple mechanisms via endogenously released serotonin and substance P. *J Neurosci*. 29(12):3720-37.

Ptak K, Zummo GG, Alheid GF, Tkatch T, Surmeier DJ & McCrimmon DR. (2005). Sodium currents in medullary neurons isolated from the pre-B¨otzinger complex region. *J Neurosci* 25, 5159–5170.

Ramirez JM, Tryba AK, Peña F. (2004) Pacemaker neurons and neuronal networks: an integrative view. *Curr Opin Neurobiol*. 14(6):665-74.

Rinzel, J., and Lee, Y. S. Dissection of a model for neuronal parabolic bursting. *J. Math. Biol.* 25: 653-675, 1987

Rush AM, Cummins TR, Waxman SG. (2007) Multiple sodium channels and their roles in electrogenesis within dorsal root ganglion neurons. *J Physiol*. 579(Pt 1):1-14.

Schäfer S, Rosenboom H, Menzel R. (1994) Ionic currents of Kenyon cells from the mushroom body of the honeybee. *J Neurosci.* 14(8):4600-12.

Smith JC, Ellenberger HH, Ballanyi K, Richter DW& Feldman JL (1991). Pre-B¨otzinger complex: a brainstem region that may generate respiratory rhythm in mammals. *Science* 254, 726–729.

Smith, J. C., Jr, R. J. B., Koshiya, N., Negro, C. D., Wilson, C. G. and Johnson, S. M. (2000) Respiratory rhythm generation in neonatal and adult mammels: The hybrid pacemaker-network model. *Respiration Physiol* 122: 131-147.

Taddese A, and Bean BP. (2002) Subthreshold sodium current from rapidly inactivating sodium channels drives spontaneous firing of tuberomammillary neurons. *Neuron* 33: 587-600.

Tazerart, S., Viemari, J. C., Darbon, P., Vinay, L. and Brocard, F. (2007) Contribution of persistent sodium current to locomotor pattern generation in neonatal rats. *J Neurophysiol* 98: 613-628.

Tazerart, S., Vinay, L. and Brocard, F. (2008) The persistent sodium current generates pacemaker activities in the central pattern generator for locomotion and regulates the locomotor rhythm. *J Neurosci* 28: 8577-8589.

Theiss RD, Kuo JJ, Heckman CJ. (2007) Persistent inward currents in rat ventral horn neurones. *J Physiol.* 580(Pt. 2):507-22

Thoby-Brisson M, and Ramirez JM. (2001) Identification of two types of inspiratory pacemaker neurons in the isolated respiratory neural network of mice. *J Neurophysiol* 86: 104-112.

Urbani, A. and Belluzzi, O. (2000) Riluzole inhibits the persistent sodium current in mammalian CNS neurons. *Eur J Neurosci* 12:3567–3574.

van Drongelen W, Koch H, Elsen FP, Lee HC, Mrejeru A, Doren E, Marcuccilli CJ, Hereld M, Stevens RL, Ramirez JM. (2006) Role of persistent sodium current

in bursting activity of mouse neocortical networks in vitro. *J Neurophysiol*. 96(5):2564-77.

Viemari JC, Ramirez JM. (2006) Norepinephrine differentially modulates different types of respiratory pacemaker and nonpacemaker neurons. *J Neurophysiol*. 95(4):2070-82

Wu N, Enomoto A, Tanaka S, Hsiao CF, Nykamp DQ, Izhikevich E, Chandler SH. (2005) Persistent sodium currents in mesencephalic v neurons participate in burst generation and control of membrane excitability. *J Neurophysiol*. 93(5):2710-22.

Wu N, Hsiao CF, and Chandler SH. (2001) Membrane resonance and subthreshold membrane oscillations in mesencephalic V neurons: participants in burst generation. *J Neurosci* 21: 3729–3739.

Yoo MH, Hyun HJ, Koh JY, Yoon YH. (2005) Riluzole inhibits VEGF-induced endothelial cell proliferation in vitro and hyperoxia-induced abnormal vessel formation in vivo. *Invest Ophthalmol Vis Sci*. 46(12):4780-7

Yvon, C., Czarnecki, A. & Streit, J.J. (2007) Riluzole-induced oscillations in cultured spinal networks. *J. Neurophysiol.* 97, 3607–3620

Zhong, G., Masino, M. A. and Harris-Warrick, R. M. (2007) Persistent sodium currents participate in fictive locomotion generation in neonatal mouse spinal cord. *J Neurosci* 27: 4507-4518.

Ziskind-Conhaim L, Wu L, Wiesner EP. (2008) Persistent sodium current contributes to induced voltage oscillations in locomotor-related hb9 interneurons in the mouse spinal cord. *J Neurophysiol.* 100(4):2254-64.

Zona C, Cavalcanti S, De Sarro G, Siniscalchi A, Marchetti C, Gaetti C, Costa N, Mercuri N, Bernardi G (2002) Kainate-induced currents in rat cortical neurons in culture are modulated by riluzole. *Synapse* 43:244–251.

Zona C, Siniscalchi A, Mercuri NB, Bernardi G (1998) Riluzole interacts with voltage-activated sodium and potassium currents in cultured rat cortical neurons. *Neuroscience* 85:931–938.

CHAPTER 5

THE SCOPE AND LIMITATIONS OF THE PRESENT STUDY AND FUTURE DIRECTIONS

Pacemaking mechanisms

Rhythmogenesis has been extensively studied in other CPG systems (respiration, mastication, whisking, and locomotion – both invertebrate and vertebrate); the cellular mechanisms are diverse and still not well understood. The role and necessity of pacemaker neurons in rhythmogenesis are widely disputed. There is currently a lack of experimental data regarding the identity or even existence of specialized pacemaker neurons in (mammalian) motor systems. For this reason, pacemaker neurons' role, necessity and sufficiency for rhythmogenesis are currently impossible to address in the mammalian systems, partly because of the technical challenges of studying the complex vertebrate circuits. Invertebrate CPGs, such as the lobster pyloric circuit, give us an opportunity to address the problem due to several factors. First, the lobster pyloric network is unarguably driven by a pacemaker neuron, the AB. Besides, this system offers a substantial technical advantage: it is a well known system, with easily identifiable components of the circuit; the ability to synaptically isolate the AB in-situ without damaging its morphology or dendritic arborizations; the ability to study intrinsic properties without interference from synaptic inputs. All this makes the STG the best model system to address the mechanisms of intrinsic bursting of a pacemaker and rhythmogenesis.

I focus on the mechanisms of monoamine-induced AB bursting. Previous work has shown the AB's unique ability to generate endogenous bursting in the presence of monoamines and the distinct ionic dependencies for each (Harris-Warrick and Flamm, 1987). Briefly, the authors previously showed that DA

oscillations are calcium –dependent and insensitive to TTX, while 5HT oscillations are highly dependent on external sodium and blocked by TTX. Building upon this work, I addressed the following questions: (1) How does the pacemaker generate an endogenous rhythmic output in the presence of each monoamine? (2) What are the ionic targets of monoamines in each bursting mode? (3) What conductances or processes are affected by monoamine in each case?

Summarizing the results that were described in detail in the previous chapters, I determined the major targets of DA and 5HT that induce bursting in the pyloric pacemaker neuron AB. DA induces bursting by an increase of cytoplasmic Ca^{2+} concentrations, most likely by triggering Ca^{2+} release from ER stores, and in so doing, DA activates I_{CAN} for initial depolarization. 5HT, in turn, induces bursting by a dual potassium conductance decrease mechanism, thus unmasking the depolarizing effect of $I_{Na(P)}$ which is necessary for the serotonin bursting.

Novelty of This Study and Contributions to the Field

I have described and characterized the physiological properties and the pharmacology of $I_{Na(P)}$ and I_{CAN} in three lobster pyloric neurons. Both currents exhibit cell-type specificity in their properties and modulation. This work brings added details to our knowledge of the inner workings of the pyloric circuit and may help to explain certain modulatory effects as well as being useful to refine existing mathematical models of the pyloric neurons and the whole circuit.

I have also established that DA induces bursting by modulation of the $[Ca^{2+}]_{in}$ dynamics. In addition to the previously known DA inhibition of influx *via* $I_{Ca(V)}$ (Johnson et al.,2003), I have obtained a direct evidence that when dopamine is applied, the intracellular calcium concentration rises before the emergence of the membrane potential oscillations. Furthermore, I have shown that a block of the

RyR and IP_3R channels prevents the DA-induced calcium increase and bursting, providing a strong evidence that these intracellular calcium channels are critically involved in the AB bursting.

Finally, I have also shown that there is voltage-dependent calcium influx during DA-induced oscillations, with the calcium peaks following the voltage peaks with a 0.2 phase delay. Hence the DA-insensitive portion of the $I_{Ca(V)}$ (which constitutes about 30% of the calcium current under control conditions, measured in the soma) still contributes to the calcium influx in the presence of DA.

The nature of the DA modulation of I_{CAN} suggests that the AB neuron switches from the external calcium-dependent bursting to the internal calcium-dependent bursting, or rather from the voltage-dependent calcium influx to the receptor- or store- dependent calcium influx during DA bursting. This indeed needs to be tested directly, and before that I cannot think of any possible explanations and advantages of such a switch to the pacemaker.

Limitations of the Conducted Study and Future Directions

The focus of this study was on the mechanisms that help to initiate the depolarizing phase of the bursting cycle, while the mechanisms of the repolarizing phase ("burst termination") were not addressed. Of course, both processes have to be controlled to generate the rhythmic oscillatory behavior and my work needs to be complemented with experimental testing of the "burst termination" mechanisms to construct a complete model.

As with any electrophysiological experiment in the STG, where the neurons have extensive dendtritic arborizations, the "space clamp" problem may interfere with accuracy of the measurements of ionic currents. Since the currents I studied (I_{CAN} and $I_{Na(P)}$) are presumed to originate in the fine neuropil, hundreds of microns away from the neuronal soma where the VC measurements are done, a significant

error may be introduced into the measurements. Additionally, this error may be magnified by the fact that the currents of interest are among the smallest in amplitude, in the range of several nA, as opposed to the potassium currents of several hundreds of nA. Therefore, due to these technical limitations, I could not carry out a full biophysical characterization of the slow inward currents in the pyloric neurons. However, I was able to show that they are expressed in the pyloric neurons in different amounts and exhibit distinct pharmacological and neuromodulatory profiles. For instance, $I_{Na(P)}$ was not detectable in the PD neuron, while it was clearly expressed in the AB and the LP. The AB's $I_{Na(P)}$ at -3 nA was much smaller in amplitude than the LP's which could reach up to -25 nA on average. Furthermore, there was a significant difference in the TTX-sensitivty of $I_{Na(P)}$: the LP it was 100 times higher than in the AB. Although I_{CAN} was present in all three types of neurons, it was much larger in the LP and the PD neurons compared to the AB. Moreover, DA significantly enhanced I_{CAN} in the AB neuron, while it did not have any effect on the same current in the LP neuron. This cell type-specificity of neuronal intrinsic properties is well-known and described for all other ionic currents in the STG (for examples, see Peck et al., 2001, 2006; Johnson et al., 2003; Kloppenburg et al., Gruhn et al., 2005 among others)

DA bursting in the AB neuron is highly dependent on calcium metabolism, which has a complex and dynamic nature involving many feedback loops and multiple regulatory mechanisms. One caveat to the use of calcium indicator dyes is that they are themselves calcium buffers: they change the calcium concentrations, distorting the readings. In addition, the kinetics of the calcium indicator's calcium binding and unbinding may be too slow for some processes to correlate the changes in the calcium signal with faster electrical phenomena.

Overall, the calcium dynamics in neurons are determined by membrane flux via ion channels and pumps, as well as by intracellular organelle release and uptake and cytoplasmic buffering. Calcium influx from the extracellular space occurs via voltage-gated or receptor-gated calcium channels, as well as store-operated calcium channels (SOCC) and the sodium-calcium exchanger (NCX) operating in a reverse mode. Additional influx may occur via non-specific cationic channels that may be activated by calcium itself or other second messengers such as cyclic nucleotides (cAMP, cGMP) or NADHP. Free calcium ions are tightly regulated: they can be pumped out by the plasma membrane calcium ATPase (PMCA) and NCX, taken up by organelles (endoplasmic reticulum ER and mitochondria), or buffered by specialized calcium-binding proteins in the cytoplasm. The ER releases calcium via two types of calcium-receptor proteins: IP3-activated (IP3R) or Ryanodine-sensitive (RyR); both may be activated or inhibited depending on the $[Ca^{2+}]_{in}$. Mitochondria release or up-take free calcium ions depending on the pH and other regulatory factors. Thus, I_{CAN} can potentially be activated by calcium ions coming from any of those sources, and DA may be targeting any of those players in the calcium metabolism. Therefore, the main challenge for me was to choose what players and processes to focus on, since controlling and measuring all aspects of the calcium dynamics was not practical. Indeed, in my DA bursting experiments I did not explore the involvement of the sodium-calcium and potassium-dependent sodium-calcium ATPases (NCX and NKCX, respectively), store-operated calcium channels (SOCE) and various receptor-activated calcium channels. Nor did I look at the role of mitochondria, which are critical in the calcium metabolism. Each of these players (channels, pumps, or receptors) was reported to be tightly linked to the prolonged depolarizations or rhythmic oscillations in different experimental systems. It is possible that some or

all of these targets are modulated by DA, and each additional player adds multiple layers of complexity due to sheer number of possible interactions with other players.

However, even with the limited number of calcium metabolism players I have chosen to focus on in the study, there are still several points that beg to be addressed. First, to test whether the IP3R and RyR are sufficient for DA bursting, one could stimulate them and look at the calcium levels and emergence of oscillations. Specifically, for the IP3R, the stimulation could be done with IP3 injection; one would expect to see bursting and $[Ca^{2+}]_{in}$ increase. To stimulate RyR one could use caffeine which does evoke spontaneous TTX-resistant oscillations in the isolated AB (Kadiri, unpublished); one would expect to see an intracellular $[Ca^{2+}]$ rise as well. Additionally, to link the activation of these receptors and intracellular calcium rise to activation of I_{CAN}, one would need to show in VC that IP3 and caffeine enhance I_{CAN}.

Another point that needs clarification is what role the extracellular calcium plays in the DA bursting. At the least, it may be the calcium store replenishment occurring via the SOC, receptor-activated calcium and/or CAN channels. At the most, it may be an active participation in the depolarization via an engagement of the high-voltage activated calcium channels. Those would need an initial depolarization to reach their threshold for activation. It is possible that I_{CAN} provides the initial (slower) ramp for depolarization, while the small portion of the voltage-activated channels unaffected by DA (see Johnson *et al.,* 2003) may be playing a critical role in the late phase (faster) depolarization. To fill in the gaps in the DA model, one could block the above-mentioned calcium-permeable pumps and channels one-by-one, while monitoring the membrane potential and intracellular calcium signal during DA application.

Finally, because of the several reports about the FFA-induced calcium release from intracellular stores, it is important to run control experiment in the STG and look at FFA's effect on intracellular Ca^{2+} release. Unfortunately, due to time limitations on the two-photon rig, we could not perform all these critical experiments.

For the 5HT bursting project, the main obstacle was that we do not know as much about its effects on the AB's conductances as we do for DA. Due to a lack of experimental evidence about the 5HT effects on other currents in the AB (V-dependent calcium current, hyperpolarization-activated current, I_h, calcium-activated potassium current, to name the few), and pumps (Na/K and Ca/Na exchangers), I cannot construct a more complete picture of the bursting mechanism. It would be worthwhile to look at the serotonin modulation of those ionic current in the AB neuron. Additionally, I cannot exclude the effect of APs in the bursting dynamics (in DA, the AB neuron can generate slow waves without APs, hence the DA bistability does not depend on the APs). Since $I_{Na(P)}$ in the AB is as sensitive to TTX as $I_{Na(T)}$ is, there is no known experimental way to separate the roles of these two currents during bursting. In this case, I think using the mathematical model of the AB (Guckenheimer, 1993) would be of great use.

Molecular underpinnings of monoamine modulation. We do not know the exact types of DA and 5HT receptors in the AB, nor the G-protein pathways they are linked to. For now, it is possible to use the 5HTR agonists and antagonists, whose pharmacology in the lobster was recently established by Baro and colleagues, to gain some insight into the signaling cascade of the 5HT modulation. Ultimately, we would like to find out the exact receptor and G-protein coupling profile of the AB neuron to pinpoint the precise pathways involved in its monoamine-induced bursting behavior and pyloric rhythmogenesis.

Mathematical models. Bursting is a non-linear behavior and as such it is difficult to study and to predict, without the knowledge gained from mathematical models and a dynamical systems approach. Mathematical models can help with better understanding of the intracellular calcium dynamics during DA bursting, and its role in burst initiation and termination. While there are numerous models of slow bursters incorporating the detailed descriptions of calcium dynamics and its role in firing properties, these models are mostly for non-neuronal cells, describing insulin secretion, hormone secretion from the hypothalamus and pituitary (Rinzel and Lee,1997; Stojilkovich, 2005) and heart pacemaker activity (Sherman; Lakkatta, 2008). It would be interesting to see whether the calcium-dependent processes that work for endocrine and muscle cells will work for the faster oscillatory behavior of the neuronal cells.

The mathematical model of the AB can help with better understanding of the 5HT bursting mechanism, and the possible importance of action potentials (APs) in the 5HT bursting: fast-slow dynamics may generate a parabolic bursting type, where APs are an integral part of the oscillatory mechanism (Aplysia R15 model). In the existing AB model (Guckenheimer, 1993), an increase of $G_{Na(P)}$ (by simply setting the inactivation of 1% of $G_{Na(T)}$ to zero) does not result in bursting, but instead in a silent depolarized state (Guckenheimer, unpublished). I believe that incorporating the findings described in this work could be used to refine this model and use it to gain deeper understanding of the oscillatory behavior of the AB neuron and map out the future experiments.